Inauguraldissertation zur Erlangung der Doktorwürde
der Naturwissenschaftlich-Mathematischen Gesamtfakultät
der Ruprecht-Karls-Universität Heidelberg

KCC2 Plays a Crucial Role during the Maturation of Spinal Neurons by Regulating the Expression of the GlyR Alpha1 Subunit and Gephyrin

vorgelegt von
Diplom-Biologe Stefanie Birgitta Schumacher
aus Bretten

Tag der mündlichen Prüfung: _____

KCC2 Plays a Crucial Role during the Maturation of Spinal Neurons by Regulating the Expression of the GlyR Alpha1 Subunit and Gephyrin

---

Referees: **Prof. Dr. Hilmar Bading**
Prof. Dr. Joachim Kirsch

Acknowledgements

First, I would like to thank Prof. Dr. Joachim Kirsch who gave me the opportunity to take part in his research group and who provided the topic. He always supported and motivated me with great patience and impressive knowledge. I was able to work independently and to experience a broad range of methods. I also want to thank Prof. Dr. Hilmar Bading for being my first referee. Whenever I needed his help, he took the time and quickly answered all my issues.

Thanks to all the people of the fourth floor for support, advice and reagents whenever I needed them and for the friendly atmosphere.

Special thanks to Jochen Kuhse who always was open to my questions and problems. He took the important critical part and had great ideas for my work. A special thank to Nicolai who was very dedicated and helped a lot during his practical course and who made a few experiments used for this thesis. Thanks to Christoph for soccer stickers, critical challenge and for informing me about every single out coming KCC2 and GlyR article. Thanks to Susanne for great help and even greater ideas in solving problems. I also would like to thank Valandis for tireless trials of measuring cells and for long and illuminating discussions. Big thanks to Kathrin who brightened every day in the lab and for her incredible friendship. Special thanks to Rita for preparing and culturing the SNs. I also would like to thank Barbara for office stuff, her great humour, funny and serious conversations and everything else. Many, many thanks to Andrea, without her I would not have succeeded. Thanks for countless protocols, advices, talks, for providing HCNs and SNs and for facilitating my life in the lab so much!

Many special thanks to my parents and my brothers for constant support and for standing by my side during my whole life!

I would like to express my deepest thanks to Christian for lightening up every day, for consolation, great support, for making me laugh and for simply being in my life.

Summary

In spinal cord and brain stem, the GlyR is the major receptor type to mediate inhibitory synaptic transmission. Together with the GlyRb subunit, the GlyRa1 subunit forms the adult form of the receptor. Activation of the pentameric GlyR by glycine results in an increased permeability of the GlyR channel for chloride. In juvenile stages, the cell is depolarized whereas adult neurons experience a hyperpolarization. Not least, the activity of KCC2, changing the intracellular chloride level from a high to a low adult state, contributes considerably to the maturation of the neurons.

In this thesis, the approximate time point of the switch to occur *in vitro* could be determined to div 14 via mRNA expression studies of the distinct GlyR subunits. The obtained mRNA data also indicate that the GlyRb subunit exhibits the highest RNA expression whereas GlyRa1 expression is even lower than that of GlyRa2. Taken together, the results suggest that adult neurons as well as juvenile neurons still express heteromeric α2β and/or homomeric α2 receptors.

Strychnine application to the SN cultures resulted in a down regulation of KCC2 expression in a dose-dependent manner at div 14. This finding indicates that the activity of the GlyR may regulate the expression of KCC2 to some extent. Subsequent treatments with Ca^{2+} channel blockers and Ca^{2+} chelators revealed a role for Ca^{2+} to destabilize the KCC2 complex. Although suppression of the entire synaptic transmission in the culture by TTX application as well as catching all free Ca^{2+} ions also reduce KCC2 expression, the latter seems not to be dependent on Ca^{2+} influx via L-type channels. However, KCC2 expression either depends on Ca^{2+} being present within the cell or Ca^{2+} influx through another type of Ca-channel than L-type.

To clarify the role of KCC2 in the GlyR subunit switch, its expression successfully was down regulated upon transduction by a silencing shRNA construct. Immunoblot and localization of immunoreactivities reveal a decrease in the expression of the adult GlyRa1 subunit following KCC2 knockdown. The expression of gephyrin is affected as well. In the main, no additionally investigated synaptic proteins are concerned. Therefore, the neurons are supposed to remain in a juvenile state in terms of the GlyR when KCC2 is not expressed properly. The question arising is, whether the pure presence or the activity of KCC2 is responsible for the correct GlyRa1 expression. It also remains unclear whether knockdown of KCC2 affects GlyRa1 expression and hence gephyrin expression, the other way around or whether even both proteins directly are affected by loss of KCC2.

I suggest that loss of KCC2 impairs the expression of the scaffolding protein gephyrin via unknown cytoskeletal mechanisms or signalling pathways. The absence of gephyrin in turn directs loss of the adult GlyR consisting of GlyRa1 and GlyRb. This loss might result from either down regulation of GlyRa1 expression or removal of the adult receptor from the membrane and subsequent degradation.

Zusammenfassung

Im Rückenmark und im Hirnstamm ist hauptsächlich der Glyzin Rezeptor (GlyR) als inhibitorisch agierender Rezeptortyp exprimiert. Die GlyRb und die GlyRa1 Untereinheiten formen zusammen den adulten Rezeptor. Wird der pentamere GlyR durch Glyzin aktiviert, erhöht sich seine Permeabilität für Chlorid, wodurch im Adultstadium eine Hyperpolarisation der postsynaptischen Membran hervorgerufen wird. Im Jugendstadium dagegen erfährt die Zelle eine Depolarisation und somit eine exzitatorische Antwort. Durch die drastische Verringerung des hohen, intrazellulären Chloridlevels trägt die Aktivität von KCC2 nicht zuletzt auch zur Reifung der Neurone bei.

In dieser Arbeit konnte ein etwaiger Zeitpunkt des GlyR Untereinheiten Switch determiniert werden. *In vitro* Daten aus mRNA Expressionsstudien der unterschiedlichen Untereinheiten zufolge findet der Switch um den Zeitpunkt div 14 statt. Aus den besagten Daten geht auch hervor, dass die GlyRb Untereinheit die höchste mRNA-Expression aufweist, wogegen das GlyRa1-Expressionslevel sogar unter dem von GlyRa2 liegt. Zusammenfassend lässt sich aussagen, dass auch reife Neurone aus dem Rückenmark noch heteromere α2β und/oder homomere α2 Rezeptoren exprimieren.

Behandelt man die SN Kulturen mit Strychnin, tritt eine dosisabhängige Abnahme der KCC2-Expression an div 14 auf. Daraus kann man schließen, dass die KCC2-Expression in gewissem Maße durch die Aktivität des GlyRs reguliert wird. Anschließend wurden die Zellen mit Ca^{2+}-Kanal Blockern und Ca^{2+}-Chelatbildnern behandelt. Daraus geht hervor, dass Ca^{2+} möglicherweise dazu imstande ist, den KCC2-Komplex, der nur als Tetramer aktiv ist, zu destabilisieren. Obwohl die Inhibierung der gesamten synaptischen Transmission der Kultur durch TTX als auch das Komplexieren aller freier Ca-Ionen zu einer verminderten KCC2-Expression führt, scheint letzteres nicht vom Ca^{2+}-Einstrom durch L-Typ Kanäle abhängig zu sein. Dennoch hängt die KCC2 Expression entweder von freien Ca^{2+}-Ionen innerhalb der Zelle oder von einströmendem Ca^{2+} durch andere Kanäle ab.

Um die Rolle von KCC2 im GlyR Untereinheiten Switch zu klären, wurden die Neurone mit einem shRNA Konstrukt transduziert, das die Expression von KCC2 fast komplett still legt. Eine daraus folgende Verminderung der adulten GlyRa1 Untereinheiten-Expression konnte in Immunoblots und Immunfärbungen aufgezeigt werden. Ebenso betroffen von dem KCC2 Knockdown war Gephyrin, welches den adulten GlyR am Zytoskelett verankert. Im Großen und Ganzen wurden alle anderen untersuchten synaptischen Proteine nicht durch den KCC2 Knockdown beeinträchtigt. Daraus folgt, dass die Zellen, im Bezug auf den GlyR, in einem jugendlichen Stadium verharren, wenn KCC2 nicht im richtigen Ausmaß exprimiert wird. Daraus resultiert die Frage, ob die bloße Anwesenheit von KCC2 oder seine Aktivität verantwortlich für die korrekte GlyRa1-Expression ist. Es bleibt auch unklar, ob der Knockdown von KCC2 die GlyRa1 Untereinheiten-Expression direkt und daraus folgend die Gephyrin-Expression beeinträchtigt oder umgekehrt oder ob sogar beide Proteine direkt durch den Verlust der KCC2-Expression betroffen sind.

Meine Vermutung ist, dass der Verlust an KCC2 das gerüstbildende Protein Gephyrin über bisher unbekannte Zytoskelett-Verbindungen oder Signalwege in Mitleidenschaft zieht. Der Verlust an

Gephyrin wiederum führt zu einer Verminderung des adulten GlyRs, bestehend aus GlyRa1 und GlyRb. Diese Verminderung könnte entweder aus der Abnahme der GlyRa1-Expression oder aus der Entfernung des GlyRs aus der Membran und anschließender Degradierung resultieren.

Table of Contents

1. Introduction

1.1. The spinal cord

1.1.1. Composition of the adult spinal cord

Extending from the *Medulla oblongata*, the spinal cord is a long, thin, tubular bundle of nervous tissue and support cells. Together with the brain, it represents the central nervous system (CNS). The spinal cord is protected by the enclosing vertebral column. In mammals, the spinal cord ranges from the *Foramen magnum* (cranium) to backmost lumbar vertebrae. This is because the backbone is developing faster than the spinal cord and thus the spinal cord's longitudinal growth drops behind that of the backbone. This phenomenon is called *Ascensus medullae spinalis*. Therefore, the roots of the spinal nerves have to cover a more and more elongated distance in caudal direction because they still break through their original intervertebral foramen. Thus, only the spinal nerve roots proceed within the vertebral canal underneath the cone-shaped spinal cord ending. The spinal cord is as well as the brain surrounded by liquor. In terms of spinal meninges, three of them are distinguished: the external *Dura mater*, the medial *Arachnoidea* and the internal *Pia mater*. The spinal cord track has two swellings: one at the *Intumescentia cervicalis* and another one at the *Intumescentia lumbosacralis*. In these regions, spinal nerves innervating the fore and hind limbs, which require more neurons than e.g. the trunk, emerge from the vertebral canal.

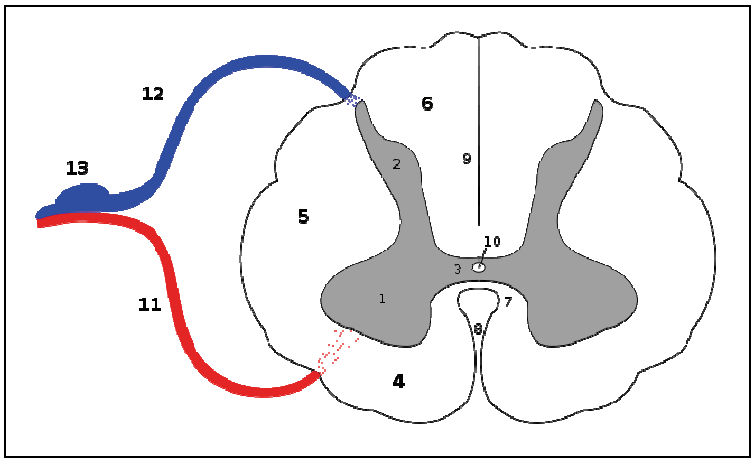

Figure 1: Structures of the spinal cord in cross-section
Source: http://www.wikipedia.de

Structures of the gray matter:
1. ventral horn
2. dorsal horn
3. Commissura grisea

Structures of the white matter:
4. ventral funiculus
5. lateral funiculus
6. dorsal funiculus
7. Commissura alba ventralis
8. Fissura mediana ventralis
9. Sulcus medianus dorsalis

Other structures:
10. Canalis centralis
11. ventral root
12. dorsal root
13. Ganglion sensorium nervi spinalis

On the ventral side of the spinal cord, the *Fissura mediana ventralis* is proceeding whereas dorsally another groove, the *Sulcus medianus posterior* is extending (Figure 1). On both sides, three strands are distinguishable: the ventral funiculus, the dorsal funiculus and in between them, the lateral funiculus of the spinal cord (Figure 1). Between the dorsal and the lateral funiculus, the dorsal root is

passing through whereas the ventral root escapes between the lateral and the ventral funiculus. The spinal nerve roots meet on the level of the intervertebral foramen where they form the spinal nerves.

According to the spinal nerve leaving points, the spinal cord is structured in five sections. The cervical part contains eight segments (C1-8) in mammals, whereas the thoracic part consists of 12 segments (Th1-12). The lumbar and the sacral part exhibit 5 segments respectively (L1-5 and S1-5) and the coccygeal part has 1-5 segments (grown together in some degree).

Regarding the longitudinal section of the fetal spinal cord, three layers are distinguishable. The one lying next to the *Canalis centralis* is called ventricular germinal zone and gives rise to neuroblasts, glioblasts and at the end ependymal cells. The intermediate zone is forming the gray matter whereas the white matter arises from the marginal zone.

Occupying cell bodies, the gray matter of the spinal cord has the shape of a butterfly. The ventral, broader part is called the ventral horn (*Cornu ventrale*). The dorsal part is narrower and called the dorsal horn (*Cornu dorsale*). In the field of the thoracic and lumbar part of the spinal cord, another smaller lateral horn is appearing (*Cornu laterale*, Figure 2, green). The “butterfly wings” of the gray matter are cross-linked by the *Commissura grisea* (Figure 1). The *Canalis centralis* filled with liquor is located in the middle of this commissure (Figure 1 and Figure 2). The gray matter is further organized into ten layers, the so-called *Laminae* (Figure 2). *Laminae* I-VII are located in the dorsal horn whereas *Laminae* VIII and IX reside in the ventral horn, *Laminae* X at last is forming the mentioned cross linkage (Figure 2). In terms of function, several nuclei can be distinguished in the spinal cord. The *Nucleus intermediolateralis* is the origin of the sympathetic nerve fibres in thoracic and lumbar spinal cord. The motor nuclei columns located in the ventral horn represent the origin of the motor fibres (Figure 2).

The dorsal horn is supplied with sensitive input coming via the dorsal, sensitive root of the spinal nerve from the periphery. The cell bodies of the sensitive nerve cells being pseudounipolar are located beyond the spinal cord within the dorsal root ganglion. Their axons enter the dorsal horn via the dorsal root. In the dorsal horn, they either are switched to a second neuron or directly project to the brain via special tracks within the white matter. The motor neurons reside within the ventral horn of the spinal cord. The axons of the motor neurons forming the ventral root are sent to the muscles and neuromuscular spindles. The lateral horn in the thoracic and lumbar part (Figure 2) of the spinal cord is formed by the cell bodies of vegetative neurons and therefore it belongs to the sympathetic nervous system. The efferent fibres of the vegetative neurons leave the spinal cord via the ventral root and project to the sympathetic trunk where they are partially switched to a second neuron. If not, they are sent to the prevertebral ganglia to be switched there. Coming from the periphery, sympathetic afferent tracks project to the lateral horn. In the sacral part, cell bodies of parasympathetic neurons are located at the same position but do not form a lateral horn.

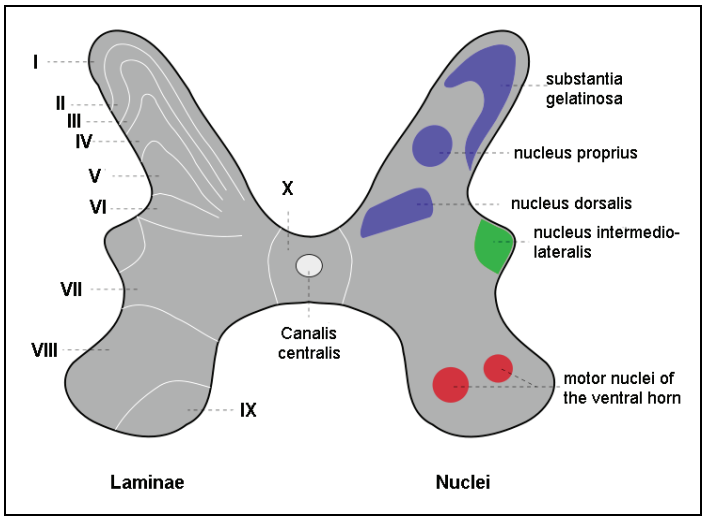

Figure 2: Laminae and nuclei of the spinal cord in cross section. The gray matter corresponds to the thoracic and lumbar region of the spinal cord.

Source: http://www.wikipedia.de

The mentioned tracks run within the white matter of the spinal cord. The afferent fibres (mostly sensitive) project to the brain whereas the efferent fibres (mostly motor) originate in the brain. The white colour arises from the myelination of the axons. Two important afferent tracks forming the dorsal fasciculus (Figure 3) whose cell bodies are located in the spinal ganglia are *Fasciculus cuneatus* and *Fasciculus gracilis*. They direct information about smooth touches and deep sensibility to the *Medulla oblongata* (afterbrain). There the initial switch appears in the accordant nuclei. Right after switching, the fibres cross to the other side. Information about rough pressure, temperature and pain (protopathic sensibility) is conducted by the *Tractus spinothalamicus* or anterolateral funiculus (Figure 3) from the dorsal horn to the Thalamus. Proprioceptive impulses about position and attitude of joints, muscles and tendons are conducted by the *Tractus spinocerebellaris* (Figure 3) arising from the *Nucleus dorsalis* in the dorsal horn and ending in the cerebellum. This track remains uncrossed.

One of the important efferent tracks is the corticospinal funiculus (*Tractus corticospinalis,* Figure 3) spanning from the motor cortex of the external granular layer of the cerebral cortex to the ventral horn. Tracks not belonging to the latter funiculus are denoted as extrapyramidal tracks.

The most important inhibitory neurotransmitter in the spinal cord is glycine. Interneurons and Renshaw cells are glycinergic, releasing glycine at their synaptic endings. The released glycine opens ligand-gated ion channels of the downstream lying neuron and thus lowers its activity. In the spinal cord, the glycinergic neurons inhibit motoneurons of the ventral horn. This process diminishes the activity of muscles innervated by the motoneurons. Strychnine is a potent antagonist of the GlyR and is able to abate the force of glycine. Abolition of the inhibition directs increased muscle activity causing life-threatening spasms.

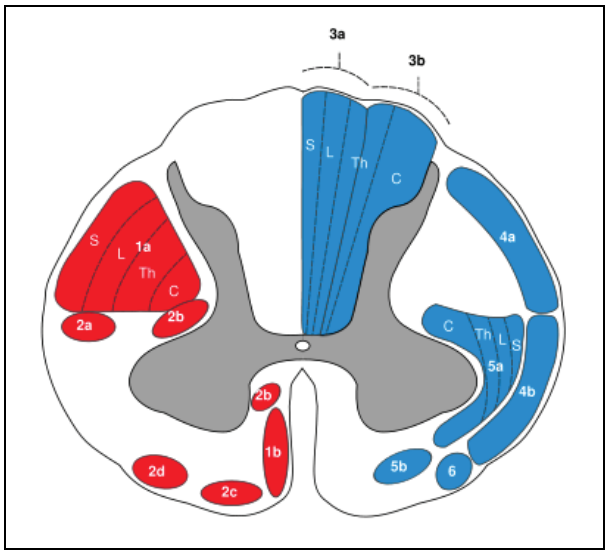

Figure 3: Afferent and efferent tracks of the white matter.

Source: http://www.wikipedia.de

Somatotopic arrangement:

S: fibres from the sacral part
L: fibres from the lumbar part
TH: fibres from the thoracic part
C: fibres from the cervical part

Motor tracks (efferent, red):

5. pyramidal funiculus
   a. Tractus corticospinalis lateralis
   b. Tractus corticospinalis anterior
6. extrasynaptic funiculi
   a. Tractus rubrospinalis
   b. Tractus reticulospinalis
   c. Tractus vestibulospinalis
   d. Tractus olivospinalis

Sensitive tracks (afferent, blue):

1. dorsal fasciculus
   a. Fasciculus gracilis
   b. Fasciculus cuneatus
2. spinocerebellar tracts
   a. Tractus spinocereballaris posterior
   b. Tractus spinocerebellaris anterior
3. sensitive anterolateral tracts
   a. Tractus spinothalamicus lateralis
   b. Tractus spinothalamicus anterior
4. Tractus spinoolivaris

Schematically, postsynaptic inhibition is functionally excitatory in the spinal cord at about one week before birth and inhibitory at about one week after birth. During this critical time window, pathways descending from the brain stem reach the lumbar cord.

1.1.2. Development of the neural tube

After gastrulation, the notochord induces the dorsomedial part of the embryonic ectoderm to form the thick and flat neural plate (Figure 4A) by secreting growth factors (e.g. sonic hedgehog). Therefore, BMP signals have to be repressed. Cells receiving BMP develop into epidermal cells. Chordin and noggin, both shown to bind directly to BMP, are responsible for the active repression of BMP (Liu and Niswander 2005). Inducing a neural fate and being created and emitted by the Spemann organiser, chordin and noggin typically are expressed on the dorsal side of the embryo whereas BMPs rather are expressed ventrally. BMPs 13-15 e.g. are able to prevent cells from a neural fate. Thus, suppression of BMP signalling on the dorsal side of the embryo is important to allow formation of neural tissue though also other pathways contribute to this process. Recent studies reveal that FGF (fibroblast growth factor) signalling also is crucial for neural induction (Liu and Niswander 2005). Thereby, FGF is thought to sensitize the tissue to respond to the BMP antagonists. FGF signalling is further shown to suppress BMP4 and BMP7 expression. Neural fate induction is also promoted by IGF (insulin-like growth factor).

At the border between the neuroectoderm and the non-neural ectoderm, a multiprogenitor population is generated. This structure, the neural crest, gives rise to a couple of different migratory cell types forming peripheral neurons, glial cells, connective tissue, bone, secretory cells, melanocytes and the outflow tract of the heart (Gammill and Bronner-Fraser 2003). Applied to naive neural tissue explants, recombinant BMP is able to induce neural crest tissue. In the BMP mutants swirl (swr or bmp2b), snailhouse (snh or bmp7) and somitobun (sbn or smad5) the precursors for trunk neural crest cells refrained from forming (Liu and Niswander 2005). Additional to BMPs, also Wnts, FGFs and Notch seem to be able to induce neural crest formation. Thus, a 'two signal model' requiring both, BMP and Wnt signalling for neural crest formation, has been postulated. FGF seems to play a role in regulating MSX1 expression, which in turn also regulates BMP signalling. Further roles for BMPs are forwarding neural crest cell migration, directing neural crest differentiation and arrangement of neural crest cell apoptosis in the hindbrain (Liu and Niswander 2005). Wnt proteins are also involved in migration, proliferation and differentiation of neural crest cells.

In the further development of neurulation, the neural groove is formed by dropping of the neural plate triggered by the generation of a ventrally localized hinge point called floor plate (Figure 4A). The final tube is formed by fusion of the lateral edges of the neural plate and afterwards is segregated from the non-neural epithelium. The neural tube represents the complete CNS anlage. Its lumen becomes the ventricular system of the brain and the spinal cord. At the dorsal midline of the tube, a new organizing centre producing BMPs, namely the roof plate, is formed. Secreting BMPs, the ectoderm and the roof plate have an important role in dorsoventral patterning of the neural tube (Figure 4B). The roof plate additionally expresses Bmp2, Bmp4, Bmp7, Gdf7, activin and dorsalin mRNA. Therefore, BMPs and members of the TGFβ family are responsible for dorsalizing the neural tube (Liu and Niswander 2005). A ligand gradient of BMPs and TGFβ members with higher levels corresponding to a more dorsal fate seems to be crucial for the patterning. Expressed in the floor plate, Shh also has an important role in patterning the ventral spinal cord. Deprivation of Shh expression ends in a loss of the most ventral cell types such as motor neurons or ventral interneurons. Furthermore, a couple of BMP antagonists (see above) is expressed in the axial and paraxial mesoderm flanking the neural tube. Dorsally, sensory interneurons, commissural neurons and neural crest cells develop whereas motoneurons and some interneurons arise ventrally. The first, rather rough determination occurs by expression of homeobox genes of the Pax and Nkx family. Dorsal progenitors exhibit Pax3 and Pax7 expression activated by BMPs. Being repressed in the dorsal spinal cord by BMPs, Pax6 is expressed in the ventral intermediate region. Nkx2, in contrast, is expressed by ventral progenitors adjacent to the floor plate (Figure 4B). Further subdivisions are achieved by expression of different basic helix-loop-helix (bHLH) and homeodomain transcription factors also tightly being regulated by BMPs. The most dorsal region is defined by Math1 expression, less dorsal cells express neurogenin 1 and 2 (NGN1/2) and Mash respectively. According to the transcription factor, being expressed in the cells, they differentiate into dorsal interneurons, ventral interneurons or motoneurons.

Patterning of the spinal cord is closely connected with proliferation. Secreted Wnt proteins as well as BMPs seem to be necessary and sufficient for cell proliferation in the dorsal spinal cord. Possibly, BMPs are thereby involved in the regulation of Wnt signalling.

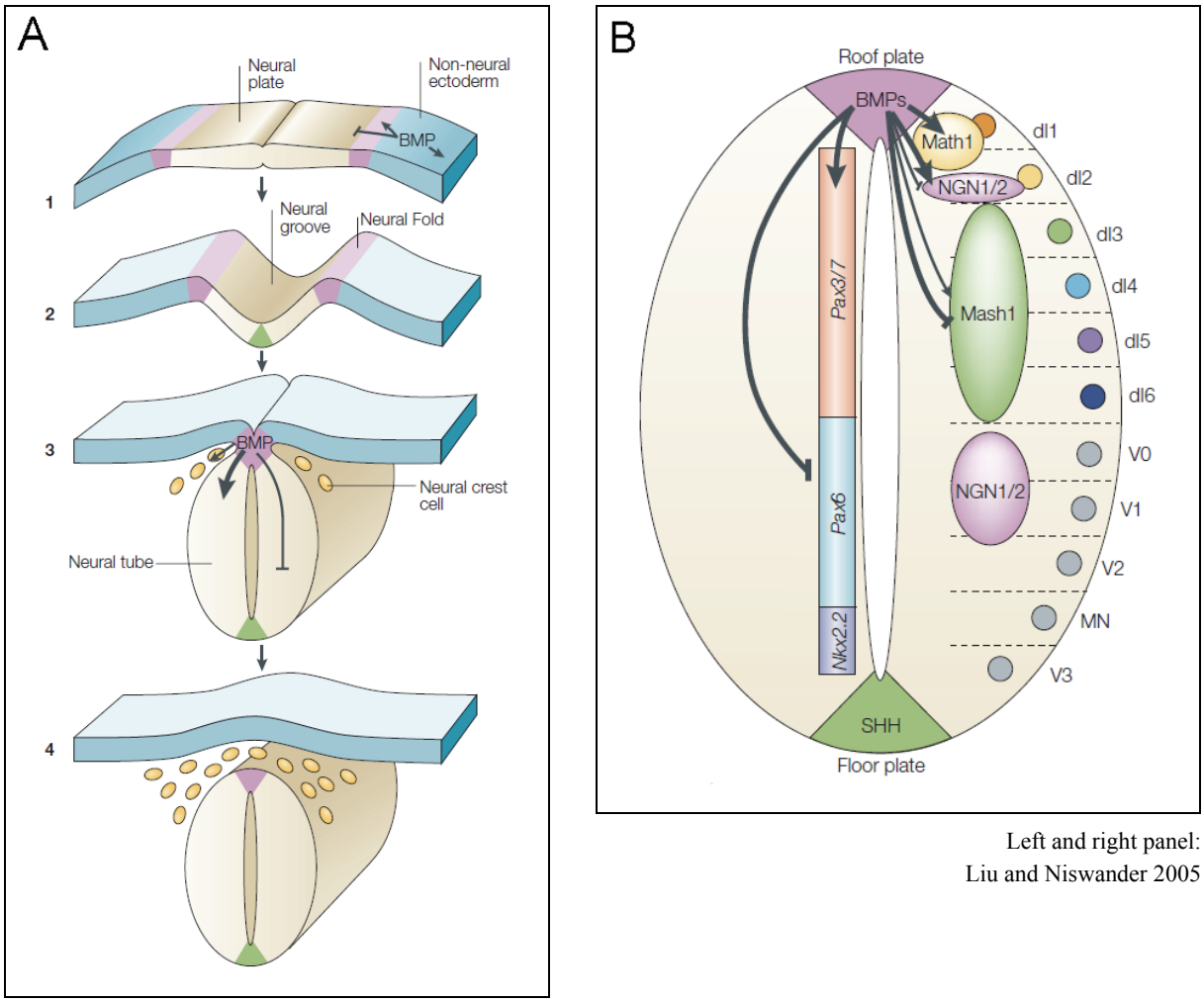

Left and right panel:
Liu and Niswander 2005

Figure 4: A, formation of the neural tube by neurulation. Green part: floor plate, purple part: roof plate. **B**, dorsoventral patterning of the spinal cord. The neural progenitor cells are first divided into broad dorsoventral domains by the differential expression of Pax homeobox genes regulated by BMPs. The spinal cord is further subdivided by the expression of basic helix–loop–helix (bHLH) family and homeodomain transcription factors. This process is also tightly regulated by BMP signalling. dI: dorsal interneurons, v: ventral interneurons, MN: motoneurons.

1.2. The Glycine receptor

1.2.1. GlyR assembly and signalling

In the adult spinal cord, brainstem and retina, the inhibitory neurotransmission is mainly mediated by the glycine receptor (GlyR). Found in the presynapse, GlyRs modulate neurotransmitter release. Postsynaptically, the amino acid glycine acts as the major agonist beside β-alanine and taurine. A high-affinity competitive antagonist is strychnine. The glycine and the strychnine binding sites indeed overlap but are not identical. In addition, cyclothiazide (Zhang et al. 2007) and caffeine (Duan et al.

2009) have recently been shown to block the GlyR. The activity of the GlyR can also be modulated by picrotoxin, zinc, alcohol, cocaine and anesthetics (Leite and Cascio 2001). To maximally activate a homomeric GlyR, three bound glycine molecules are sufficient (Lewis et al. 2003, Beato et al. 2004). Two related subunits named α (GlyRa, 48 kDa) and β (GlyRb, 58 kDa) are known. Currently, four different vertebrate isoforms of the GlyR alpha genes (GlyRa1-4) and the single GlyR beta gene are identified (Lynch 2004). The GlyR β subunit shares 47% amino acid sequence homology with the α1 subunit whereas the α subunits share more than 90% amino acid sequence homology with each other. Each of the subunits contains a large extracellular ligand-binding domain at the N-terminus, mainly consisting of β-sheets as well as four α-helical transmembrane domains (TM1-4, Figure 5) and a short extracellular C-Terminus. The β-sheets are connected by flexible loops. TM3 and TM4 are connected by a large, among ligand-binding ion channels poorly conserved, intracellular domain holding phosphorylation sites and other sites for interaction with cytoplasmic factors. Belonging to the Cys-loop ion channel superfamily, the GlyR owns a disulfide bond-mediated loop in the mentioned N-terminal domain. The amphipathic TM2 domain is responsible for the formation of the central water-filled channel pore. The unusual large cytoplasmic loop (130 residues) between TM3 and TM4 of the GlyRb subunit includes a gephyrin binding domain consisting of an 18-amino-acid motif (Kim et al. 2006, Meyer et al. 1995, Sola et al. 2004). Interacting with GlyRb, gephyrin might serve as a connection point between the GlyR and the actin-filaments via profilin and Mena/VASP. The pentameric GlyR is believed to consist of two α1 and three β subunits in its adult state (Grudzinska et al. 2005). The juvenile form of the GlyR is either a homo-oligomer built of only α2 subunits or a hetero-oligomer composed of α2 and β subunits. The homo-oligomer is not thought to bind directly to gephyrin. Although forming homomeric GlyRs in recombinant expression systems, α1, α3 and α4 GlyR homo-oligomers weakly are expressed in adult neurons. α2 homo-oligomers, in contrast, are abundantly expressed in embryonic neurons.

The high intracellular chloride level of embryonic or rather neonatal neurons generates an outwardly directed chloride flux toward the Cl^- equilibrium potential. The outcome is a depolarisation of the postsynaptic neuron, when the GlyR is activated. Hence, Ca^{2+} fluxes through voltage-gated Ca^{2+}-channels, leading to intracellular signalling, are induced. Joachim Kirsch and Heinrich Betz could show that the mentioned Ca^{2+}-signal is crucial for the formation and maintenance of the GlyR clusters and that GlyR activity and Ca^{2+}-signalling are associated in juvenile spinal neurons (Kirsch and Betz 1998). Still little is known about GlyR mediated gene and protein expression. Raphael Blüm could recently reveal that the juvenile GlyRa2 subunit may bind eEF1A, calcineurin and p70S6 kinase (Bluem et al. 2007). Being crucial for protein synthesis and actin bundling, eEF1A might act as a connection partner between the α2 subunit and actin-filaments, which could be an explanation for GlyRa2 clusters in young neurons.

Activation of the adult GlyR generates a hyperpolarisation of the postsynaptic cell evoked by chloride influx into the cell resulting in an inhibition of the postsynaptic neuron (Betz and Laube 2006, Kirsch 2006).

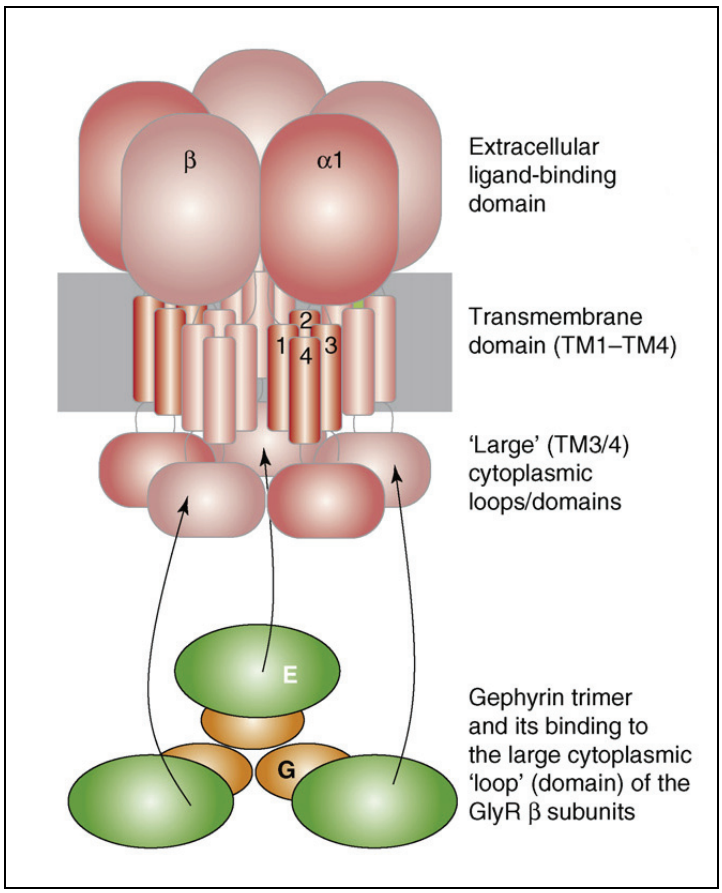

Figure 5: GlyR assembly.
Pentameric GlyR with its three functional domains: the extracellular ligand-binding, the transmembrane and the cytoplasmic (loop) domains. Interaction with the gephyrin trimer is depicted.

Fritschy et al. 2008

1.2.2. Anchoring, trafficking and motility of the GlyR

Additional to the GlyR subunits, Pfeiffer could purify a third protein of 93 kDa in size (Pfeiffer et al. 1982). This peripheral membrane protein named gephyrin is able to bind polymerized tubulin (Kirsch et al. 1991). Gephyrin can interact with the large intracellular loop of GlyRb via a high-affinity binding site. The identified α subunits of the GlyR as well as many $GABA_A$ receptors cannot form connections with gephyrin (Kirsch et al. 1995). Gephyrin consists of three major domains: the N-terminal G (20 kDa) and the C-terminal E domain (43 kDa, Figure 5 and Figure 6) got their denomination because of their sequence analogy with the bacterial Moco-synthesizing enzymes (MogA and MoeA). The two mentioned domains are linked by the so-called C (central) domain (18-21 kDa). The isolated G domain is able to form stable trimers depending on yet identified residues. In contrast, the isolated E domain forms dimers and includes the alluded binding site for the GlyR β subunit (Figure 6A). The "linker region" or C domain of gephyrin occupies several binding sites for interacting proteins such as dynein light chain 1 and 2 (Dlc 1 and 2) and collybistin.

The clustering of the GlyR at postsynaptic sites is dependent on synaptic activity (Kirsch and Betz 1998). Since GlyR clustering is abolished in gephyrin knockout mice as well as in SN cultures treated with antisense-oligonucleotides, that process is obviously mediated by gephyrin (Kirsch et al. 1993, Feng et al. 1998). Blocking GlyR activity in cultured spinal neurons by strychnine, results in the loss of GlyR as well as gephyrin cluster formation. Instead, the GlyR was observed to reside in large intracellular vesicles probably being endosomes (Kirsch and Betz 1998). Gephyrin is believed to build a scaffold submembranously. The linkage of gephyrin trimers and dimers forms this scaffold (Figure 6B and C). Onto the described structure, the GlyR molecules are sitting thereby achieving a three-dimensional shape (Figure 6D).

Furthermore, it has been shown, that in young cultured spinal neurons (div 5-7) the peak amplitude and frequency of spontaneous glycinergic mIPSCs severely are decreased upon microtubule disruption via colchicine. After 15-17 days in culture or by the use of GTP as microtubule stabiliser, this effect is not occurring any more. Van Zundert et al. propose that in later stages either the microtubules are stabilized by e.g. acetylation or MAPs or that the GlyR/gephyrin complexes become independent on microtubules (van Zundert et al. 2004).

Both, GlyR and gephyrin are shown to be co-transported to the plasma membrane, which indicates that non-clustered gephyrin binds to the receptor (Hanus et al. 2004). The binding affinity of gephyrin to the GlyRb loop can be enhanced by the phosphorylation-dependent binding of Pin1 (peptidyl-prolyl isomerase NIMA interacting protein 1), which directs conformational changes to the C domain. Furthermore, there is evidence for the binding of gephyrin to the GlyR to be important for intracellular transport, the lateral motility in the membrane (Ehrensperger et al. 2007, Hanus et al. 2006, Dahan et al. 2003) and interaction with the cytoskeleton (Charrier et al. 2006). Dlc 1 and 2 are shown to bind to the C domain of gephyrin. They are components of motor proteins which likely contribute to gephyrin transport along microtubules (Figure 6E) and hence along neuronal processes. Gephyrin located in the cytoplasm, mainly represents gephyrin in transit (Maas et al. 2006). Via biochemical, immunocytochemical and time-lapse studies, Maas could recently demonstrate the co-transport of gephyrin and GlyRs. He also shows co-localization of dynein and GlyR-gephyrin transport units forming a triple-complex together (Maas et al. 2006). Mobile transport units are attached to microtubules whereas a small proportion of the mentioned triple-complexes are not bound to microtubules. This transport occurs in a retrograde direction. Since Maas shows GlyR-gephyrin complexes not only to move retrogradely but also in an anterograde manner, it would be of great interest to identify the responsible machinery. Supporting Kirsch's data in 1998, chronic strychnine application increased the number of mobile gephyrin by more than 100% together with a clear shift to retrogradely directed transport. Thus, there is functional evidence of GlyR-gephyrin co-transport to be likely sensitive to GlyR blockade. In this context, strychnine may trigger the disappearance of GlyRs from synapses (Rasmussen et al. 2002). After exocytosis at extrasynaptic sites, GlyRs are mainly inserted into synapses by lateral diffusion. Endocytosis of GlyRs also occurs at extrasynaptic localizations. In the extrasynaptic mem-

brane, GlyRs exhibit fast Brownian diffusion. These movements slow down and become confined, when the GlyR reaches a synapse and interacts with synaptic gephyrin clusters (Meier et al. 2001). Thereby gephyrin enters and leaves active synapses within minutes.

Furthermore, the gephyrin-associated protein collybistin is able to translocate gephyrin to the membrane (Kins et al. 2000) and is necessary for its synaptic targeting (Papadopoulos et al. 2007). Since the SH3 domain of collybistin inhibits its membrane-targeting function (Harvey et al., 2004; Kins et al., 2000), the domain has to be deactivated in neurons. Interacting with the gephyrin E domain and being specific for inhibitory synapses (Varoqueaux et al. 2004), NL2 has been found to possess such a capacity (Poulopoulos et al. 2009).

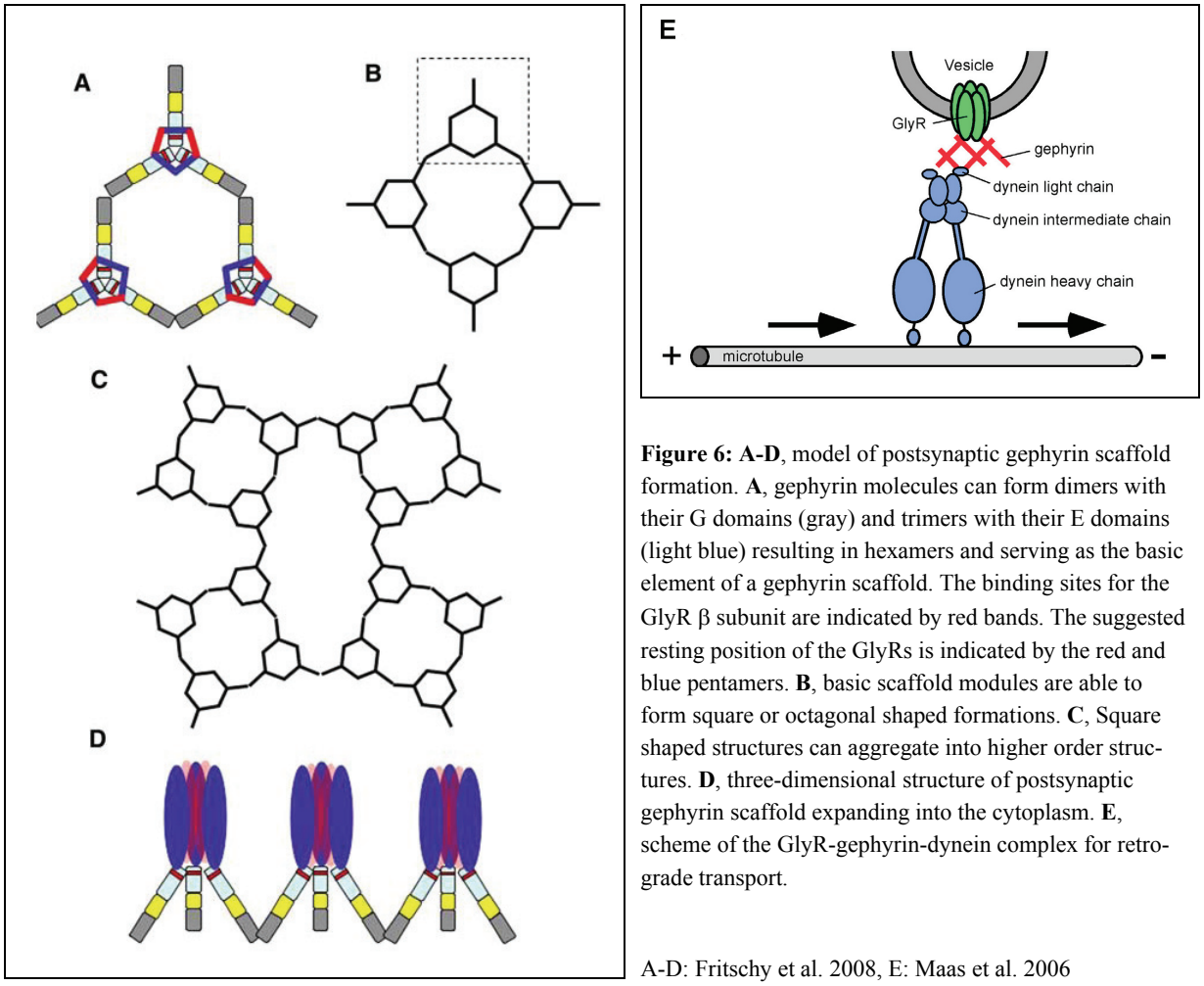

Figure 6: A-D, model of postsynaptic gephyrin scaffold formation. **A**, gephyrin molecules can form dimers with their G domains (gray) and trimers with their E domains (light blue) resulting in hexamers and serving as the basic element of a gephyrin scaffold. The binding sites for the GlyR β subunit are indicated by red bands. The suggested resting position of the GlyRs is indicated by the red and blue pentamers. **B**, basic scaffold modules are able to form square or octagonal shaped formations. **C**, Square shaped structures can aggregate into higher order structures. **D**, three-dimensional structure of postsynaptic gephyrin scaffold expanding into the cytoplasm. **E**, scheme of the GlyR-gephyrin-dynein complex for retrograde transport.

A-D: Fritschy et al. 2008, E: Maas et al. 2006

1.2.3. The GlyR subunit switch

In the fetal rat, predominantly α2 homomers are expressed (Becker et al. 1988, Malosio et al. 1991, Watanabe and Akagi 1995). However, the number of homomeric α2 GlyRs decreases strongly between birth and postnatal week three, while expression of α1 and β subunits increases over the same period. Thus, in the rat, a developmental switch from α2 homomeric GlyRs to α1β heteromeric GlyRs

takes place during the mentioned time period (Figure 7). If actually existent, homomeric α1 or α3 GlyRs are probably located extrasynaptically because they fail to bind gephyrin. Because α1 exhibits the highest expression level of all α subunits in the adult rat (Becker et al. 1988, Malosio et al.1991), it is believed that most glycinergic synapses in the adult rat are mediated by α1β GlyRs. Since α2 subunit mRNA and protein expression levels dramatically are reduced in early postnatal stages, synapses holding α2β GlyRs are probable to be seldom in adulthood. However, a relevant number of glycinergic synapses in the inner plexiform layer of the adult mouse retina displays co-localization of immunoreactivity for the α2 subunit and gephyrin (Haverkamp et al. 2004). Hence, α2 subunits are possibly localized at synapses. Indeed, Veruki recently demonstrated functional evidence for α2β-mediated synapses on wide-field amacrine cells in the adult rat retina (Veruki et al. 2007). Since α2 knockout mice lack obvious neurological and visible defects it seems likely that the properties of α2-containing GlyRs are not essential for normal central nervous system function and that the required procedures are replaced appropriately. Obviously, activation of the GlyRs themselves is not required for the mechanism triggering the developmental switch.

The developmental alteration from depolarizing to hyperpolarizing is believed to happen at the same time as the GlyRa2 subunit is exchanged by the adult α1 and α3 subunits. Nevertheless, no complete GlyRa2 down regulation is shown in retina, auditory brainstem and hippocampus (Piechotta et al. 2001). The hetero-oligomeric 2α1/3β GlyR is characterized by a single channel conductance of about 50 pS and low sensitivity to picrotoxin and β-carboline whereas homo-oligomeric α2 receptors exhibit a larger channel conductivity (85 pS) and slower kinetics. Homomeric α GlyRs are also potentially inhibited by picrotoxin. Hetero-oligomeric α2β receptors, in contrast, develop a channel conductivity of 48 pS. The open time of native GlyR channels in spinal cord slices decreases from 40 ms (E20) to 6 ms (P22, Takahashi et al. 1992). This confirms Beckers and van Zunderts data that the α2 subunit is replaced by the α1 subunit during development (Becker et al. 1988, van Zundert et al. 2004, Figure 7). Hence, synapses of immature spinal neurons probably contain α2β hetero-oligomers.

A brief glycine application onto an in vitro E15 rat spinal cord causes an excitatory response being abolished by strychnine (Vinay and Jean-Xavier 2008). Development therefore is beside the subunit switch marked by a decline in $[Cl^-]_i$ resulting in a shift of E_{Cl} toward negative potentials and hence from depolarization to hyperpolarization. The reversal potential of IPSPs (E_{IPSP}) shifts from above (~ -69 mV) to below (~ -74 mV) the resting membrane potential, which holds about -72 mV during the first postnatal week.

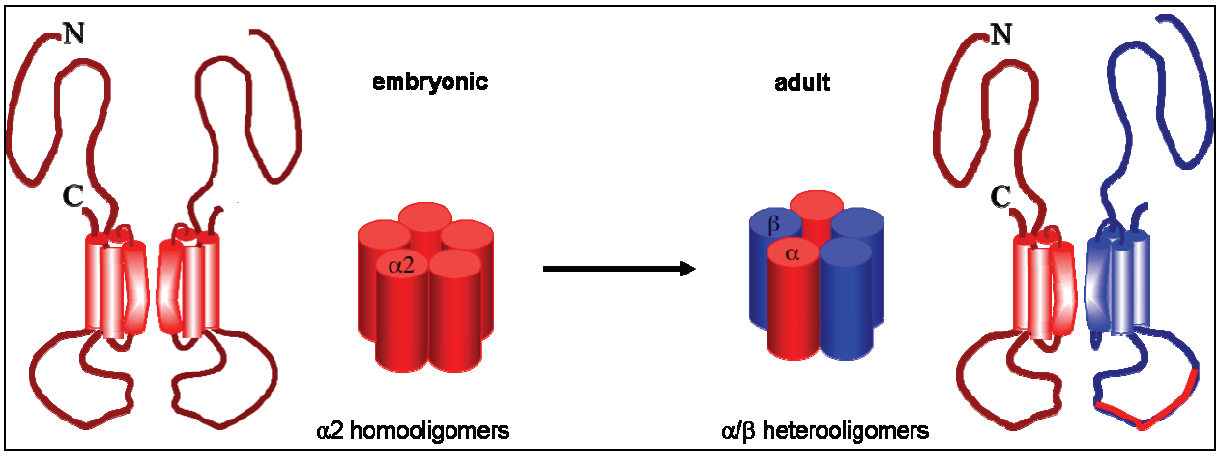

Figure 7: GlyR subunit composition.
The red barrels represent the α subunit, the blue barrels represent the β subunit of the GlyR. Shown is the alteration of the GlyR composition during maturation. Adapted from J. Kirsch

1.2.4. Splice variants of the GlyR genes

Different splice variants are yet identified. One of them is $\alpha1^{ins}$, a rat α1 splice variant characterized by an insertion of eight amino acids within the large intracellular loop (between TM3 and TM4) owning a potential phosphorylation site (Malosio et al. 1991b). The rat GlyR α2 subunit exhibits two splice variants namely α2A and α2B (Kuhse et al. 1991). α2A and α2B differ from each other by V58 and T59 substitutions in α2B. An additional form of the α2 subunit is α2* which includes the single G167E substitution giving rise to strychnine insensitivity. Alternative splicing of the human α3 subunit also creates two variants termed α3K and α3L (Nikolic et al. 1998). α3K misses a 15-amino acid section in the large intracellular loop. A zebrafish splice variant of GlyR α4 possesses a 15-amino acid insert within the ligand-binding domain (Devignot et al. 2003). All GlyR genes share a similar exon-intron organization. Thereby, the coding region is distributed over nine exons. This indicates phylogenetic gene duplications.

1.2.5. Disease

Since α1β GlyRs most likely mediate the main part of the glycinergic transmission in spinal cord, brainstem and retina, knockdown or knockout of either subunit may direct intense and similar neurological effects. Indeed reduced expression of either gene causes a hyperplexia phenotype. Mice and humans concerned by such a defect exhibit excessive startle reflexes to unexpected stimuli and often additional temporary muscular rigidity, which frequently causes an unprotected fall. The human hyperplexia or startle disease is hereditary. Characteristic for this disease is the augmented sensitivity to the startle response by emotional exertion, nervousness and exhaustion. The described falls result in typical chronic injuries. The symptoms are present from birth on. Because of either disruption of GlyR surface expression or of reduced ability to conduct chloride ions, the efficiency of glycinergic trans-

mission in reflex circuits of the spinal cord and brain stem is affected. Thereby the general level of motor neuron excitability is elevated.

The human GlyR α1 gene, which is responsible for the described disorder, is localized at the distal part of chromosome 5q (Ryan et al. 1992). R271L or R271Q substitutions in the human GlyR α1 gene give rise to the most common autosomal dominant form of the startle disease (Shiang et al. 1993). There are also several autosomal recessive forms of the disease, e.g. deletion of one base pair leading to a frame shift and thereby to a stop codon prior to the TM1 domain. In the β subunit, compound heterozygous mutations have been identified. The missense mutation G229D and a splice site mutation resulting in a cutting-out of exon 5 appear simultaneously. The G229D mutation alone directs a moderate (4-fold) decline of the glycine sensitivity of recombinant α1β GlyRs, whereas the excision of exon 5 would probably exclude the expression of functional β subunits. No startle mutations have been found until now in the α2 and α3 gene. Likewise, it has not been determined whether up regulation of these subunits compensates α1 subunit expression deficits. The startle disease is medicated by clonazepam likely to potentiate the $GABA_AR$. Indeed GABAergic neurotransmission in the spinal cord may be up regulated during development in spastic mice and myoclonic cattle to compensate the loss of glycinergic transmission (Graham et al. 2003, Lummis et al. 1990). A hereditary mutation in the GlyR binding partner gephyrin gene also gives rise to a hyperplexia phenotype in humans (Rees et al. 2003). In mice, targeted deletion of the GlyT2 gene leads to this phenotype (Gomeza et al. 2003).

Mice also are shown to develop startle syndromes. The symptoms of the three naturally occurring hyperplexias resemble those of humans. In contrast to humans, the startle symptoms appear not until P20, when the developmental subunit switch is supposed to be completed. Thereby, the so-called *spastic* mouse, that already was identified in the 1960s, (Meier and Chai 1970) is best described. The function of expressed receptors is normal, but the number of GlyR α1 subunits is diminished in this autosomal recessive disorder. Aberrant splicing of the GlyR β subunit gene caused by an insertion within intron 5 produces an accumulation of unfinished protein and hence reduced surface expression of functional β subunits (Mulhardt et al. 1994). Probably the loss of the β subunit anchoring function impairs efficient recruitment of receptors to the membrane or rather postsynaptic sites. Electrophysiological measurements reveal significantly reduced dimensions of glycinergic IPSPs in motor and sensory neurons compared to wild type (Graham et al. 2003).

In *spasmodic* mice, the α1 subunit carries the point mutation A52S leading to a modest 6-fold reduction in glycine sensitivity (Ryan et al. 1994).

Homozygous mice suffering from the *oscillator* variant of the *spasmodic* form, die of a strong motor tremor three weeks after birth (Kling et al 1997). Caused by a frameshift mutation in the TM3-TM4 domain the translation of the α1 subunit rests incomplete. Predicted not to possess the α1β heteromers mediating glycinergic transmission at P20, *oscillator* mice indeed exhibit a 90%-reduction in strychnine binding in isolated membranes of the spinal cord. This suggests a loss of functional α1 subunit expression (Buckwalter et al. 1994). However, the dimension of strychnine-sensitive

synaptic currents was only reduced by 50% in dorsal horn sensory neurons of homozygous mice (Graham et al. 2003). The examination of this phenomenon and discovering of compensating mechanisms would be of great interest.

1.3. Cation-chloride cotransporters (CCCs)

1.3.1. Isoforms and splice variants

Beside ion channels, also ion transporters mediate ion trafficking across biological membranes. Therefore, ion transporters are as important in generating electrical signals as ion channels.

In mammals, nine members of the CCC family, encoded by the genes Slc12a 1-9, are currently known (Blasse et al. 2009). According to their function, three categories have been determined: two members belong to the loop diuretic-sensitive Na-K-2Cl cotransporters (NKCCs) represented by the two isoforms NKCC1 and NKCC2. One is a thiazide-sensitive Na-Cl cotransporter (NCC) and four isoforms display K-Cl cotransporters (KCC1-4). The remaining CCCs (Slc12a8 and Slc12a9 or CIP and CCC9 respectively) are physiologically not sufficient characterized. NKCC1 is expressed in non-epithelial cells and in basolateral membrane of epithelial cells whereas NKCC2 as apical form only is expressed in the thick ascending limb of the Henle's loop in kidney. The other apical isoform NCC is exclusively present in the distal convoluted tubule of the kidney (Figure 8A). KCC1 seems to work as a "household" isoform in glial and other cell types but not in neurons. KCC2, in contrast, is exclusively present in CNS neurons (Blaesse et al. 2009). KCC3 is expressed in diverse brain regions, muscle, lung, heart and also kidney and exhibits a developmental increase in protein expression similar to that of KCC2. KCC4 is strongly expressed in muscle, pancreas and the embryonic brain (Figure 8A) but its role in the nervous system still is unknown.

The CCCs possess a relative small intracellular N-terminus, adjacent 12 α-helical transmembrane domains and a large intracellular C-terminus (about half of the protein, Figure 8B). From TM5 to TM6, a large extracellular loop comprising a couple of consensus N-linked glycosylation sites ranges in KCCs and CCC8. The same appears between TM7 and TM8 in NKCC1, NKCC2 and NCC. All members are glycoproteins with molecular weights in the range of 120-200 kDa (Payne et al. 2003).

Relating to alternative splicing, variants are known for KCC1, KCC2, KCC3, NKCC1 and NKCC2. KCC3a is exclusively expressed in glial cells, KCC3b is found in organs outside the CNS and KCC3c is restricted to neurons. The NKCC1 gene offers two variants: NKCC1a and NKCC1b both being expressed ubiquitously. NKCC2 even offers six alternative isoforms differing in function. Of KCC2 (Slc12a5), two isoforms named KCC2a and KCC2b, differing in promoters and first exons, are currently known. Interestingly, the mRNA expression of both isoforms is similar in the neonatal mouse but postnatally, the overall expression of KCC2a remains constant and that of KCC2b is excessively up regulated. This suggests KCC2b to be responsible for the yet mentioned developmental shift

of the intracellular chloride level. Indeed GABAergic responses remain depolarizing in cortical cultures from KCC2b knockout mice (Zhu et al. 2005). These mice are viable but exhibit abnormal posture and movement as well as numerous seizures within a few postnatal days. They die about 2 weeks after birth. Mice missing KCC2 expression completely die instantly after birth of respiratory failure (Hübner et al. 2001).

In tissue, CCC homo-oligomers have been detected whereas exogenously expressed CCCs are also able to form hetero-oligomers.

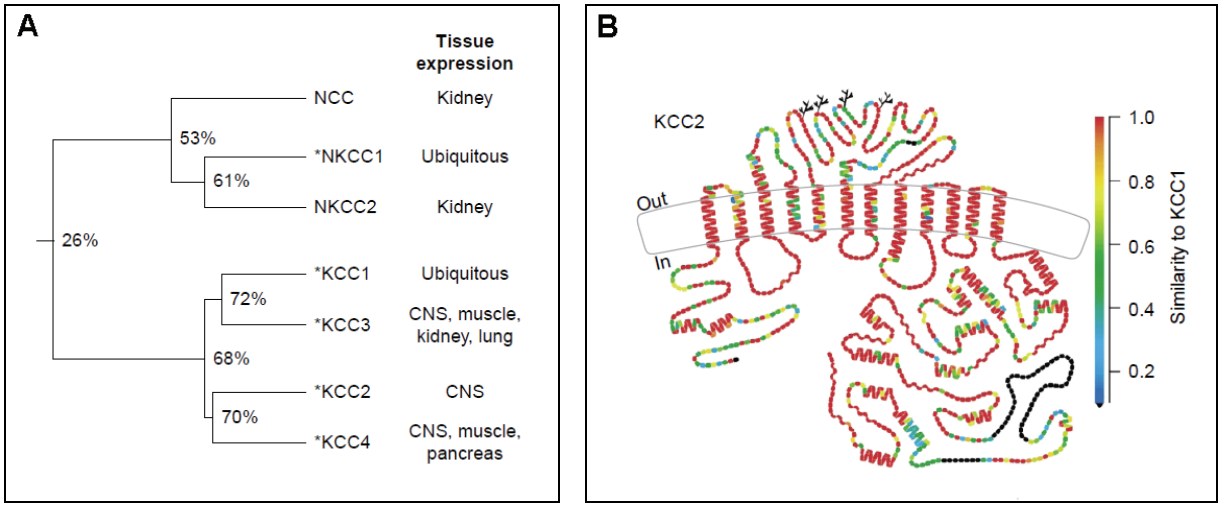

Figure 8: Phylogenetic tree of human cation–chloride cotransporters (CCCs) and structure of the K^+–Cl^- cotransporter 2 (KCC2). **A**, The percentage of identical residues between aligned protein sequences is shown at branch points. Human protein sequences were aligned and the phylogenetic tree constructed using CLUSTALW. The predominant tissue expression is listed for each CCC and those identified in nervous tissue are indicated by asterisks. **B**, Model of the KCC2 protein and similarity to KCC1. Putative transmembrane segments were predicted based on hydropathy analysis using the Kyte–Doolittle algorithm. Secondary structural elements were predicted using the PHD server (helices represent α structures; wavy lines represent β structures). Rat KCC2 and rabbit KCC1 are compared with one another: red residues are identical between KCC2 and KCC1; black residues are absent from KCC1. Potential asparagine-linked glycosylation sites between putative transmembrane segments 5 and 6 are indicated with branched lines. Payne et al. 2003

1.3.2. Function and regulation

The potassium-chloride co-transport is the electroneutral-coupled movement of K^+ and Cl^- ions without changing the net charge across the membrane. All potassium-chloride cotransporters are secondary active transporters getting the energy for the transport of the driven ion from the electrochemical gradient of another ion species. This gradient is established by the work of the Na^+/K^+-ATPase. In addition, other secondary active transporters like Na^+-dependent and Na^+-independent anion exchangers (NDAE and AE respectively) can take part in the neuronal Cl^- homeostasis by exchanging Cl^- for HCO_3^-. As being electroneutral, they can work bi-directional and thus are able to conduct net ion influx or efflux depending on the concentration gradients of the transported ions (Gamba et al. 1994).

In most neurons, chloride accumulation within the cell is mediated by NKCC1 utilizing plasmalemmal Na^+ gradients as energy source for Na-K-2Cl co-transport. Expulsion of chloride in contrast

is offered by the K^+-gradient. In nervous tissue, KCC2 and NKCC1 seem to be the essential players in maintaining Cl^- balance.

NKCC1 and KCC2 are regulated by different kinases modulating their activity. Nevertheless, their role for regulating the intracellular chloride level seems to be dependent on gene expression.

The ubiquitously present potassium-chloride co-transport regulates cell homeostasis namely constancy of cell volume and chemical composition of intracellular compartments. Many studies demonstrated that K-Cl co-transport is among others activated by cell swelling and in turn regulates the cell volume (regulatory volume decrease or RVD, Adragna et al. 2004) in non-neuronal cells. Cell swelling in non-neuronal cells is evoked by hypotonia and thus water influx whereas in neurons intense synaptic activity and thereby channel-mediated cation- and chloride-influx induce water inflow. The recovery in neurons can be mediated by a volume sensor, being able to activate the K-Cl co-transport or/and an augmented driving force for the transport caused by an increased Cl^--level inside the cell. KCC3 knockout mice show impaired cell volume recovery in cortical neurons after hypotonic swelling suggesting a role of KCC3 in neuronal volume regulation (Boettger et al. 2003).

Recently, it was shown that the K-Cl cotransporter is critical for controlling the electrochemical Cl^--gradient being required for the hyperpolarization mediated by $GABA_A$Rs and GlyRs (Figure 9). The depolarization evoked by GABA in early development induces Ca^{2+}-influx via NMDARs as well as voltage-dependent Ca^{2+}-channels (Figure 9). The latter leads to significant neurodevelopmental consequences in proliferation and migration of neurons and neural precursors (Mercado et al. 2004).

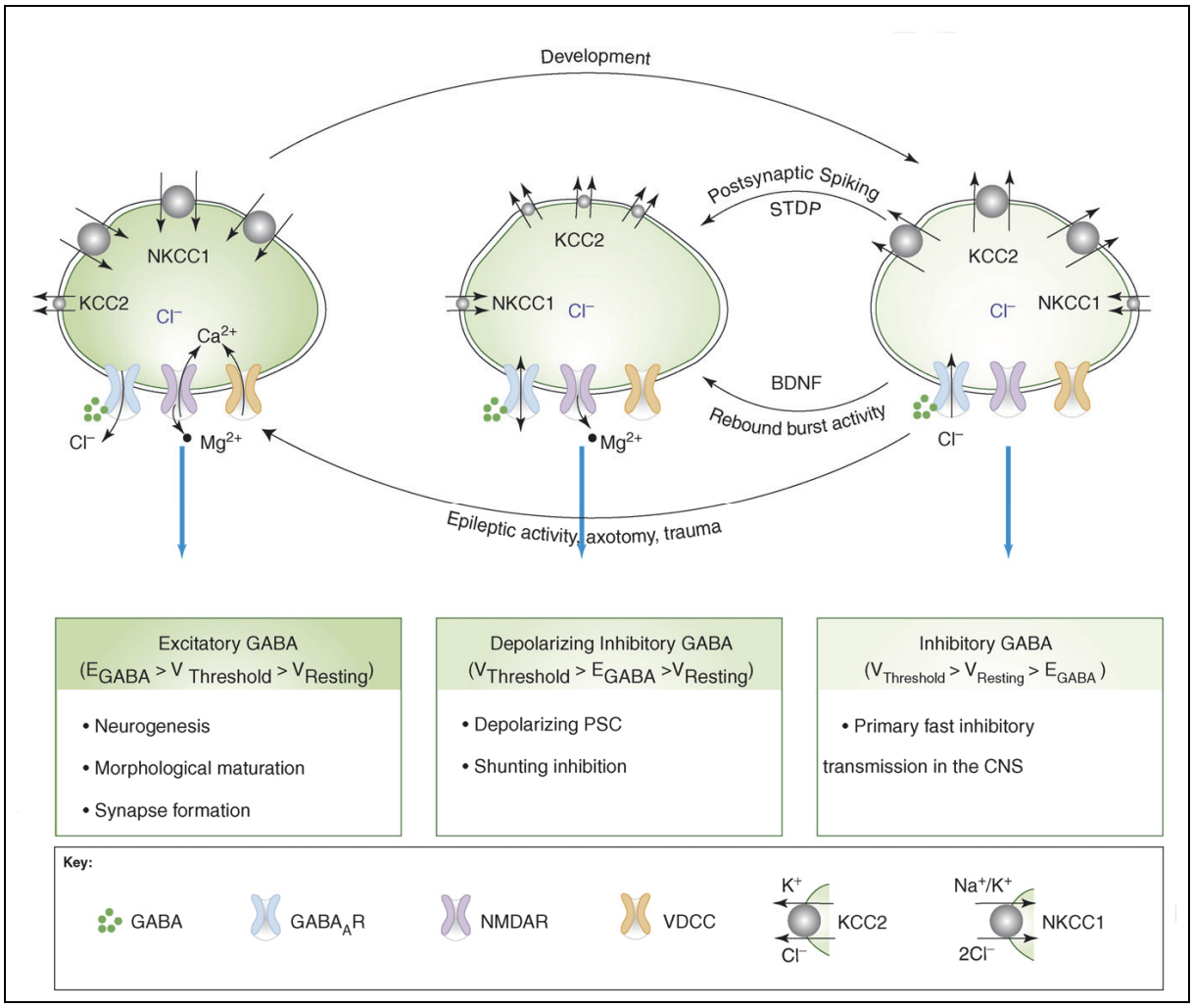

Figure 9: Ion-Transport mechanisms underlying $GABA_AR$- (and not shown GlyR) mediated responses in immature and mature neurons. Left: early in development NKCC1 mediates Cl^--uptake in immature hippocampal and cortical neurons maintaining high $[Cl^-]_i$. Binding of GABA to its receptor directs Cl^--efflux and induces excitation which in turn removes the Mg^{2+}-block from the NMDAR and permits Ca^{2+}-influx through voltage-gated Ca^{2+}-channels (VDCCs) and NMDARs (in presence of glutamate). Right: in mature CNS neurons, KCC2 is the principal K-Cl cotransporter producing low chloride levels within the cell. Upon $GABA_AR$ activation, inhibition occurs, VDCCs are failed to be opened and Mg^{2+} is not removed from NMDARs. Following epileptic activity, axotomy or neuronal trauma, the Cl^- homeostasis is reversed resulting in excitatory responses to GABA (arrow to the left). Middle: in response to more physiological levels of activity (e.g. postsynaptic spiking and rebound burst activity), or in the presence of neurotrophic factors, a decrease in the Cl^--extruding capacity of KCC2 leads to a positive shift in E_{GABA}. Depending on the extent of Cl^- accumulation in the neuron, GABAergic neurotransmission might activate VDCCs and remove the Mg^{2+} block from the NMDAR. The positive shift in E_{GABA} might result in a depolarizing postsynaptic current that does not reach the threshold for generating an action potential and still exerts an inhibitory effect by shunting excitatory current. Fiumelli and Woodin 2007

1.3.3. Pharmacology

The site responsible for Na^+ transport is also able to accept Li^+ whereas the K^+ accepting site also takes Rb^+, NH_4^+ or Cs^+ but with different affinities. In terms of anions, only Br^- can be transported in part by NKCC1 and KCC instead of Cl^-. The 'loop' diuretic furosemide has an equal potency to inhibit both NKCC1 and KCC. Another member of the mentioned diuretics, bumetanide, has a 500fold greater affinity for NKCC1 and therefore is able to inhibit NKCC1 significantly in low concentrations without concerning KCC.

1.3.4. The potassium-chloride cotransporter KCC2

As an electroneutral ion transporter located in the membrane, KCC2 expels chloride from the cell by utilizing the outwardly directed driving force of K^+ and thus is not dependent on the membrane potential. Thereby, KCC2 maintains the intracellular Cl^--level lower than predicted by the electrochemical equilibrium. The transport is therefore determined by the sum of the chemical potential differences of K^+ and Cl^- (Vinay and Jean-Xavier 2008). Since the intracellular chloride level is low in many neurons (7-9 mM), the driving-force for the K-Cl transport is nearby the thermodynamic equilibrium. Therefore, KCC2 possesses the sensitivity to recognize minimal changes in $[Cl^-]_i$ or $[K^+]_o$. In a neuron with relative low intracellular chloride, a 5 mM increase in $[K^+]_o$ is sufficient to reverse the driving-force.

1.3.4.1. KCC2 expression and localization

KCC2 expression is closely restricted to central neurons. Its mRNA expression is opulent in most neurons of the mature CNS but marginally in non-neuronal cells or neuronal precursor cells. KCC2 is found in cerebellar granule cells, thalamic relay cells, auditory brainstem neurons and cortical neurons (Blaesse et al. 2009). According to the preferred localization of glutamatergic synapses to spines and GABAergic ones to dendritic shafts and somata, it might be inspiring that also high levels of KCC2 are shown to be present in dendritic spines of rat cortical pyramidal neurons and interneurons (Gulyas et al. 2001). However Li et al. recently demonstrated a morphogenic role for KCC2 in spine formation (Li et al. 2007). In immature neurons of the auditory brainstem and of primary cortical cultures, functionally inactive KCC2 has been found.

In altricial species such as rats, KCC2 expression at birth is delayed in hippocampus and neocortex compared to species with precocious neonates. Within a single species, high expression levels of KCC2 are first seen in the spinal cord and subcortical brain regions (Blaesse et al. 2006). In the ventral rostral spinal cord of rodents, KCC2 mRNA already is expressed at E12.5 (Hübner et al. 2001, Li et al. 2002). Its protein level rises until P3-7.

1.3.4.2. KCC2 function and interaction partners

Early in development, NKCC1 activity leads to accumulation and maintenance of intracellular Cl^- resulting in depolarizing and hence excitatory GABAergic transmission. During the first neonatal weeks, KCC2 is up regulated and starts Cl^- extrusion. This process is accompanied by a negative shift of the reversal potential for chloride beyond the resting membrane potential. Thus, GABAergic transmission switches from excitatory to inhibitory (Fiumelli and Woodin, 2007). Subsequently, KCC2 is responsible for maintaining the low Cl^- concentration in mature neurons (Rivera et al. 1999, Hubner et al. 2001).

The number of GABAergic synapses and the frequency of GABAergic mIPSCs were elevated in early hippocampal cultures upon KCC2 overexpression (Chudotvorova et al. 2005). Fitting to that, the mIPSC frequency in mice with reduced KCC2 levels is lower. As already mentioned, Li et al. show that KCC2 owns a morphogenic role in cortical spine formation during development. Neurons achieved from $KCC2^{-/-}$ mice exhibit high motile and branched long dendritic protrusions (5 µm) representing morphological aberrant "filopodia-like" spines (Li et al. 2007). Transfecting these neurons with an N-terminal deletion construct, not being able to mediate transport, could rescue that phenotype. Therefore, the role of KCC2 in spine maturation might be based on cytoskeletal interactions and not on its transport activity. Via immunoprecipitation assays, the cytoskeletal 4.1N protein was shown to interact with the KCC2 C-terminal domain (Li et al. 2007). 4.1N is highly expressed in the postsynaptic density and is thought to own an anchoring and targeting function for glutamate receptor subunits.

Ca^{2+}-dependent down regulation of KCC2 activity can be achieved within minutes via postsynaptic spiking (10 Hz for 5 min). Consistent with that is an alteration in membrane trafficking and/or post-translational modifications of KCC2 and not in gene transcription or protein synthesis, which would last longer.

Uvarov et al. demonstrated that the KCC2 gene possesses ten putative transcription factor binding sites within its core promoter. EGR4 is shown to bind to one of these sites and it furthermore induces KCC2 transcription in neurons (Uvarov et al. 2006).

Besides its function in both, regulating neuronal activity and activity-dependent synaptic plasticity, such as inducing and maintaining hippocampal long-term potentiation, BDNF also is thought to regulate GABAergic transmission and plasticity via coordinating KCC2 expression. During development, overexpression of BDNF induces augmented KCC2 expression in the prenatal hippocampus, giving rise to an increase of the onset of spontaneous correlated network activity. Mice lacking the BDNF receptor TrKB, in contrast, exhibit diminished KCC2 expression and lower intrinsic activity in pyramidal neurons as neonates (Fiumelli and Woodin 2007). P8-19 TrKB knockout mice also show reduced KCC2 mRNA levels compared to wild-type littermates. Nevertheless, the mRNA levels are high enough to maintain the switch from excitation to inhibition. Therefore, BDNF is believed to contribute to the developmental up regulation of KCC2. Premature KCC2 expression in neurons alters GABA transmission from excitation to inhibition thereby preventing GABA-induced increase in $[Ca^{2+}]_i$ (Fiumelli and Woodin 2007).

In adult networks, KCC2 expression is reduced upon neuronal damage and hyperexcitation. Thereby transcription and synthesis of KCC2 is decreased via a BDNF-TrKB pathway. Acute application of BDNF to HCN cultures even directs a depolarization of E_{GABA} together with a fast down regulation of KCC2 activity. This might be possible due to a quick turnover of the KCC2 pool provided in the membrane.

CIP1 has been demonstrated to interact with NKCC1 and to inhibit its transport activity (Caron et al. 2000). Regarding the amino acid sequence, CIP1 shares 25% identity with both NKCC1 and KCC2 but in terms of topology it is closer to KCC2 (Caron et al. 2000). Therefore, it is predicted to interact with KCC2 as well. Indeed, CIP1 itself is transport-inactive (Wenz et al. 2009) but expressed together with KCC2 in HEK cells, the transport activity of KCC2 is enhanced significantly (Wenz et al. 2009). The effect is believed to be achieved by formation of KCC2/CIP hetero-oligomers. Thus, CIP1 has a reciprocal effect on KCC2 and NKCC1 respectively. So does the protein phosphatase PP1, which activates KCCs and deactivates NKCC1 (Adragna et al. 2004). In contrast, the kinases WNK3 or SPAK together with WNK4 activate NKCC1 but inactivate KCC2 activity in Xenopus laevis oocytes (Gagnon et al. 2006).

1.3.4.3. Disease

In accordance to the increase in KCC2 expression during development, nociceptive withdrawal reflexes are low right after birth and grow with age (Price at al. 2005).

No or few KCC2 protein leads to a depolarizing (excitatory) action of GABA and glycine in the mammalian spinal cord. Beside early development, the same can be observed in a number of pathological conditions, such as epilepsy, neuronal injury and chronic pain. In cortical neurons missing KCC2 expression, no developmental reduction of intracellular chloride occurs (Zhu et al., 2005). KCC2 knockout mice are signed by serious motor defects and are unable to breathe resulting in suffocation shortly after birth. 'Hypomorphic' KCC2 gene-targeted mice, containing 20-30% of normal KCC2 levels, are viable and exhibit no obvious behaviour abnormalities. Mice with only 5–10% of KCC2 in contrast show spontaneous, generalized seizures and die shortly after birth.

Jean-Xavier et al. investigated effects of spinal cord injury by transection and concomitant removal of all descending inputs to the lumbar enlargement. E_{IPSP} in lumbar motoneurons at P4-7 was significantly higher depolarized (above resting potential) in cord-transected than in control animals (below resting potential, Jean-Xavier et al. 2006) and therefore was similar to P0-2control animals. The increase in KCC2 immunoreactivity in lumbar motoneurons occurring during the first postnatal week in control animals was absent due to spinal cord transection. Motoneurons recorded from treated animals were less sensitive to different manipulations as $[K^+]_o$-modifications or application of bumetanide to block CCCs. These results indicate that pathways, descending from brainstem, play a fundamental role in the maturation of inhibitory synaptic transmission by augmenting KCC2 expression in development.

GABA- and glycinergic transmission can rapidly switch from inhibition to excitation in a couple of regions of the CNS caused by pathological conditions. Upon epileptiform activity, neuronal damage and peripheral nerve-induced chronic pain, KCC2 expression in adult rat neurons is reduced (Vinay and Jean-Xavier 2008). This and the concomitant $[Cl^-]_i$ increases may represent an first response to neuronal trauma (Figure 10). Recapitulating early developmental stages, GABA and glycine evoke a

depolarization of injured neurons. Hence, Ca^{2+}-channels are activated and Mg^{2+}-blocks are removed from NMDARs (Figure 9). These procedures may direct Ca^{2+}-dependent excitotoxicity. Upon adult spinal cord injury (SCI), BDNF, being able to down regulate KCC2 expression via TrKB receptor, is up regulated within a short time window of 6-24 hrs after SCI. This might rapidly diminish KCC2 expression. The long term down regulation of KCC2 destabilizes synaptic contacts to motoneurons analogue to the decrease of inhibitory reflex mechanisms after SCI. Interestingly, BDNF is down regulated in the lumbar cord seven and fifteen days after SCI compared to control animals.

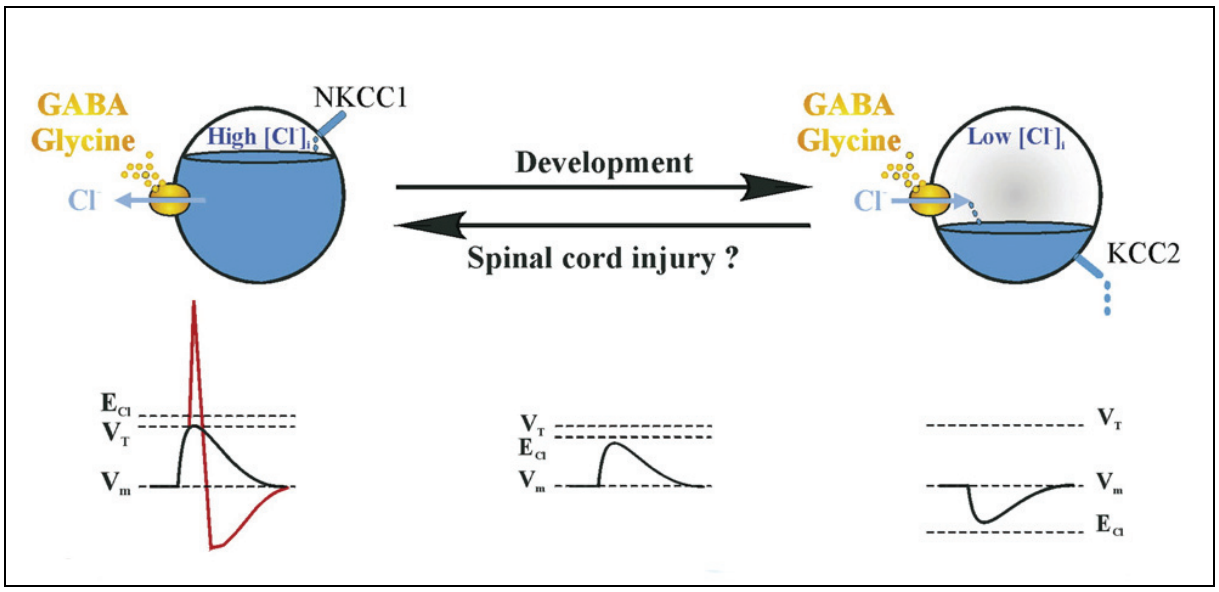

Figure 10: Hypothetical relationship between cation-chloride cotransporters and spinal cord injury. CCCs are responsible for the regulation of $[Cl^-]_i$. In immature neurons, $[Cl^-]_i$ is high and the equilibrium potential of chloride (E_{Cl}) is above the resting membrane potential (V_m). Activation of $GABA_A$Rs and GlyRs may even trigger cell firing, when E_{Cl} is above action potential threshold (V_T). Consequently, "inhibitory" interneurons, within the spinal locomotor network, may have a physiological role similar to that of excitatory interneurons. NKCC1 is responsible for intracellular Cl^- accumulation. $[Cl^-]_i$ decreases with age upon up-regulation of KCC2; E_{Cl} shifts to values below V_m. As a result, the strength of inhibitory connections increases.Vii

2. Aim of study

The aim of this study was to get deeper insights in the still unknown process of the developmental switch occurring in spinal neurons. During this process, the GlyR assembly is altered and the juvenile GlyRa2 subunit recedes for the benefit of the adult GlyRa1 subunit. Therefore, expression profiles of the distinct subunits should be performed *in vitro*. To address the question whether the activity of the GlyR contributes to the switch, strychnine treatments are intended. Since KCC2 plays a major role in reversing the chloride level within the neurons during the critical time window and therefore being crucial for the switch, its expression profile also has to be determined. The role of KCC2 is further investigated utilizing RNAi technology.

The expression profiles for the GlyR subunits and KCC2 of embryonic rat spinal neurons were obtained via RT-PCR as well as RTq-PCR. The latter allows a semi-quantitative determination of mRNA expression in the cells. Furthermore, protein levels were determined if possible. The experimental approach was to culture the cells for a certain number of days, take protein and RNA extracts followed by immunoblot or RT-PCR analysis. By means of these studies, an approximate time window of the subunit switch to occur could be established.

Towards the observation that GlyR blockade might negatively regulate KCC2 protein expression, distinct treatments were carried out to specialize the effects. SN cultures were treated with given concentrations of Ca^{2+} channel inhibitors, Ca^{2+} chelators and other receptor blockers, protein extracts were prepared and the results were obtained by immunoblot analysis. These experiments should shed light on the question whether Ca^{2+}-influx or presence is involved in regulating KCC2 expression.

To address the upcoming question whether KCC2 contributes to the developmental switch of the GlyR subunits, shRNA oligos silencing KCC2 expression were designed, cloned into lentiviral vectors and transduced to the neurons. Uninfected cells or cells transduced by mismatch shRNA oligos without the ability to induce KCC2 knockdown acted as controls. The neurons were cultured, infected by the lentivirus and incubated for 4-32 days. Then cells were either lysed, protein extracts were taken and immunoblots were prepared, or cells were fixed and immunohistochemistry against different synaptic proteins was performed. Therewith, effects of KCC2 knockdown onto the different GlyR subunits, gephyrin and some other synaptic proteins should be clarified.

3. Material and Methods

3.1. Material

3.1.1. Chemicals

AppliChem	DTT
	EDTA
	Glycerol
	Glycine
	Na_2HPO_4* 2 H_2O
	NaH_2PO_4* H_2O
BD	Bacto Trypton
BioRad	Acrylamide/Bisacrylamide 30 % (w/v)
Braun	Aqua ad injectabilia
Finnzymes	Phusion® High-Fidelity DNA Polymerase
	5x Phusion HF Buffer
Fluka	NP-40
Grüssing	Di-Sodiumtetraborate* 10 H_2O
Invitrogen	Kanamycine
	Select Agar
	Agarose (electrophoresis grade)
	DMEM
	D-PBS
	FCS
	HBSS
	L-Glutamine, 100x
	Neurobasal
	Optimem
	Pen/Strep, 100x
	Horse serum
	Trypsin
	Trypsin/EDTA
	Cell culture water
	Zeocin, 2000x
J.T. Baker	Boric acid
Merck	Ethanol
	Isopropanol
	Methanol
	Triton X-100
PAA Laboratories	BSA

PAN Biotech GMBH	Neuropan 27 Supplement, 50x
Riedel de Haën	PFA
Roche Biochemicals	Protease-Inhibitors, tablets EDTA-free
Roth	Ampicillin
	APS
	Beta-Mercaptoethanol
	DABCO
	Ethidiumbromide
	Yeast extract
	Milk powder
	Mowiol 4.88
	TRIS
	Tween-20
Serva	SDS
Sigma-Aldrich	Bromphenol Blau
	DOC
	Poly-DL-Ornithine
	Poly-L-Lysine
	TEMED
	Trypan Blue
	PEI
VWR	Sodiumchloride

3.1.2. Equipment

AGFA Gewaert	Developing Machine Curix 60
Amersham Bioscience	Spectrophotometer UltroSpec 3100 pro UV/Visible
Applied Biosystems	ABI Prism sequence detection system
Astacus	Water Preparation Membra Pure
Beckman Coulter	Ultracentrifuge (Optima LE-80K)
	Ultracentrifuge rotor SW32Ti
	Avanti J-25 Centrifuge
Bender und Hobein AG	Vortex Genie 2 G-560E
BioRad	Trans-Blot SD cell
	GS-800 Calibrated Densitometer
	PCR Machine
	Power Supply PowerPac 200
	Mini protean III Gel System
CAT	Rocker ST5
Eppendorf	Heating block
GFL	Water Bath Type 1008
Heidolph	Magnet stir MR 2002

Heraeus Instruments	Shaking Incubator
	Oven
Herolab	Gel Documentation System
Hettich	Micro 200R table-top centrifuge
	Table centrifuge
Hirschmann	Pipet aid
	Glass Pipet (1 ml, 2 ml, 5 ml, 10 ml)
Holten	Sterile Workflow LaminAir Model 1.2
IBS Integra Bioscience	Autoclave
Kendro Laboratory Products GmbH	Sterile Workflow HERA safe
Kern und Sohn GmbH	Analytical Balance 440-33N
Leica	S6E Binocular
	KL 1500 LCD light source
Marienfeld	Neubauer counting chamber
Mettler Toledo	pH Meter
MS Laborgeräte	Incubator
Nuaire	CO_2 Incubator, water-jacketed
Supplier	Equipment
Visitron Systems	CCD Camera (SpotRT)
Zeiss	Objective Plan NeoFLUAR 40x/1.3 Oil
	Objective Plan Apochromat 63x/1.4 Oil
	Objective Plan FLUAR 100x/1.45 Oil
	Microscope Axiovert 200M
	Light Source FluoArc

3.1.3. Software

Adobe	Photoshop
	InDesign
	Acrobat
Applied Biosystems	ABI Prism 7000
Bio-Rad Laboratories	GeneX
	QuantityOne
Microsoft	Excel
	Word
	PowerPoint
Visitron Systems	Metamorph Software (Version 6.2r6)

3.1.4. Disposables

BD Falcon	Cell Strainer 100 µm
BD Microlance	Injection Needles (20 G, 21 G, 24 G)
BD Plastipak	Syringes (1 ml)
Beranek	Ultracentrifugation tubes (25 x 89 mm)
Corning Incorporated	Cell scraper
Falcon	Cell culture dishes (3,5 cm, 6-well, 24-well)
	Reaction tubes (15 ml, 50 ml)
GE Healthcare	Amersham Hyperfilm ECL
Greiner bio-one	Reaction tubes (0,5 ml, 1,5 ml, 2 ml)
	Petri dishes
	Pipet tips (10 µl, 20 µl, 200 µl, 1 ml)
	PET tubes (14 ml)
Hartmann	Gloves S, Peha-soft
Kisker	Quali-PCR-Plates
Marienfeld	Glass slides
	Cover slips (12 mm, 13 mm)
Millipore	Sterile filter 0,22 µm, 150 ml (Steritop-GP) 45 mm width
	PVDF-Membrane
	Syringe filter 0,45 µm
Nerbe plus	adhesive cover for RTq-PCR Plates
Pechiney	Parafilm
Sarstedt	Plastic cuvettes 1 ml
	Serological Pipets (5 ml, 10 ml, 25 ml)
Schleicher und Schuell	Whatman
Starlab	Pipet tips (10 µl, 20 µl, 200 µl, 1 ml)
VWR	Gloves S, Nitril
Zeiss	Immersol Immersionoil

3.1.5. Kits

Applied Biosystems	TaqMan Master Mix
	TaqMan Gene Expr. Assay Rn00592624_m1, inventoried (KCC2)
	TaqMan Gene Expr. Assay Rn00595017_m1, inventoried (Enolase)
	TaqMan Gene Expr. Assay Rn00565582_m1, inventoried (GlyRa1)
	TaqMan Gene Expr. Assay Rn01420724_m1, inventoried (GlyRa2)
	TaqMan Gene Expr. Assay Rn01638847_m1, inventoried (GlyRa3)
	TaqMan Gene Expr. Assay Rn00583966_m1, inventoried (GlyRb)
	TaqMan Gene Expr. Assay Rn99999916_s1, inventoried (GAPDH)
	TaqMan Gene Expr. Assay Rn00575867_m1, inventoried (gephyrin)
GE Healthcare	Amersham™ ECL™ Plus
Invitrogen	SuperScript® III First-Strand Synthesis System

Macherey-Nagel	NucleoBond® Xtra Midi/Maxi-Kit NucleoSpin® RNA II
Qiagen	QIAquick Gel Extraction Kit
Roche Applied Science	Rapid DNA Ligation Kit
Stratagene	QuikChange Site-Directed Mutagenesis Kit
Thermo Scientific	BCA Protein Assay

3.1.6. Buffers, Solutions, Culture Media

3.1.6.1. Cell Culture

Boric acid	150 mM H_3BO_3 in Milli-Q, pH8.3
DMEM^{+++}	10 % (v/v) FCS, 1 % (v/v) P/S, 0,5 % (v/v) Glutamine in NB
D-PBS/Glucose	5 % 20x Glucose in D-PBS
Glucose, 20x	12 % (w/v) Glucose (for cell culture) in cell culture water
MEF medium	10 % (v/v) FCS, 1 % (v/v) P/S in DMEM
NB^{+++}	0,25 % (v/v) Glutamine, 1 % (v/v) P/S, 2 % (v/v) Neuropan 27 in NB
NB^{++++}	1 % (v/v) Glutamine, 0,1 % (v/v) P/S, 2 % (v/v) Neuropan 27, 0.2 % (v/v) Holo-Transferrin in NB
o/n medium	10 % (v/v) FCS, 1 % (v/v) P/S in NB
Poly-Ornithine, 5x	500 mg/l in H_3BO_3

3.1.6.2. Molecular Biology

Annealing buffer	100mM Kaliumacetate, 30 mM HEPES (pH7.4), 2 mM Magnesium-acetate in autoclaved Milli-Q
DNA loading buffer, 10x	30 % (v/v) Glycerol, 0.1 % (w/v) OrangeG in autoclaved Milli-Q
Innou transformation buffer	55 mM $MnCl_2$* 4 H_2O, 15 mM $CaCl_2$* 2 H_2O, 250 mM KCl, 10 mM PIPES in Milli-Q
LB agar	1.5 % (w/v) Select-Agar in LB-Medium
LB medium	1 % (w/v) NaCl, 1 % (w/v) Bacto-Trypton, 0.5 % (w/v) yeast extract in Milli-Q
Lysis buffer P2	200 mM NaOH, 1 % (w/v) SDS in autoclaved Milli-Q
Neutralisation buffer P3	3 M KOAc, pH5.5 in Milli-Q
PIPES	0.5 M PIPES, pH6.7
Resuspension buffer P1	50 mM Tris-HCl pH8, 10 mM EDTA,10 % (w/v) RNase A
SOB-Medium	0.05 % (w/v) NaCl, 2 % (w/v) Bacto-Trypton, 0.5 % (w/v) yeast extract, 2.5 mM KCl (pH7) in Milli-Q; add 10 mM $MgCl_2$ before use
TAE, 50x	242 g/l Tris base, 37.2 g/l Na_2EDTA* 2 H_2O, 5.71 % (v/v) Acetic acid in Milli-Q

3.1.6.3. Immunohistochemistry

Blocking solution A	1 % (w/v) BSA, 5 % (v/v) Horse Serum, 0.5 % (v/v) Triton X-100 in 1xPBS
Blocking solution B	1 % (w/v) BSA, 5 % (v/v) Horse Serum in 1xPBS
PBS, 10x	137 mM NaCl, 2.7 mM KCl, 4.3 mM Na_2HPO_4* 2 H_2O, 1.4 mM KH_2PO_4 in Milli-Q, pH7.3

3.1.6.4. Biochemistry

Blocking buffer	5 % milk powder in TBS-T
Complete Solution	1 tablet in 2 ml of autoclaved Milli-Q
RIPA	50 mM Tris-HCl, 1 % (v/v) Triton X-100, 1 % (w/v) SDS, 150 mM NaCl, 1 mM EDTA, 1% (w/v) DOC, 4 % (v/v) Complete Solution in autoclaved Milli-Q
SDS running buffer, 10x	3.029 % (w/v) Tris-base, 14.413 % (w/v) Glycine, 1 % (w/v) SDS in Milli-Q
TBS, 10x	1.5 M NaCl, 1.18 % (w/v) Tris-base, 6.35 % (w/v) Tris-acid in Milli-Q
TBS-T	0.05 % (v/v) Tween-20 in 1xTBS
Transfer buffer (semi-dry blot)	25 mM Tris-HCl, 150 mM Glycine, 10 % (v/v) MeOH in Milli-Q
Transfer Buffer (tankblot)	0.381 % (w/v) $Na_2B_4O_7$*10 H_2O in Milli-Q
Urea sample buffer, 2x	8 M Urea, 20 mM DTT, 125 mM Tris-HCl, 5 % (w/v) SDS, 0.01 % (w/v) Bromphenolblue, 20 % (v/v) Glycerol in Milli-Q

3.1.7. Antibodies

3.1.7.1. Primary Antibodies

Antigen/Antibody	Species	Dilution IF/IB	[kDa]	Source
β-tubulin	ms	-/1:25.000	50	Sigma-Aldrich
408 (gephyrin AA 175-191)	rb	1:500/1:200	93	Nawrotzki (unpubl.)
GABAAR bd17, β-chain	ms	1:100/1:500	55	Chemicon, Fritschy et al. 1992
$GABA_A\gamma_2$	gpig	1:100/1:25	43	Fritschy and Mohler 1995
mAb2 (GlyRa1)	ms	1:100/1:100	48	Pfeiffer et al. 1984
mAb4 (all GlyRa subunits)	ms	1:100/1:100	48	Pfeiffer et al. 1984
mAb7 (gephyrin)	ms	1:200/1:500	93	Pfeiffer et al. 1984
Neuron specific enolase γ2	ms	1:10/1:2000	47	Chemicon
NMDAR1	ms	-/1:5000	106	Millipore
Phospho-eEF2 (Thr56)	rb	-/1:1000	95	CellSignaling

Antigen/Antibody	Species	Dilution IF/IB	[kDa]	Source
Phospho-S6 Ribosomal Protein	rb	1:50/1:5000	32	CellSignaling
VIAAT	ms	1:500/-	-	Sigma-Aldrich
αGFP/FITC	gt	1:1000/-	27	USBiological
αGlyRβC-20	gt	-/1:100	58	Santa Cruz
αGlyRα_2	gt	1:100/1:100	48	Santa Cruz
αGlyRα1	rb	-/1:1000	48	Millipore
αKCC2-1 (N-Terminal)	rb	1:1000/1:5000	124	Kind gift of Prof. Friauf
αPSD 95	ms	1:250/1:5000	95	Transduction Laboratories

3.1.7.2. Secondary Antibodies

Antibody	Conjugation	Dilution	Source
dk anti gt IgG	cy2	1:200	Dianova
dk anti gt IgG	HRP	1:10,000	BioRad
dk anti ms IgG	cy3	1:1000	Dianova
dk anti ms IgG	HRP	1:10,000	BioRad
dk anti rb IgG	HRP	1:10,000	BioRad
gt anti rb IgG	cy3	1:1000	Dianova
ms β-Actin/	HRP	1:200,000	Sigma-Aldrich

3.1.8. Plasmids and Sequences

3.1.8.1. ShRNA

The shRNA Oligos were synthesized either at BioSpring or at Eurofins MWG Operon.

shRNA Oligos inducing KCC2 knockdown	
KCC2kd1, sense (located in the 3'UTR)	5'-TTTGCCGGAGTAGACGTTGCAATAAGTGAAGCC ACAGATGTTATTGCAACGTCTACTCCGGTTTTT-3'
KCC2kd1, antisense	5'-CGAAAAACCGGAGTAGACGTTGCAATAACATCT GTGGCTTCACTTATTGCAACGTCTACTCCGG-3'
KCC2kd2, sense (kd2) (located in the ORF)	5'-TTTGAGAGCGACATCTCAGCATACAGTGAAGCC ACAGATGTGTATGCTGAGATGTCGCTCTTTTTT-3'
KCC2kd2, antisense	5'-CGAAAAAAGAGCGACATCTCAGCATACACATCT GTGGCTTCACTGTATGCTGAGATGTCGCTCT-3'
KCC2kd3 sense (located in the ORF)	5'-TTTGAGAGTATGATGGCAGGAACATGTGAAGCC ACAGATGATGTTCCTGCCATCATACTCTTTTTT-3'
KCC2kd3 antisense	5'-CGAAAAAAGAGTATGATGGCAGGAACATCATCT GTGGCTTCACATGTTCCTGCCATCATACTCT-3'

shRNA Oligos inducing KCC2 knockdown	
KCC2kd4, sense (located in the ORF)	5′-TTTGGCTGTCTCGCCATGGCTTTGAGTGAAGCC ACAGATGTCAAAGCCATGGCGAGACAGCTTTTT-3′
KCC2kd4, antisense	5′-CGAAAAAGCTGTCTCGCCATGGCTTTGACATCT GTGGCTTCACTCAAAGCCATGGCGAGACAGC-3′

Mismatch shRNA Oligo accordant to KCC2kd2 without silencing effect	
KCC2kd2mm, sense	5′-TTTGAGAGCGATATTTCAGCGTACAGTGAAGCC ACAGATGTGTACGCTGAAATATCGCTCTTTTTT-3′
KCC2kd2mm, antisense	5′-CGAAAAAAGAGCGATATTTCAGCGTACACATCT GTGGCTTCACTGTACGCTGAAATATCGCTCT-3′

3.1.8.2. Vectors, Plasmids

Plasmid	Description	Source
pCMV-U6	Eukaryotic expression vector carrying the MCS downstream to the U6-Promoter	Dittgen et al. 2004
pCMV-U6_KCC2kd1	shRNA Oligo against KCC2 in pCMV-U6 via BbsI/BstBI restriction sites	this thesis
pCMV-U6_KCC2kd2	shRNA Oligo against KCC2 in pCMV-U6 via BbsI/BstBI restriction sites	this thesis
pCMV-U6_KCC2kd3	shRNA Oligo against KCC2 in pCMV-U6 via BbsI/BstBI restriction sites	this thesis
pCMV-U6_KCC2kd4	shRNA Oligo against KCC2 in pCMV-U6 via BbsI/BstBI restriction sites	this thesis
pCMV-U6_KCC2kd2mm	mmshRNA Oligo against KCC2 in pCMV-U6 via BbsI/BstBI restriction sites	this thesis
pCMV Δ8.9	Lentiviral packaging vector	Zufferey et al. 1997
pVSVG	Lentiviral envelope vector	Naldini et al. 1996
pFSGW	Based on pFUGW; the ubiquitin promoter was replaced by the human synapsin promoter	Thomas Kremer
pFSGW_KCC2kd2	shRNA Oligo against KCC2 under the U6 promoter in pFSGW via BstBI/NheI restriction sites	this thesis
pFSGW_KCC2mm	shRNA Oligo against KCC2; contains 3 mismatches compared to the KCC2kd2 Oligo, under the U6 promoter in pFSGW via BstBI/NheI restriction sites	this thesis
hGlyRa1 in pcis	Eukaryotic expression vector for the human GlyRa1 subunit	Grenningloh et al. 1990
hGlyRa2 in pcis	Eukaryotic expression vector for the human GlyRa2 subunit	Grenningloh et al. 1990
rGlyRa3 in pcis	Eukaryotic expression vector for the rat GlyRa3 subunit	Kuhse et al. 1990

Plasmid	Description	Source
rGlyRb in pcis	Eukaryotic expression vector for the rat GlyRb subunit	Grenningloh et al. 1990
KCC2_rn in pEFGP-N3	Eukaryotic expression vector for rat KCC2, C-terminally tagged to EGFP	Kai Kaila
KCC2_rn in pEGFP-C1	Eukaryotic expression vector for rat KCC2, N-terminally tagged to EGFP	Kai Kaila
KCC2-IRES	Eukaryotic expression vector for rat KCC2, N-terminally tagged to IRES and EGFP	Kai Kaila

3.1.8.3. Primer

The primers for GlyRa2, GlyRa3 und GlyRb subunits originate from Jochen Kuhse. The remaining ones were synthesized at BioSpring or GATC.

Primer	Sequence
GlyRa1-F	5′-TTTTTTGCCCCCATAACTCGTGG-3′
GlyRa1-R	5′-TGCTGTAGAGGACATTCCCATTCCG-3′
GlyRa2 3UTRs1	5′-CCTGGGACCTTCTTTGCCTAAGTG-3′
GlyRa2 3UTR AS1	5′-ATGGTAGTCACTATTGTCAGATGG-3′
GlyRa3 3UTRs1	5′-CTATGAAGGCATACAAAAACAGAGC-3′
GlyRa3 3UTR AS1	5′-GTGTTCTGACATGAGTGACCTTGAC-3′
GlyRβ s1	5′-TTGGCCTCAGAGTGCACCACCCTC-3′
GlyRβ AS1	5′-CGTGGGGATGACAGGCTTGGCAGG-3′
KCC2mut, sense	5′-CTCGTAGGTGTACGCTGATATGTCACTCTCGTGCATC-3′
KCC2mut, antisense	5′-GATGCACGAGAGTGACATATCAGCGTACACCTACGAG-3′
NheI/5’ U6pro	5′-CCCGCTAGCATCCGACGCCGCCATCTCTA-3′
pCMV-U6oligo3’	5′-CCACCGCATCCCCAGCATGCC-3′

3.1.9. Antibiotics

Antibiotic	Dilution
Ampicillin	1:1000 from stock (150 mg/ml)
Kanamycin	1:1000 from stock (30 mg/ml)
Zeocin	1:2000

3.1.10. Cells

3.1.10.1. Bacteria

Stratagene E.coli XL-1 blue

3.1.10.2. Cell lines

ATCC HEK293, CRL-1537 human embryonic kidney cells

HEK293T, CRL-11268 HEK293T cells, stably express the SV-40 T antigen

3.1.11. Inhibitors

Inhibitor	Function	concentration	solvent
APV	Blocks the NMDAR	30 µM	H_2O
bicuculline	Blocks the $GABA_AR$ and Ca^{2+}-activated K^+-channels	20 µM	H_2O
cnqx	Blocks AMPAR and KainateR	2 µM	H_2O
gabazine	Blocks the $GABA_AR$	10 µM	H_2O
mk 801	Blocks the NMDAR (not competitive)	5 µM	H_2O
nifedipine	Blocks L-type Ca^{2+}-channels	5-10 µM	DMSO
strychnine	Blocks the GlyR	1 µM	H_2O
tetrodotoxin	Blocks voltage depending Na^+-channels	1 µM	H_2O
verapamil	Blocks L-type Ca^{2+}-channels	2 µM	H_2O

3.1.12. DNA and Protein standards

Bio-Rad Precision Plus Protein Dual Colour standards

Invitrogen 100 bp ladder

1 kb ladder

Fermentas Gene Ruler Express

3.2. Methods

3.2.1. Cell culture techniques

3.2.1.1. Cell lines

Culture and passaging of HEK293 and HEK293T cells

Cells are grown in MEF medium on 10 cm cell culture dishes and passaged three times a week as follows: cells are rinsed with D-PBS (37°C) and incubated with Trypsin/EDTA for 2 min. They are resuspended in fresh medium and centrifuged for 5 min at 500 rpm. The supernatant is removed and the cells are resuspended in fresh medium. The cell suspension is diluted 1:5 and 1:10 in fresh medium and plated on 10 cm dishes (10 ml) or seeded on poly-L-lysine coated cover slips (500 µl).

PEI-Transfection of cells

The cells are transfected when they reach 60-70 % density. For one well of a 24-well plate, 1 µg DNA is diluted in 50 µl Optimem and 2-3 µl PEI is added quickly followed by 10 s vortexing. After 30 min of incubation at the dark and RT, the mixture is added to the cell culture medium and distributed equally. Cells are incubated for 4 h under normal growth conditions, then the medium is replaced with fresh MEF medium. The amount of components for the transfection is increased relative to the surface of the dish or well.

3.2.1.2. Primary cultures

Hippocampal neurons (E 19)

Hippocampi are dissected from Wistar/Crl rats at E 19 and propagated as described previously (Dresbach et al. 2003). Briefly, a pregnant rat is anaesthetised and sacrificed. The embryos are taken out of the mother and decapitated. The heads are opened and the Hippocampi are removed, treated with Trypsin, washed three times with serum containing DMEM and triturated first by a 20 G then by a 24 G needle. The cells are counted and plated at a density of 10,000-15,000 cells/cm^2 on poly-L-lysine coated cover slips or 6-well plates in DMEM^{+++}. After 4 h or 1 day, the DMEM is exchanged by NB^{+++}.

Spinal neurons (E 15)

Spinal cords are dissected from Wistar/Crl rats at E 15 and propagated as described previously (Kirsch and Betz 1995). Briefly, a pregnant rat is anaesthetised and sacrificed. The embryos are removed and after opening of the back, the spinal cords are removed and collected in D-PBS/Glucose. After cutting the cords into small pieces, the cells are dissociated by trituration with glass pipettes. The single cell suspension is centrifuged, the supernatant is removed and the pellet is solved in NB^{++++}. Finally, cells are counted and plated on poly-L-ornithine coated 6-well plates (containing four cover slips per well for immunoreactivity or without cover slips for extracts). Per well 400,000 cells are filled in.

3.2.2. Molecular biology

3.2.2.1. Transformation of bacteria (Holger Stuck)

One Aliquot of competent cells is gently thawed on ice. 50 µl of the cell suspension is mixed with 0.5 µl of DNA and incubated on ice for 30 min. After a heat shock at 42°C for 30 sec and incubation on ice for 1 min, 450 µl of LB medium without antibiotics is added. The mixture is shaken for 45 min at 37°C and 180 rpm. At the end 50-100 µl of the cell suspension are streaked on agar dishes containing the accordant antibiotic.

3.2.2.2. Mini Plasmid Preparation

A colony is picked with a baked toothpick and thrown into 3 ml of LB medium containing the accordant antibiotic. The sample is shaken o/n at 37°C. The next day, the cell suspension is centrifuged for 5 min at 5000 rpm and 4°C to get the cells pelleted. The pellet is solved in 400 µl P1 containing 0.4 µl RNaseA. 400 µl P2 are added and the suspension is inverted 2-3 times. After incubation at RT for 5 min, another 400 µl ice-cold P3 are added to the mixture. Again, the suspension is inverted and incubated for 5 min on ice. Cell debris and denatured proteins are pelleted by centrifugation for 10 min at 4°C and 13,000 rpm. The clear supernatant is carefully taken up and filled into a new 2 ml reaction tube. The tube is filled to a volume of 2 ml with isopropanol and inverted. The DNA pellet is produced by centrifugation for 30 min at RT and full speed. The supernatant is discarded and the DNA pellet is washed with 870 µl of 70% EtOH. Finally, the tube is centrifuged again for 10 min at RT and full speed, the supernatant is discarded and the pellet is allowed to dry until it becomes transparent. The isolated DNA is solved in autoclaved Milli-Q and is prepared for sequencing or stored at -20°C.

3.2.2.3. Maxi plasmid preparation

For the o/d culture, one colony of an agar dish or a glycerol stock is picked with a sterile yellow pipet tip and thrown into 5 ml of LB medium without antibiotics. In the evening 2 ml of the cell suspension are added to 500 ml LB medium containing the accordant antibiotic. The mixture is shaken o/n at 37°C and 250 rpm. The next day, the DNA is purified using the NucleoBond® Xtra Midi/Maxi-Kit following the manufacturer's instructions. The plasmid DNA is eluted in Milli-Q and the $OD_{260/280}$ is determined using the photometer. The DNA solution is adjusted to 1 µg/µl and stored at -20°C.

3.2.2.4. Agarose gel electrophoresis

DNA loading buffer is added to the DNA to a final concentration of 1x. The samples are loaded on an agarose gel (0.7-2 % (w/v) in 1x TAE) and the DNA is separated at 80 V for the first 10 min followed by 100 V for the rest of the run. Afterwards, the gel is applied to an EtBr bath (in 1x TAE) to visualize the DNA and is photographed for documentation.

3.2.2.5. Gel extraction

For the extraction of DNA out of the agarose gels, the QIAquick Gel Extraction Kit is used. The manufacturer's instructions are followed.

3.2.2.6. Restriction digest

All used enzymes and buffers originate from NEB. The proposed time durations, temperatures and concentration are adopted. For double digests, the optimal conditions are worked out.

3.2.2.7. Mutational assay

The production of a construct containing mutations at defined sites in the targeted sequence is done using the QuikChange Site-Directed Mutagenesis Kit. Primers are designed following the kit's instructions. The PCR was performed as proposed in the manual.

3.2.2.8. Annealing of shRNA

To anneal the shRNA Oligos, 2 µl of each, sense and antisense solution, are diluted in 46 µl of annealing buffer and heated for 3 min at 90°C in the heating block. Still containing the samples, the block is turned off and is allowed to cool down to 37°C. After reaching this temperature, the block is turned on again and the RNA is incubated for 1 h at 37°C. The dsRNA is kept at -20°C.

3.2.2.9. RNA isolation

According to the manufacturer's instructions, total cellular RNA is isolated from 1.2 million cells using the Nucleobond RNA II kit. Finally, the RNA is eluted with 30 µl water. To further increase the concentration, the eluate was used to elute remaining RNA from the membrane one more time. The concentration is determined by UV spectrophotometry at 260 nm. The RNA is stored at -20°C.

3.2.2.10. CDNA synthesis

The following components of the SuperScript® III First-Strand Synthesis System are mixed in a PCR tube.

RNA	8 µl
OligodT	1 µl
dNTPs	1 µl

The mixture is incubated at 65°C for 5 min, placed on ice for 1 min and the DNA synthesis mix is added.

10x RT Puffer	2 µl
25 mM MgCl2	4 µl
0.1 M DTT	2 µl
RNaseOut	1 µl
SuperScript III RT	1 µl

This mixture is incubated for 58 min at 50°C and then for 5 min at 85°C. Subsequently it is placed on ice and 1 µl of RNaseH is added. Digest of the RNA takes place at 37°C for 20 min.

3.2.2.11. RT-PCR

The reaction of the RT-PCR takes place in 50 µl volume. Therefore 27 µl of autoclaved Milli-Q are mixed with 10 µl 5xPhusion HF Buffer, 5 µl 2.5 mM dNTPs, 1.5 µl DMSO, 2 µl sense and antisense primers respectively, 0.5 µl Phusion Polymerase und 2 µl cDNA. The following conditions are applied:

a) 2 min at 94°C
b) 50 sec at 94°C
c) 50 sec at 53°C (GlyRa1), 60°C (GlyRa2, GlyRa3), 68°C (GlyRb)
d) 50 sec at 72°C
e) 20 min at 72°C

Steps b)-d) are repeated 35 times.

3.2.2.12. RTq-PCR

For the PCR samples, a DNA and a reaction mix are prepared. For the DNA mix, 50-100 ng of cDNA is solved in autoclaved Milli-Q in a final volume of 13.5 µl. For the reaction mix, 15 µl TaqMan Master Mix and 1.5 µl of the accordant Gene Expr. Assay are mixed. The two mixtures are combined in the wells of a 96-well plate. Doublets or triplets of each sample are performed. Autoclaved Milli-Q serves as the negative control. The plate is sealed with an adhesive cover. Before the PCR reaction takes place, the plate is centrifuged for 2 min at 1500 rpm to avoid air bubbles within the samples. Afterwards, 50 cycles of amplification with the recommended PCR program (a) 2 min 50°C, b) 10 min 95°C, c) 15 sec 95°C, d) 1 min 60°C) are performed. For all genes together, the auto-baseline is adjusted to get rid of noise. For each single gene, the Auto-CT value is adjusted to determine the point, at which the enzyme-substrate curve switches from linear to the plateau-phase. The data are analyzed with the help of the genex.xls macro, which employs the ΔΔ-CT method.

3.2.2.13. Lentivirus

Production

The following mixture is prepared to transfect HEK293T cells for virus production:

plasmid	per 10 cm dish
pCMV R8.9	7.5 µg
pVSVG	5 µg
pFSGW + shRNA	10 µg
PEI	75 µl
Optimem	925 µl

For an effective approach, four 10 cm dishes of cells are transfected with this mixture respectively. After 4 h, the medium is aspirated and replaced by fresh MEF medium (37°C). Two days later, the medium is removed, pooled and centrifuged for 5 min at 1291 rpm and RT. The supernatant is sterile filtered through a 0.45 µm syringe and transferred to an ultracentrifuge tube (no cap). The virus is centrifuged in the following UZ step within a SW32Ti rotor at 25,300 rpm and at 4°C for 90 min. Afterwards, the supernatant is carefully aspirated and the viral pellet (yellow-brown) is allowed to dissolve in the reflux for 4 h on ice. The reflux volume is measured and filled up with D-PBS to a final volume of 500 µl. 15 µl virus aliquots are deep frozen in liquid nitrogen and stored at -80°C.

Infection

One virus aliquot is gently thawed on ice and filled with NB to a volume of 1 ml. 10-80 µl of this mixture are dropped to one well of a 6-well plate and well distributed. The cells are incubated at least 4 days with the virus. Protein extracts or immunoreactivity assays are prepared at div 8, 15, 22 and 36.

3.2.3. Biochemistry

3.2.3.1. Protein extracts (modified from Santa Cruz)

The medium is removed and cells are washed once with D-PBS. 1.2 million cells are scraped off in 150 µl RIPA buffer and transferred to a 1.5 ml reaction tube. The lysate is passed through a 21 G needle 10-15 times to shear genomic DNA. The lysate is cleared by centrifugation at 4°C and full speed for 15 min in a tabletop centrifuge. The supernatant is transferred to a new 1.5 ml reaction tube and stored at -80°C.

3.2.3.2. BCA-Assay

The following standards are prepared:

BSA: 2 mg/ml		RIPA [µl]	Milli-Q [µl]
[µl]	[µg]		
0	0	10	40
0.5	1	10	39.5
1.25	2.5	10	38.75
2.5	5	10	37.5
5	10	10	35
10	20	10	30
20	40	10	20
30	60	10	10
40	80	10	0

10 µl of the protein extract are mixed with 40 µl of Milli-Q. Doublets or triplets are performed. For the BCA reagent, Solution A and B of the BCA Protein Assay are mixed at the ratio of 50:1. 1 ml of the BCA reagent is pipetted into each sample. Afterwards the samples are first incubated at 37°C, then at RT for 30 min respectively. The protein concentration is measured using the photometer.

3.2.3.3. Acrylamide Gels

The gels for the poly acrylamide gel electrophoresis (PAGE) and adjacent immunoblot analysis are mixed as in the following instruction.

Separation gel, 10%

2 x 1.5 mm gels	
8 ml	H_2O
6.6 ml	Acrylamide
5 ml	1.5 M Tris pH8.8
200 µl	10% SDS
200 µl	10% APS
16 µl	TEMED

Stacking gel

2 x 1.5 mm gels	
5.4 ml	H_2O
1340 µl	Acrylamide
1000 µl	1 M Tris pH6.8
80 µl	10% SDS
80 µl	10% APS
16 µl	TEMED

The solution is immediately filled between two glass plates. First, the separation gel and, after its polymerization, the stacking gel is filled in.

3.2.3.4. PAGE

The protein extracts are thawed on ice and are drugged with 2x Urea buffer. The samples are heated for 5 min at 42°C. 15-40 µg of protein per lane are separated on the acrylamide gel using the mini protean III gel system. The separation was performed at 35 mA. The proteins are transferred to a PVDF membrane via a tank blot (3 h at 400 mA or o/n at 180 mA) or a semi-dry-blot system (1-1.5 h at 150-200 mA). The transfer is performed at 4°C. The membrane is blocked for 1 h in blocking buffer. Subsequently, it is incubated with the primary antibody diluted in blocking buffer for 1 h at RT or o/n at 4°C. Then, the membrane is washed 3x 15 min with TBS-T and incubated with the secondary antibody diluted in blocking buffer for 30-45 min at RT. After 3x 15 min washing in TBS-T and once in TBS, ECL plus solution is applied to the membrane as instructed by the manufacturer. The membrane is rinsed once with TBS. Subsequently it is dried, before detection using a Hyperfilm in the Curix developing machine takes place.

For semi-quantitative studies, immunoblots are scanned with the BioRad GS-800 Calibrated Densitometer. Therefore, the bands of interest are encircled and subsequent measured by use of QuantityOne. All statistical results are produced using actin or tubulin bands as a reference.

3.2.4. Histological Techniques

3.2.4.1. Fixation methods

PFA/MeOH

Sitting on cover slips, the targeted cells are washed once with warm D-PBS (37°C). At once, 4 % PFA (RT) is added to the cells followed by incubation for 2-3 min at RT. The PFA is removed and the prefixed cells are washed once with D-PBS (RT). Afterwards, cold MeOH (-20°C) is added to the cells. The cover slips are incubated on dry ice or in the freezer (-20°C) for additional 10-15 min. After the MeOH is removed, cover slips are allowed to dry for a few seconds and then they are washed three times with D-PBS.

PFA

The cover slips, which carry the targeted cells, are washed once with warm D-PBS (37°C), fixed with 4% PFA for 15 min and washed three times with D-PBS (RT).

3.2.4.2. Immunoreactivity assay of fixed cells

The cover slips carrying the fixed cells are placed into a humid chamber. There they are blocked for 1 h with blocking solution A. Afterwards, the cells are incubated for 1 h at RT with the primary antibody diluted in blocking solution B. The cover slips are three times washed in 1x PBS and incubated for another 45 min-1 h with the secondary antibody diluted in blocking solution B. After washing the cells three times in 1x PBS, the cover slips are dunked into Milli-Q and mounted with Mowiol+DABCO on a glass slide.

4. Results

4.1. Specificity of attached antibodies

For investigation of the protein expression levels and immunoreactivities, different "new" antibodies were established. Some of them just work in immunoblots, some only in immunostainings and others can be used for both. Each of the used antibodies was initially tested in HEK293 cells transfected with the accordant GlyR subunit or KCC2 expression construct. In the following figures, the "new" antibodies rb αGlyRa1 (Figure 12A), gt αGlyRa2 (Figure 11A and Figure 12B), gt αGlyRb (Figure 11B and Figure 12C) and rb αKCC2-1 (Figure 11C and Figure 12D) are applied to transfected HEK cells to demonstrate function and specificity.

Figure 11: HEK cells transfected with the indicated expression construct. Immunoreactivity visualized by **A**, antibody αGlyRa2. **B**, antibody αGlyRb. **C**, antibody αKCC2-1. Scale bar=50 µm

αGlyRa2 (gt), αGlyRb (gt) and αKCC2-1 respectively recognize the native proteins (Figure **11**). αGlyRa1 (rb) was not tested for immunoreactivity because it was only used for immunoblots. Instead, the well-characterized antibody mAb2 was used to visualize the GlyRa1 subunit in immunostainings. All four presented antibodies recognize the accordant denatured protein in immunoblots (Figure 12). The GlyRb subunit exhibits 3-5 different bands (Figure 12C), which indicate different splice variants expressed in HEK cells or degradation products. Furthermore, the bands run lower than expected (58 kDa) which points to the small fragment of the GlyRb gene (1900 bp) cloned into the pcis vector and to degradation. αKCC2-1 recognizes two bands in HEK cell protein extracts (Figure 12D). The lower band at about 150 kDa represents the KCC2 monomer (126 kDa), the upper band (above 250 kDa) represents KCC2 oligomers (e.g dimers or tetramers).

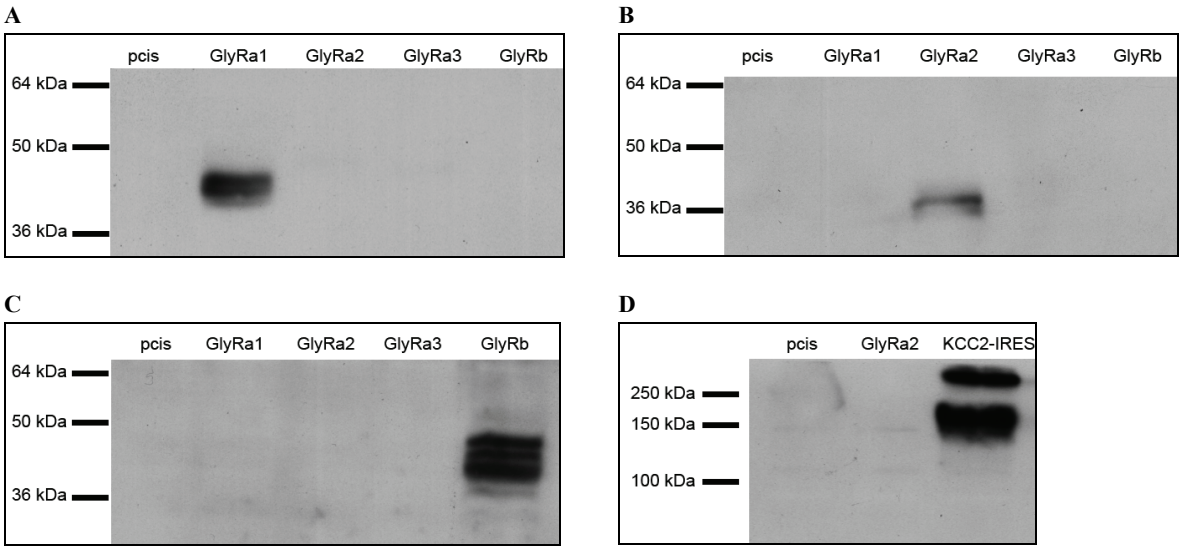

Figure 12: Immunoblots from HEK293 cells transfected with the indicated expression construct respectively. **A**, antibody αGlyRa1. **B**, antibody αGlyRa2. **C**, antibody αGlyRb. **D**, antibody αKCC2-1.

The well-characterized antibodies mAb2, mAb4 and mAb7 (Pfeiffer et al. 1984), as well as different commercial antibodies, were also used in this thesis.

4.2. Expression profiles of the GlyR subunits

To characterize the expression of the four GlyR subunits in cultured rat spinal or hippocampal neurons respectively, different div stages were investigated. Therefore, the RNA as well as the protein levels were determined. After preparation, the cells were cultured for 4, 7, 11, 14, 20, 21 or 28 days. Div 28 neurons serve as the adult stage according to GlyR expression. At the indicated stages, the cells were lysed and RNA or protein extraction was performed. Afterwards, the RNA was reversely transcribed into cDNA, which then was used for subsequent RT-PCR or RTq-PCR studies. The qualitative analysis, indicating the presence of different subunits, was followed by the quantitative study. The RTq-PCR results are shown as values normalized to one div stage. Thereby, values achieved from div 28 cells were determined as "1". In the case of the GlyRa2 subunit, the youngest stage (div 4) served as the control value because at that time point a cell should contain the biggest amount of GlyRa2 transcripts.

It was not possible to quantify the results of the immunoblot analysis, because the existing antibodies against the GlyR subunits do not work properly when being applied to neuronal protein extracts. However, some of those blots are shown.

4.2.1. Dynamics of GlyR subunit expression in HCNs

During the analysis of the hippocampal cultures, it appeared that RNA of all GlyR subunits is expressed without GlyRa1 (Figure 13). The same was already shown via *in situ* hybridizations of Maria-Luisa Malosio (Malosio et al. 1991b) and in this thesis confirmed by RT-PCR data. RNA expression of the GlyRa2 subunit decreases with development. In contrast, RNA expression of the GlyRb subunit remains unchanged.

A: GlyRa1 primer

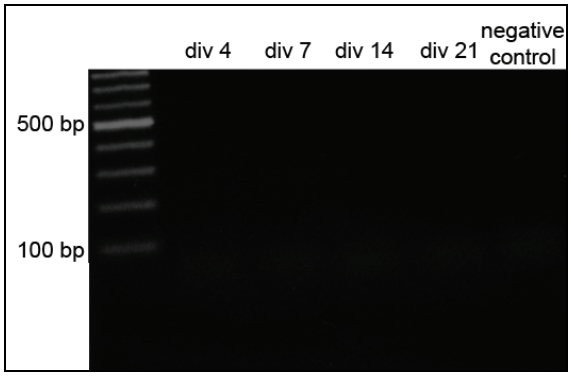

B: GlyRa2 primer

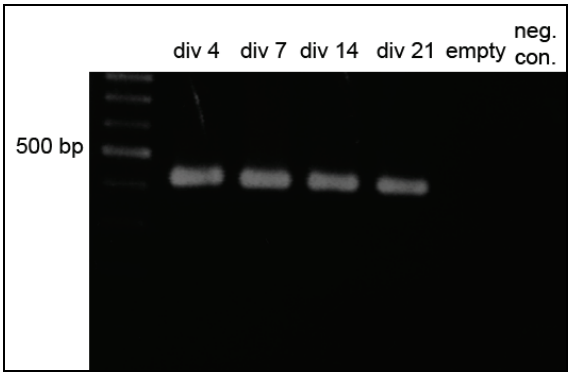

C: GlyRa3 primer

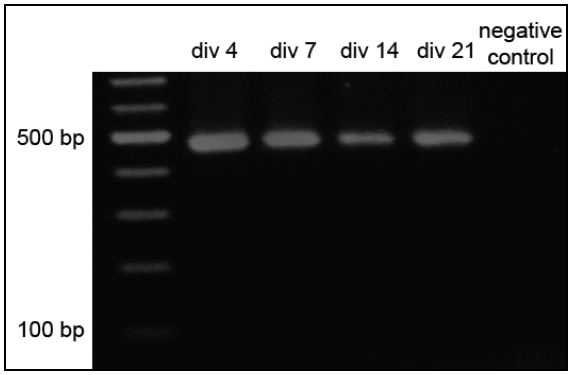

D: GlyRb primer

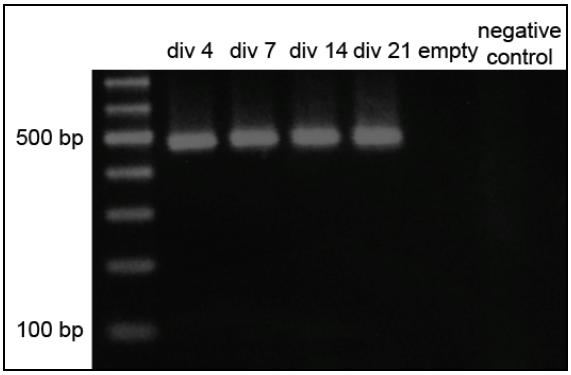

Figure 13: RT-PCR from HCN cDNA prepared at the indicated time points. **A**, GlyRa1 primer. **B**, GlyRa2 primer. **C**, GlyRa3 primer. **D**, GlyRb primer. Negative control: Master Mix without cDNA.

Additional to the RT-PCR studies, RTq-PCR was performed to calculate the relative changes in GlyR subunit RNA expression during *in vitro* development. The following investigations confirm the *in situ* data of Maria-Luisa Malosio (Malosio et al. 1991b), who also showed, that the RNA level of the GlyRa2 subunit decreases during development (Figure 14A). Furthermore, GlyRa3 RNA reaches a high peak at div 7 remaining unmatched during the other investigated div stages (Figure 14B). GlyRa3 RNA expression also increases during the first three weeks in culture compared to div 4 but reaches the same state in adulthood (div 28). GlyRb transcripts, in contrast, already show 60% of the adulthood level at div 4. During development, the RNA level befalls a slight decrease in order to reach its maximum at div 21 and to stay there (Figure 14C).

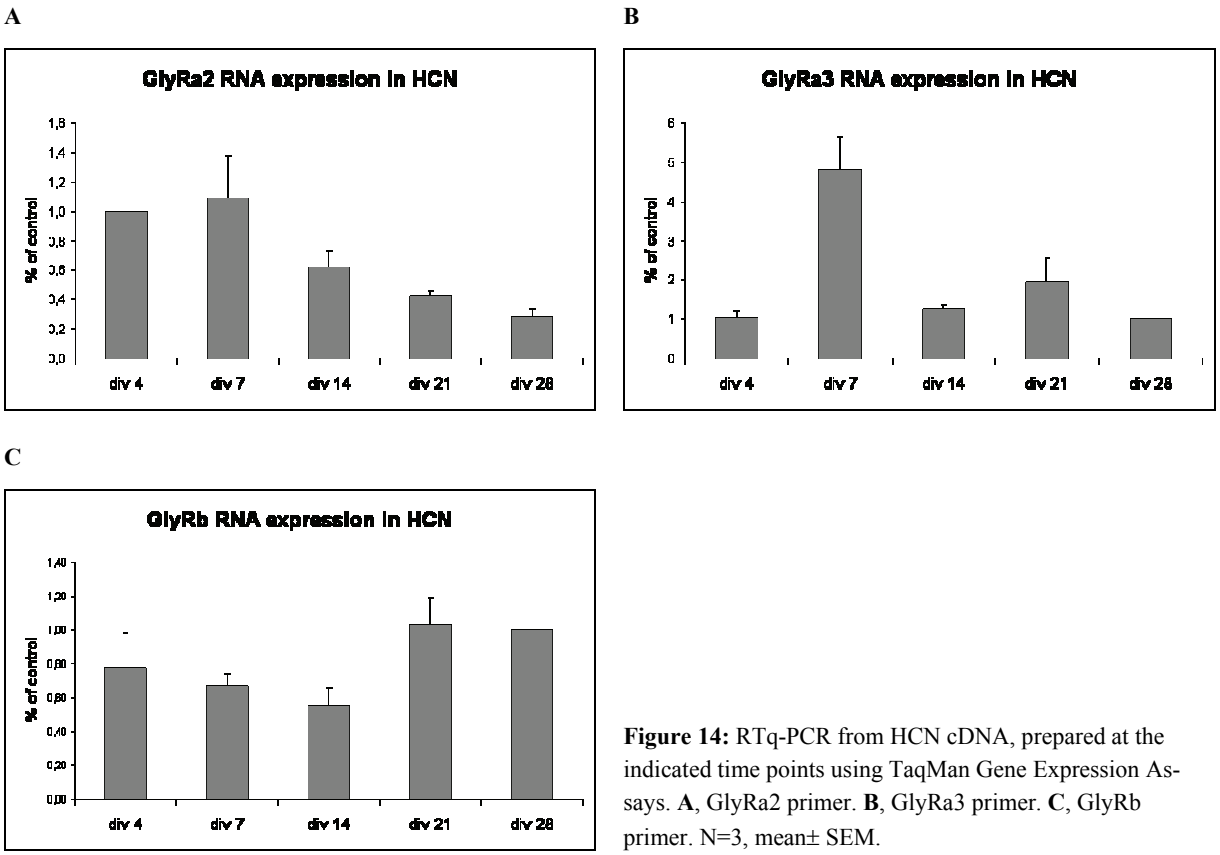

Figure 14: RTq-PCR from HCN cDNA, prepared at the indicated time points using TaqMan Gene Expression Assays. **A**, GlyRa2 primer. **B**, GlyRa3 primer. **C**, GlyRb primer. N=3, mean± SEM.

Regarding the curves of the three examined GlyR subunits combined in one diagram (Figure 15A), the GlyRb and GlyRa2 trajectories cross around div 14. To that time point, the mentioned subunit switch is predicted to occur. By generating the reciprocal of the ΔCT values, the absolute RNA amounts of the subunits can be compared (Figure 15B). While the GlyRb subunit exhibits the highest amount of transcripts even increasing during development, the GlyRa3 subunit only reaches one fourth of it. In between them, the GlyRa2 transcript amount is slightly decreasing with time.

A **B**

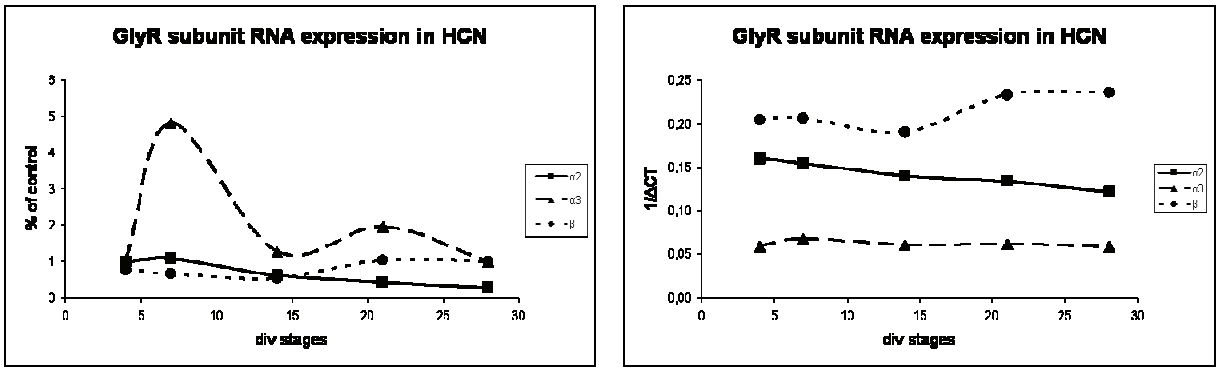

Figure 15: RTq-PCR summary. **A**, relative RNA expression of all GlyR subunits in cultured HCNs. Trajectories cannot be set in relation to each other in terms of absolute amount of RNA. **B**, amount of GlyR subunit RNA, calculated by the reciprocal of the ΔCT values. Mean of 3 experiments.

At the protein level, only GlyRa2 and GlyRb subunit could be investigated. Clearly visible is the augmentation of the GlyRa2 expression during development (Figure 16A). As well as the GlyRa2 band, the GlyRb band runs higher than expected. This phenomenon probably results from the imprecision of the prestained protein standard. GlyRb expression is present from the beginning of the examination and stays until div 28, where it reaches a maximum (Figure 16B, lower bands).

A: GlyRa2 **B:** GlyRb

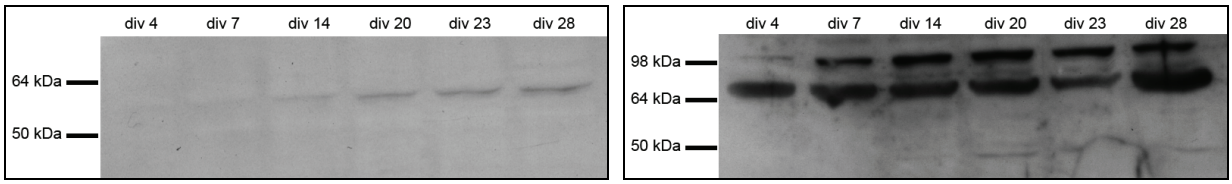

Figure 16: Immunoblots from HCN protein extracts taken at the indicated time points. **A**, antibody αGlyRa2. **B**, antibody αGlyRb (lower bands).

Since the GlyR is mainly expressed in spinal cord and lower brain regions, GlyR subunit expression also should be determined in SNs.

4.2.2. Dynamics of GlyR subunit expression in SNs

In contrast to the HCN cultures, the RNA of all GlyR subunits is expressed in the SN cultures (Figure 17). The level of GlyRa1 RNA increases within the time course (Figure 17A). The GlyRa2 and GlyRb RNA expression remains unchanged (Figure 17B and D), whereas that of GlyRa3 exhibits small variations (Figure 17C).

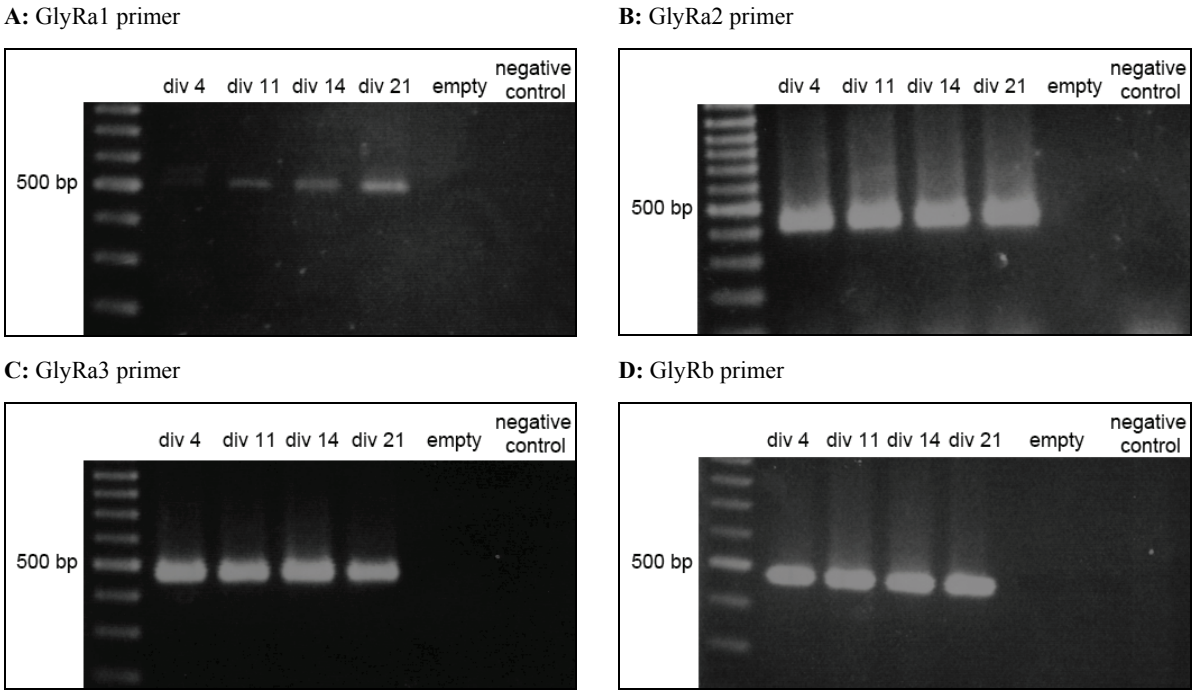

Figure 17: RT-PCR from SN cDNA prepared at the indicated time points. **A**, GlyRa1 primer. **B**, GlyRa2 primer. **C**, GlyRa3 primer. **D**, GlyRb primer. Negative control: Master Mix without cDNA.

Regarding the semi-quantitative study, the increase of the GlyRa1 RNA level (Figure 18A) reminds of the increase in the protein level, shown in the work of Cord-Michael Becker (Becker et al. 1988). He also demonstrated a decrease of the GlyRa2 protein level. Cord-Michael Becker could distinguish the two subunits by the size (GlyRa1: 48 kDa, GlyRa2: 49 kDa) using the mAb4 antibody, which recognizes all GlyRa subunits. Additionally, this study demonstrates that the RNA levels of the GlyRa3 and the GlyRb subunits rise during *in vitro* development (Figure 18C and D). However, the expression patterns of the GlyR subunits differ from each other. The amount of the GlyRa1 RNA remains almost constant until div 14 before it rises erratically (Figure 18A). In contrast, the RNA level of the GlyRa3 subunit increases continuously, but steeply (Figure 18C). The GlyRb RNA level also increases continuously, but faster (Figure 18D). The adult stage is achieved one week earlier compared to the other subunits. During the first week in culture the GlyRa2 subunit RNA level remains similar, and then it decreases, rests for another week and reaches the minimum level during the last week before adulthood (Figure 18B).

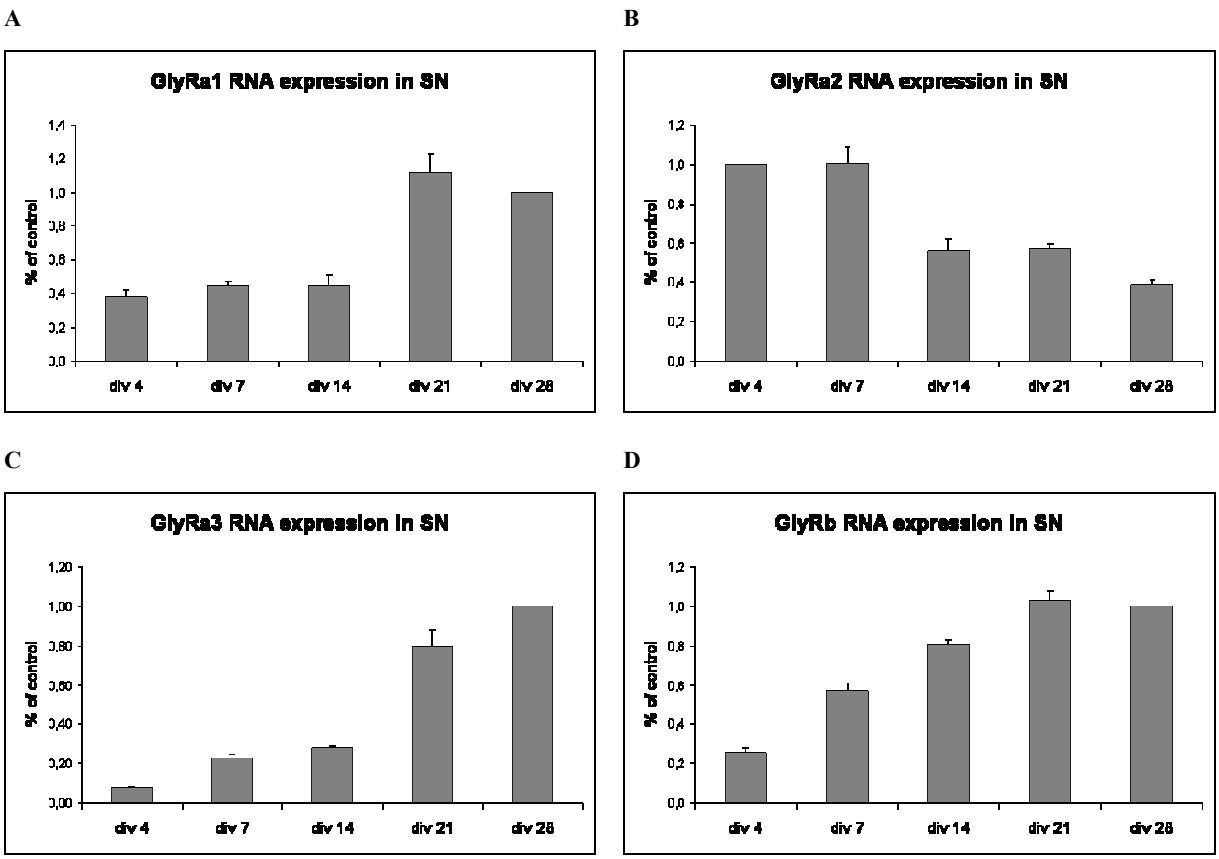

Figure 18: RTq-PCR from SN cDNA, prepared at the indicated time points using TaqMan Gene Expression Assays. **A**, GlyRa1 primer. **B**, GlyRa2 primer. **C**, GlyRa3 primer. **D**, GlyRb primer. N=4, mean ± SEM.

Figure 19A impressively clarifies the GlyR subunit switch. The GlyRa1 and GlyRa2 curves cross at div 15 indicating the switch to occur at this point. It also shows that GlyRa3 subunit expression increases together with the GlyRa1 subunit, but is slightly shifted backwards. By generating the reciprocal of the ΔCT, values the absolute RNA amounts of the four investigated subunits can be compared (Figure 19B). One can observe that from the beginning most of the transcripts exist of the GlyRb subunit. This subunit already seems to be important at early div stages. At the beginning of the measurement, there is more GlyRa1 RNA than GlyRa3 RNA, but until adulthood, the ratio is surprisingly inverted (Figure 19B). The GlyRa2 RNA curve shows the mentioned jump between div 7 and div 14 (Figure 19A and B). However, in adulthood, more GlyRa2 material than GlyRa1 or GlyRa3 RNA remains in the cells (Figure 19B).

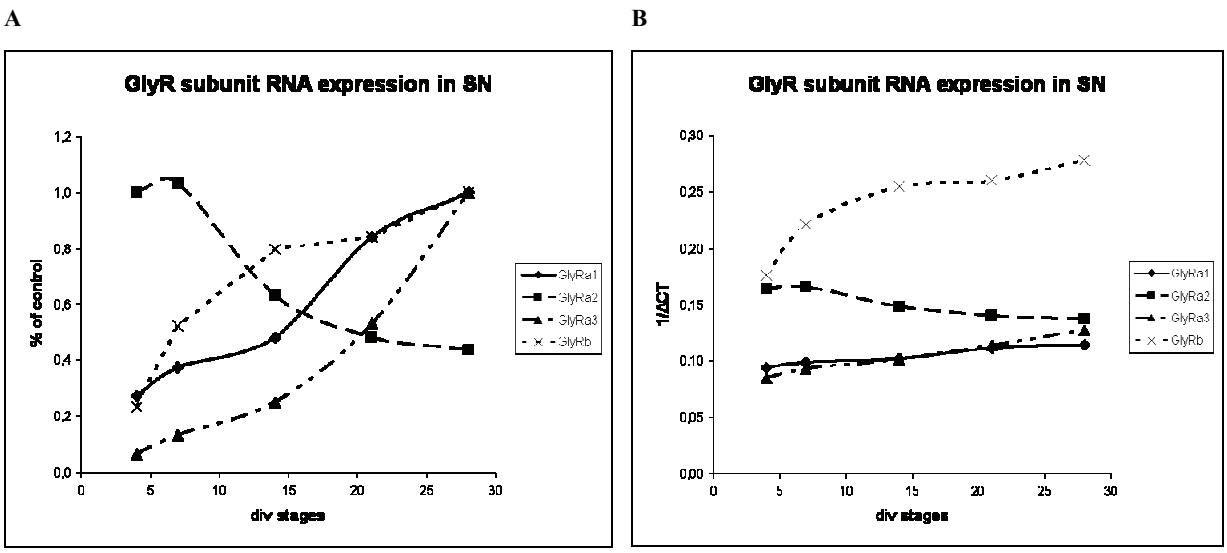

Figure 19: RTq-PCR summary. **A**, relative RNA expression of all GlyR subunits in cultured SNs. Trajectories cannot be set in relation to each other in terms of absolute amount of RNA. **B**, amount of GlyR subunit RNA calculated by the reciprocal of the ΔCT values. Mean of 4 experiments.

At the protein level, GlyRa2 is present from the first investigated div stage and stays until adulthood (div 28, Figure 20A). GlyRb expression also starts not later than div 7, increases during development but then decreases until adulthood (Figure 20B).

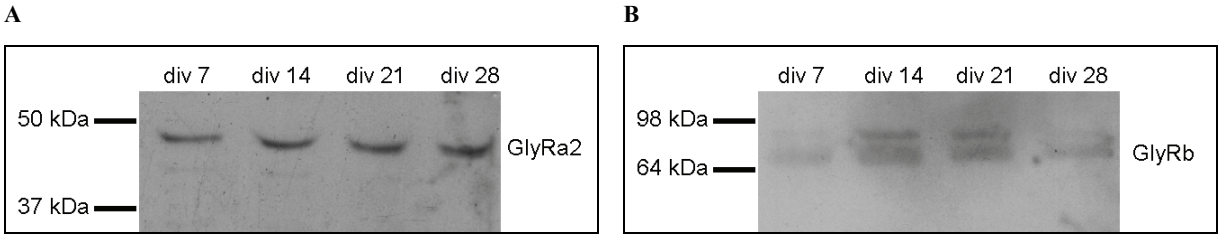

Figure 20: Immunoblots from SN protein extracts taken at the indicated time points. **A**, antibody αGlyRa2. **B**, antibody αGlyRb (lower bands).

The ion transporter KCC2 is up regulated in the rat brain during development (Lu et al. 1999). Because this transporter is essential for inverting the extra- versus the intracellular chloride ratio, its expression dynamics in spinal cord also were investigated.

4.3. Characterization of the KCC2 expression in spinal neurons

The ion transporter KCC2 plays an important role during neuronal development. KCC2 is responsible for changing the ion ratio inside the cell versus the extracellular space. Its function thereby is, to reduce the intracellular chloride level by expelling chloride ions together with potassium ions out of the cell. In contrast to the juvenile stage, more chloride ions are located extracellularly than inside the cell in adulthood. If a chloride channel in the latter stage is opened by a neurotransmitter, chloride

does no longer flow out of the cell but rather into the cell. This directs a hyperpolarisation of the post-synaptic cell instead of a depolarisation. To investigate the contribution of KCC2 expression to the subunit switch, *in situ* and *in vitro* protein and RNA expression studies were performed.

As expected, the expression of KCC2 RNA increases during development. Thereby, the amount of transcripts is approximately duplicated (Figure 21A).

At the protein level, there also is an increase of KCC2 expression during development. However, the protein amount reaches its maximum at div 14 and subsequently decreases to a lower level (Figure 21B). The *in situ* data show a similar pattern, but the maximum expression is achieved at P 22 (Figure 21C).

A: in vitro

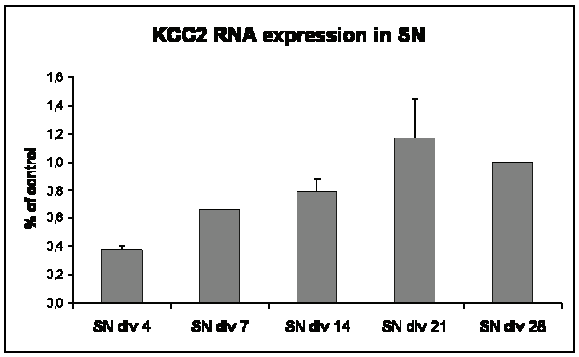

Figure 21: KCC2 expression in spinal neurons. **A**, relative KCC2 RNA expression in cultured SNs. N=6, mean ± SEM. **B**, endogenous KCC2 protein expression in SN cultures (upper panel) and actin control (lower panel). **C**, endogenous KCC2 protein expression in spinal cord homogenates. RNA extracts, protein extracts and homogenates are taken at the indicated time points.

B: in vitro

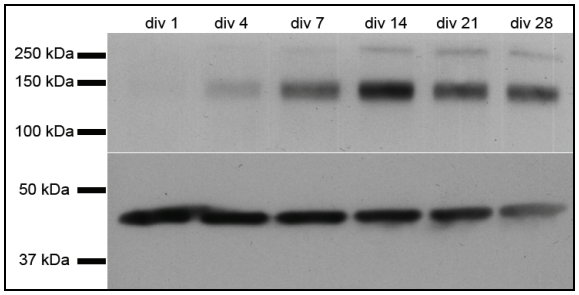

C: in situ

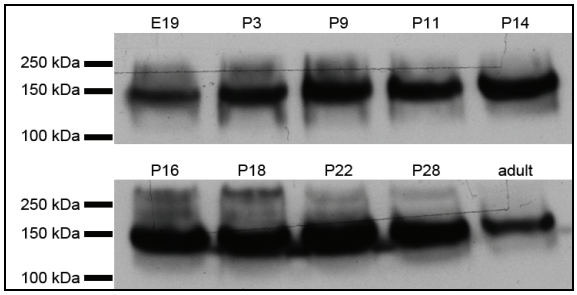

The next step was to check if blockade of glycinergic transmission alters the expression of KCC2 and the GlyR subunits and therewith the subunit switch.

4.4. Altered expression of GlyR subunits and KCC2 upon blockade of glycinergic transmission and Ca^{2+} influx

The first idea, after characterization of the GlyR subunit and KCC2 expression dynamics in development, was to block glycinergic transmission by strychnine application. Therefore spinal neurons were cultured as described and 1µmol/l strychnine was added three times a week beginning at div 1. The following immunoblots gave an initial impression of upcoming effects. Comparing protein extracts of untreated (Figure 22A) and treated cultures (Figure 22B), KCC2 expression seems to be down regulated in cultures with impaired glycinergic transmission.

A: control

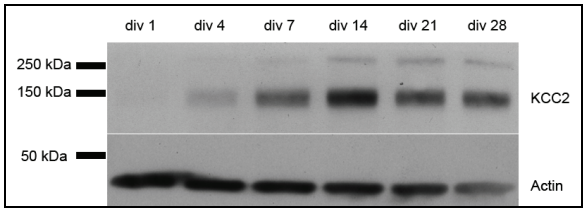

B: strychnine treated

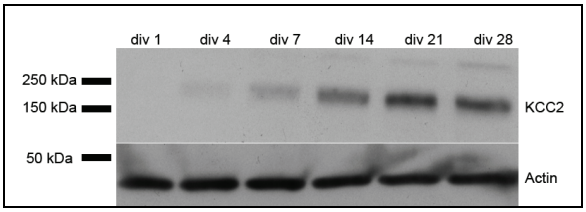

Figure 22: Endogenous KCC2 (upper panels) and actin (lower panels) expression in SN cultures. **A**, untreated cells. **B**, cells treated with 1 µM strychnine. Protein extracts were taken at the indicated time points.

Towards this finding a dose-response assay using different strychnine concentrations was performed. Three trials of three different time points respectively were produced and the data were quantified (Figure 23). Cells were treated as described above. Only at div 14, a significant dose-dependent decrease in KCC2 expression arises (Figure 23A and D).

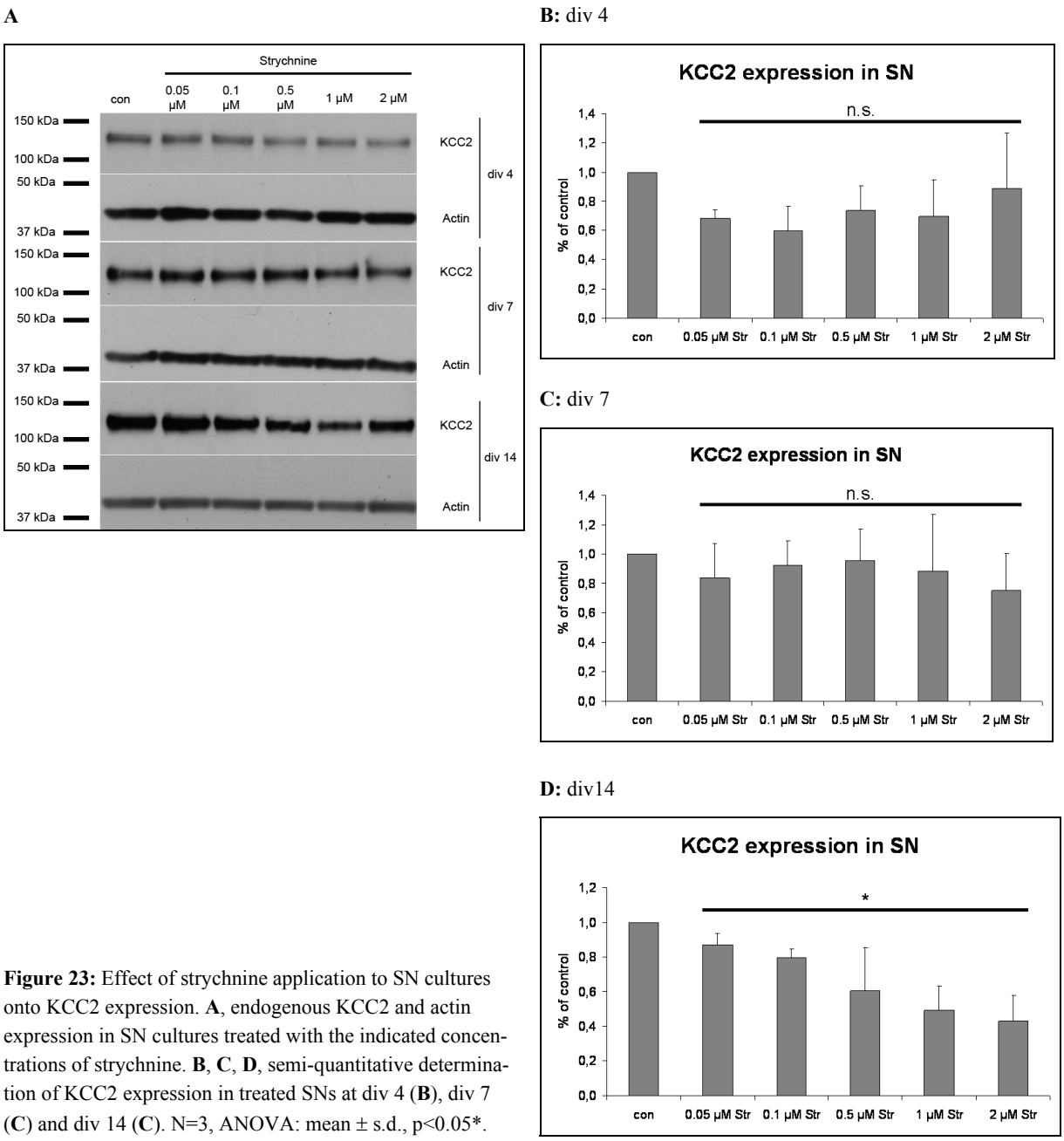

Figure 23: Effect of strychnine application to SN cultures onto KCC2 expression. **A**, endogenous KCC2 and actin expression in SN cultures treated with the indicated concentrations of strychnine. **B**, **C**, **D**, semi-quantitative determination of KCC2 expression in treated SNs at div 4 (**B**), div 7 (**C**) and div 14 (**C**). N=3, ANOVA: mean ± s.d., $p<0.05$*.

The resulting question was, if the reduction in KCC2 expression arises from the lacking glycinergic transmission or from reduced Ca^{2+}-influx into the cells. To determine these considerations, different inhibitors were applied to the SN cultures. First, 1 µmol/l TTX was applied twice a week to completely abolish transmission. Application of TTX leads to a significant decrease in KCC2 and mAb7 expression (Figure 24A and B). GlyR subunits were not concerned. To block Ca^{2+}-signalling, 10 µmol/l BAPTA was added to the cultures. BAPTA is able to enter the cells and therefore can form complexes with the entire free Ca^{2+} in the cultures. Cells were incubated for one night with BAPTA before they were lysed. BAPTA altered the KCC2 expression and to a small extent GlyRa expression (mAb4) but not gephyrin expression (mAb7). This treatment was done once and not quantified because the phenomenon of Ca^{2+}-influx should be investigated and not the presence of Ca^{2+} inside the

cell. Furthermore, to check if blockade of other ion channels affects KCC2 expression different inhibitors were applied to SNs (Figure 24C). To block NMDAR activity, AP5 (30 µmol/l) and mk801 (5 µmol/l) were used; cnqx (20 µmol/l) blocks AMPAR while $GABA_AR$ is blocked by gabazine (10 µmol/l) or bicuculline (20 µmol/l). All inhibitors were added three times a week. The activity of none of these receptors seems to be important for KCC2 expression without gabazine, which leads to an increase in KCC2 expression. Gephyrin expression seems to be decreased to a small extent upon inhibiting activity of excitatory receptors. Interestingly, only mAb7 signal exhibits this effect, the 408 signal remains unchanged. GlyRa subunit expression possibly is up regulated upon $GABA_AR$ blockade. However, these findings were not investigated further.

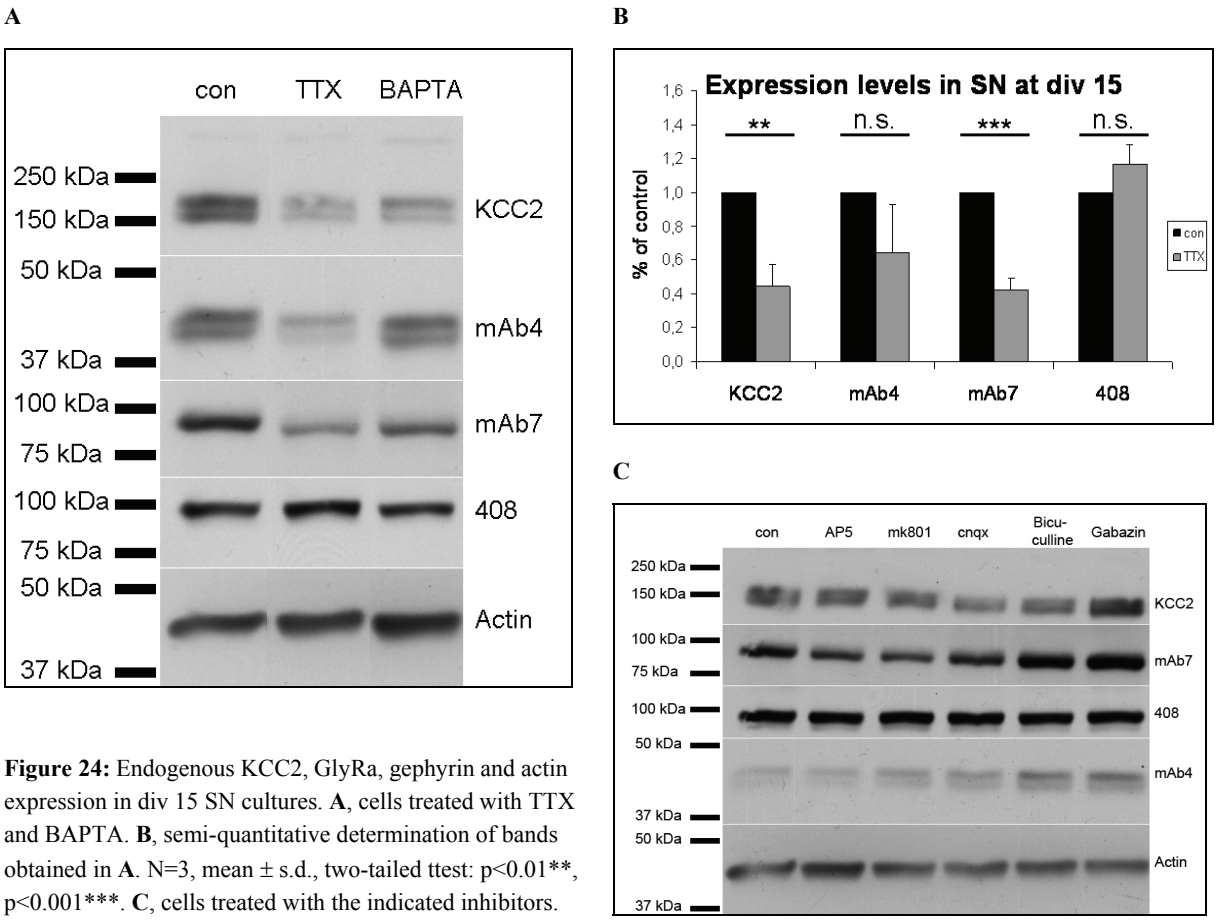

Figure 24: Endogenous KCC2, GlyRa, gephyrin and actin expression in div 15 SN cultures. **A**, cells treated with TTX and BAPTA. **B**, semi-quantitative determination of bands obtained in **A**. N=3, mean ± s.d., two-tailed ttest: $p<0.01$**, $p<0.001$***. **C**, cells treated with the indicated inhibitors.

In addition, different blockers for Ca^{2+}-channels were used. EGTA binds the entire free Ca^{2+} of the medium but is not able to enter the cell. EGTA (5 mmol/l) as well as verapamil (1 µmol/l) and nifedipine (20 µmol/l) were applied the day before lysates were taken (Figure 25A). KCC2 expression was not affected by application of these drugs but interestingly, KCC2 oligomers (KCC2/oligo) were formed to a significant higher extent (Figure 25B). Because mAb7 signal completely is abolished upon EGTA application and decreased following BAPTA application (but not 408 signal, Figure 25A), it may be that gephyrin is modified by e.g. phosphorylation. This implies mAb7 to be a phosphorylation-specific antibody. To check this consideration, the phosphorylation-specific antibody Phospho-S6

Ribosomal Protein (P-S6) was applied to the immunoblot. In fact, the signal was decreased or almost completely abolished in EGTA- and BAPTA-treated cultures (Figure 25C). Therefore, it is highly probable that mAb7 is phospho-specific and that loss of free Ca^{2+} affects the phosphorylation states of certain proteins such as gephyrin. Thus, the activity of kinases and/or phosphatases might be concerned. At least, KCC2 oligomers seem to be dependent on either phosphorylation or another influence arisen by Ca^{2+}.

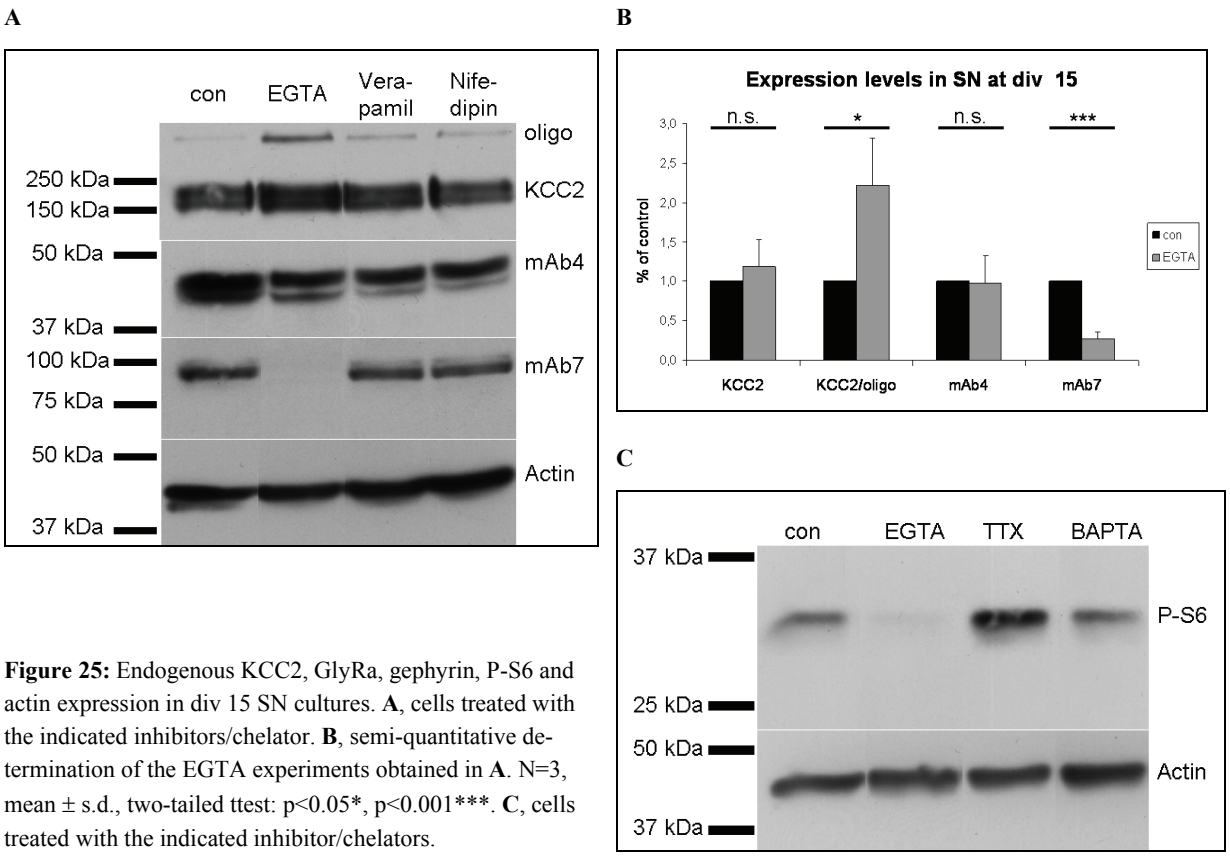

Figure 25: Endogenous KCC2, GlyRa, gephyrin, P-S6 and actin expression in div 15 SN cultures. **A**, cells treated with the indicated inhibitors/chelator. **B**, semi-quantitative determination of the EGTA experiments obtained in **A**. N=3, mean ± s.d., two-tailed ttest: $p<0.05$*, $p<0.001$***. **C**, cells treated with the indicated inhibitor/chelators.

Subsequently, the opposite effect should be achieved by treating cells grown in glycine-free medium with 2 mmol/l glycine over night. Cells grown in NB^{++++} as well as cells grown in glycine-free NB^{++++} served as controls. The expectation was an increased KCC2 expression in glycine treated or glycine-containing cells compared to cells grown in glycine-free medium. Unfortunately, this speculation was not confirmed (Figure 26).

A

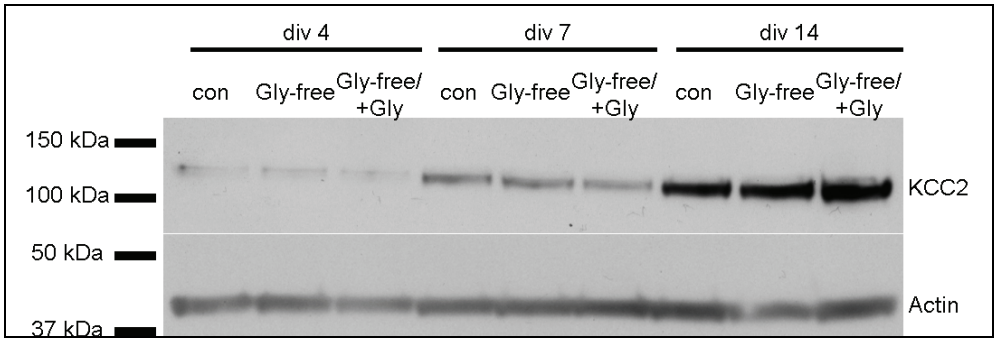

B

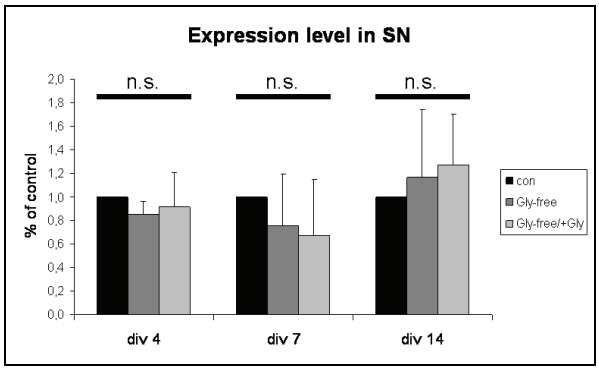

Figure 26: Glycine treatment. **A**, endogenous KCC2 and actin expression in div 4, 7 and 15 SN cultures kept in NB^{++++} (con), glycine-free NB^{++++} (Gly-free) or glycine-free NB^{++++} and treated with glycine over night (Gly-free/+Gly). **B**, semi-quantitative determination of **A**. N=3, mean ± s.d. ANOVA.

At the end, the assumption came up that not only GlyR activity influences KCC2 expression but rather KCC2 expression or activity influences GlyR expression or even the subunit switch. Therefore, the next step was to knock down KCC2 expression and analyze the upcoming effects.

4.5. Effects of KCC2 Knockdown

To test whether KCC2 influences the subunit switch of the GlyR, its expression in SN cultures ought to be silenced by RNA interference (RNAi). RNAi represents a complex process of small RNAs of 21-25 nucleotides in length evoking sequence-specific silencing of genetic information. In metazoa the silencing can occur either via degradation of the mRNA or translational inhibition. Transcribed in the nucleus, the pri-miRNA (primary micro RNA) is first processed by an enzyme called Drosha resulting in the pre-miRNA. Exportin 5 guides the pre-miRNA into the cytoplasm where it is further processed by Dicer. Afterwards, the unwound and single-stranded siRNA forms a complex with RISC (RNA-induced silencing complex), binds residing in the complex to the targeted mRNA and leads to

its degradation or translational repression. In this study, short hairpin RNAs (shRNAs), which belong to the siRNAs, were used to evoke KCC2 silencing. Therefore, four different shRNA oligos composed of sequences complementary to the KCC2 sequence were designed.

4.5.1. Design of shRNA sequences

4.5.1.1. Identification of silencing Knockdown-Sequences

HEK cells were transfected with both, a KCC2 expression construct (KCC2_rn in pEFGP-N3; short: KCC2-N3) and the vector pCMV-U6 expressing the accordant shRNAs under the U6 promoter (pCMV-U6_KCC2kd, short: KCC2kd). Control cells only were transfected with the KCC2 expression construct. Untransfected cells served as an additional control. The immunoblot shows that only the constructs KCC2kd2 and KCC2kd3 are able to direct a silencing effect in KCC2 expression (Figure 27). The other two oligos have no effect. Due to these results, only the KCC2kd2 and KCC2kd3 oligos together with the U6 promoter are cut off the pCMV-U6 vector and ligated into the pFSGW vector to create lentiviral particles for infecting neurons.

A

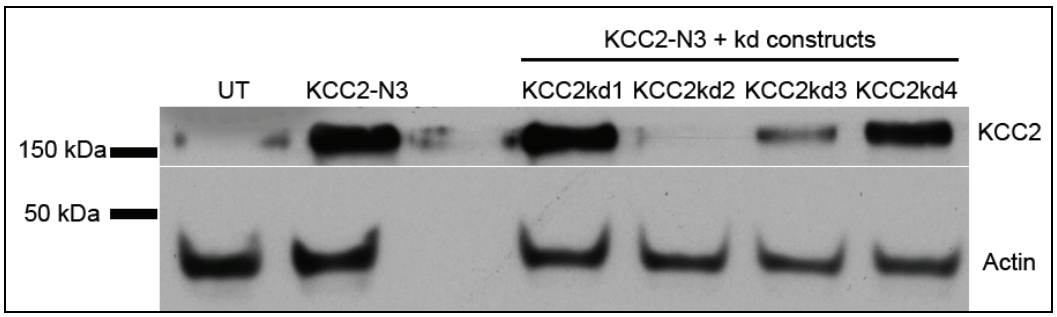

B

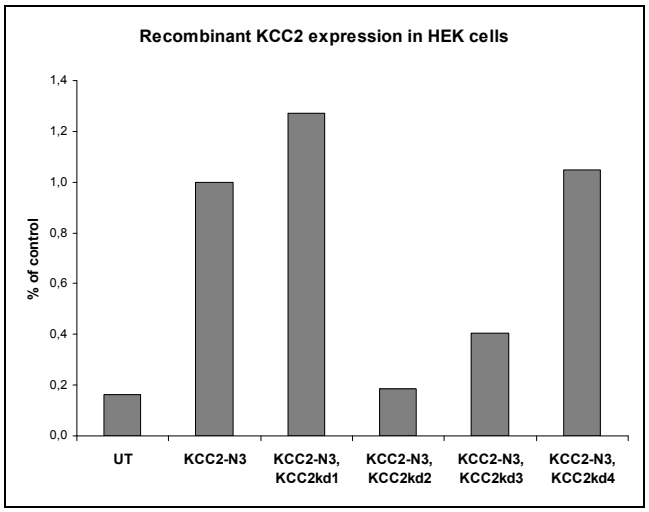

Figure 27: Recombinant KCC2 expression in either untransfected HEK293 cells (UT) and HEK cells transfected with the indicated constructs. **A**, KCC2 and endogenous actin expression. **B**, quantification of the immunoblots shown in **A**.

Additional to the knockdown constructs, it was necessary to create functional non-silencing sequences.

4.5.1.2. Determination of non-silencing controls

As a control additional to uninfected cells, a mismatch construct (KCC2kd2mm) appropriate to the most potent knockdown oligo KCC2kd2 was created. The sequence of is similar to that of KCC2kd2 but contains three mutations. These mismatches avoid binding of the shRNA to the targeted mRNA and thus silencing of KCC2. For testing the construct, HEK cells were co-transfected with the expression construct KCC2-N3 and pCMV-U6_KCC2kd2mm or as a control the empty pCMV-U6 vector. Protein extracts of the cells were taken and analyzed via immunoblot (Figure 28). The diagram clearly shows that the mismatch sequence is not able to generate a knockdown of KCC2. The KCC2 expression in cells co-transfected with KCC2kd2mm and KCC2-N3 is as strong as in cells co-transfected with KCC2-N3 and pCMV-U6, which serve as control cells. In contrast, KCC2kd2 induces an almost complete loss of recombinant KCC2 expression in HEK cells co-transfected with KCC2-N3 (Figure 28B).

A

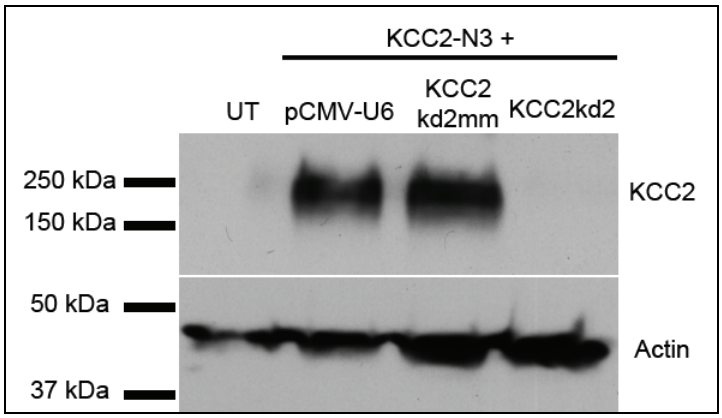

B

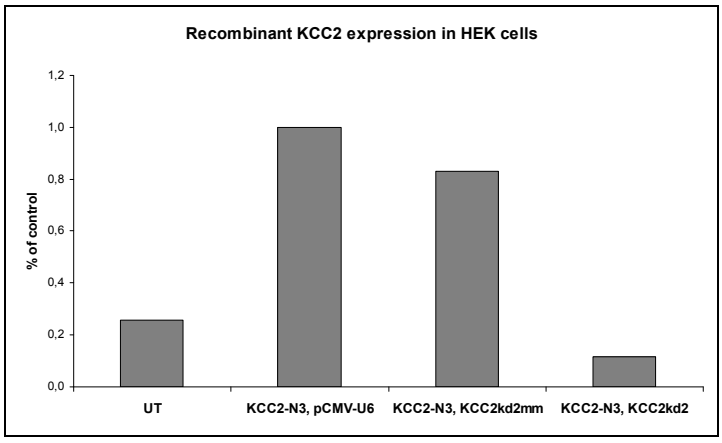

Figure 28: Recombinant KCC2 expression in either untransfected HEK293 cells (UT) or HEK cells transfected with the indicated constructs. **A**, KCC2 and endogenous actin expression. **B**, quantification of the immunoblots shown in **A**.

As a rescue control, an expression construct of KCC2-N3 containing three silent mutations compared to the original KCC2-N3 was created. These mutations are localized in exactly the same region where the shRNA of KCC2kd2 is able to bind. Occupying these mutations, the so-called KCC2-N3mut should be resistant against the silencing effect. Indeed, recombinant KCC2 expression, which was abolished in cells co-transfected with KCC2kd2 and KCC2-N3, was not affected in cells co-transfected with KCC2kd2 and KCC2-N3mut (Figure 29).

A

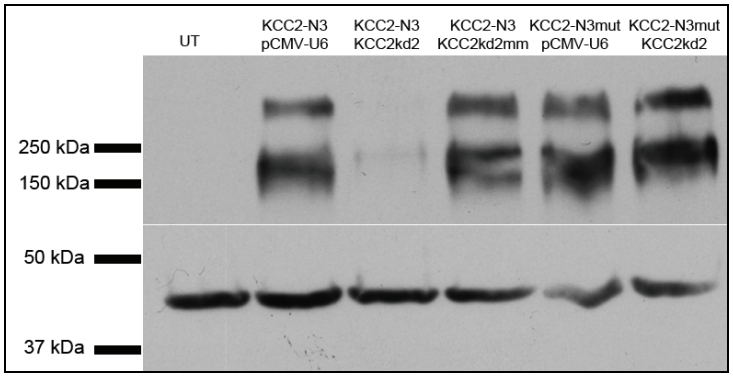

B

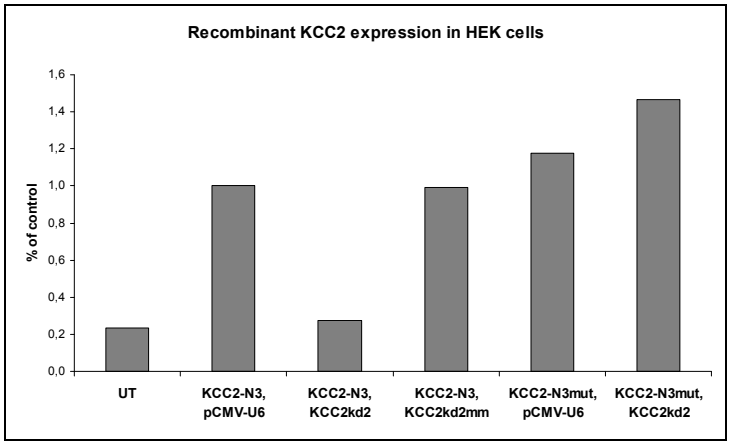

Figure 29: Recombinant KCC2 expression in either untransfected HEK293 cells (UT) or HEK cells transfected with the indicated constructs. **A**, KCC2 (upper panel) and endogenous actin expression (lower panel). **B**, quantification of the immunoblots shown in **A**.

Transfections, SDS-PAGE and immunoblotting were performed by Nicolai Nagelpusch.

Unfortunately, it was not possible to clone the KCC2-N3mut sequence into the viral pFSGW vector in this thesis. Hence, it could not be used as a rescue control in SNs. Nevertheless, the HEK cell studies demonstrate that the mutated construct is functional and resistant against the shRNA oligo. As shown in immunoblot studies there are no KCC2 or rather GFP immunoreactivities in untransfected HEK cells (Figure 30A). Control cells co-transfected with KCC2-N3 and pCMV-U6 exhibit a normal GFP and KCC2 signal (Figure 30B), whereas cells co-transfected with KCC2-N3 and KCC2kd2 develop a much lower signal (Figure 30C). Cells co-transfected with KCC2-N3 and KCC2kd2mm reveal a normal KCC2 and GFP expression because the mismatch sequence is not able to silence KCC2 expression (Figure 30D). To demonstrate the normal expression of the mutated construct, cells were co-transfected with KCC2-N3mut and pCMV-U6 (Figure 30E). At last, cells were co-transfected with KCC2-N3mut and KCC2kd2 to show that the shRNA is indeed no longer able to bind to the KCC2 RNA and thus induce a knockdown of KCC2 expression (Figure 30F).

Towards these findings in HEK cells, the effects of the lentiviral particles containing the knockdown sequences onto KCC2 expression in SNs and HCNs ought to be investigated next.

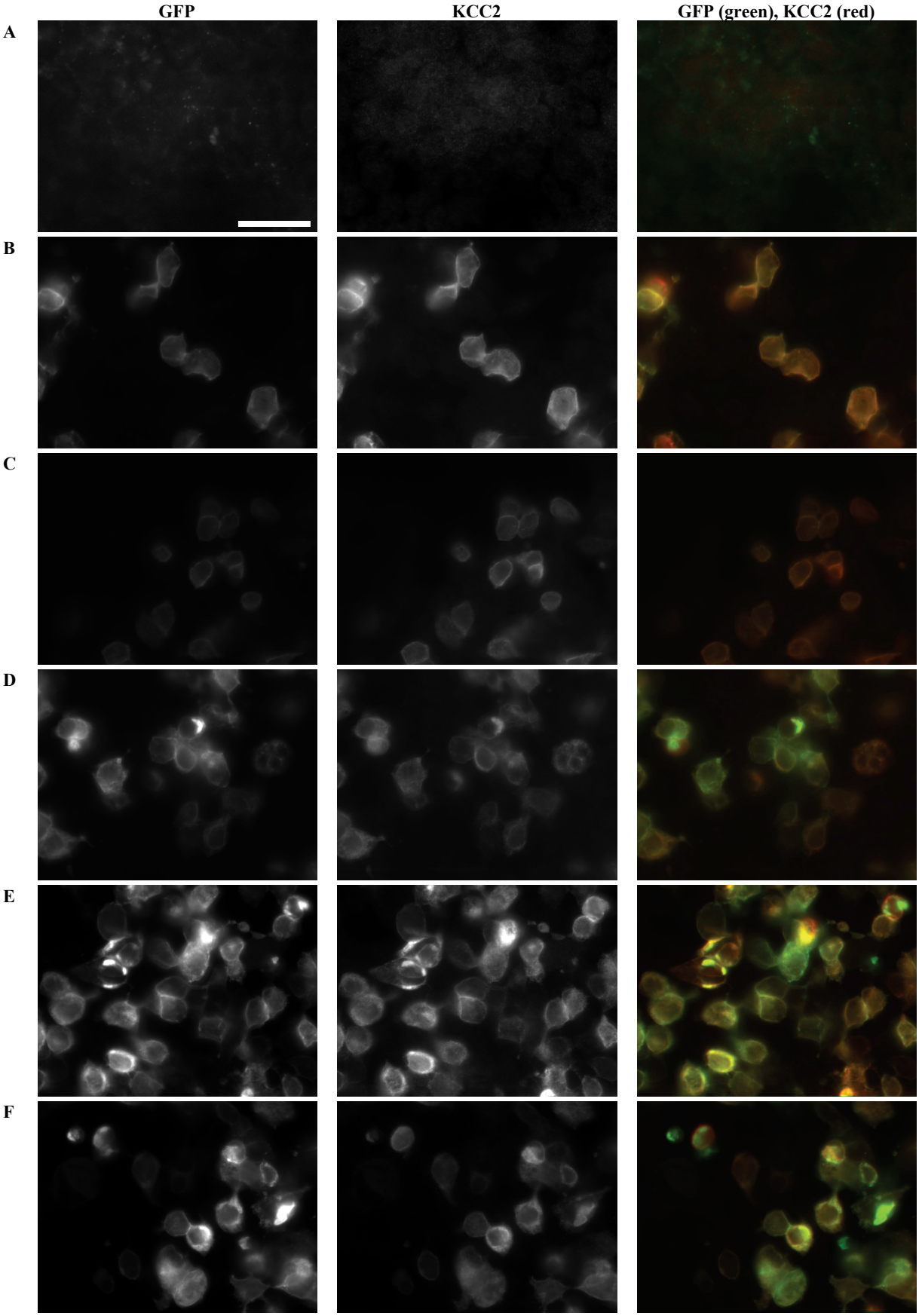

Figure 30: Recombinant GFP- and KCC2-immunoreactivities in HEK cells. **A**, untransfected cells. Cells co-transfected with KCC2-N3 and pCMV-U6 (**B**) KCC2-N3 and KCC2kd2 (**C**), KCC2-N3 and KCC2kd2mm (**D**), KCC2-N3mut and pCMV-U6 (**E**), KCC2-N3mut and KCC2kd2 (**F**). Scale bar=30 µm. Transfections and images were performed by Nicolai Nagelpusch.

4.5.2. Effects of KCC2 knockdown in HCNs and SNs

For the production of lentiviral particles HEK293T cells were transfected with three different plasmids: pFSGW, expressing the shRNA sequence under the synapsin promoter, pVSVG, the envelope vector and finally pCMV Δ8.9, the packaging vector for the virus. Given, that all three constructs are expressed in the cell, the virus particles carrying the shRNA are allowed to form and break out of the cell. Hence, they are found in the medium, can be isolated and stored at -80°C. SNs as well as HCNs were infected with lentiviral particles. Therefore, one aliquot of virus was gently thawed on ice, filled with NB to 1 ml final volume (virus suspension) and was added to the medium of the neurons. The cells were infected at div 4 and treated with AraC to stop glial proliferation at div 11. The analysis took place at div 8, 15, 22 or 36.

4.5.2.1. Effects of KCC2-Knockdown in HCNs

This short investigation should simply show that the shRNA also induces a down regulation of KCC2 in HCNs. Cells were infected as indicated and analyzed at div 20. The experiment was done once. A clear knockdown of KCC2 appears in the infected cultures (Figure 31). Gephyrin expression seems not to be decreased in the form, antibody 408 recognizes, but mAb7 signal is reduced. This supports the idea that at least two forms of gephyrin exist. These two forms probably differ in their phosphorylation state. The GlyRa subunits also are down regulated. Generally, more amount of virus suspension (80 µl) is necessary to evoke down regulation of other genes than KCC2.

Because the GlyR is mainly expressed in spinal cord, all following studies were exclusively done using SN cultures.

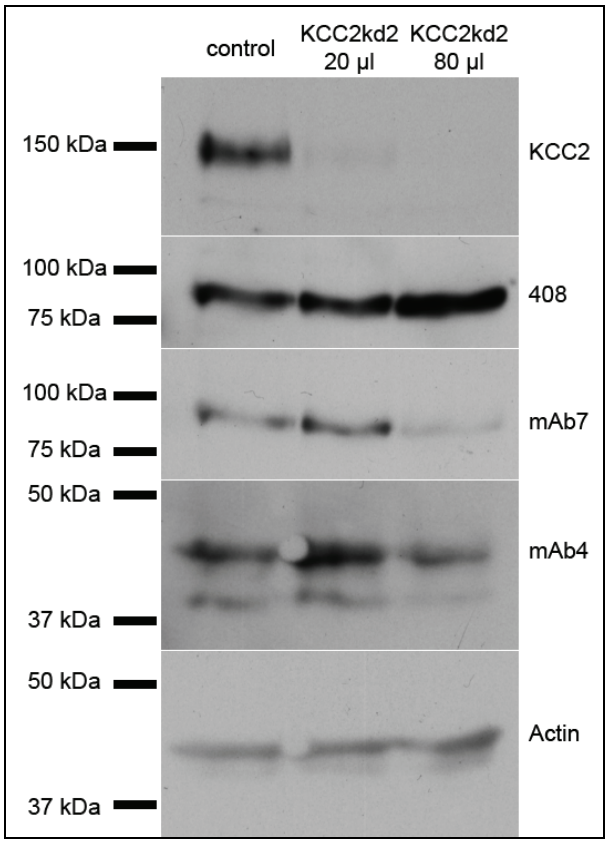

Figure 31: Endogenous KCC2, gephyrin (mAb7 and 408), GlyRa (mAb4) and actin expression in div 20 HCNs after infection with KCC2kd2.

4.5.2.2. Effects of KCC2-Knockdown in SNs

The effects of the KCC2 knockdown in SNs were examined in much more detail. Cells were infected, treated with AraC and lysed as mentioned above. Immunostainings as well as immunoblots were performed.

Semi-quantitative determination of receptor and KCC2 protein

For the immunoblots, protein extracts were taken at div 15. For the first experiments, uninfected cells served as control. Later cells infected with KCC2kd2mm virus were used as control cells. Different proteins were tested for altered expression. The first thing to clarify was the existence of the knockdown effect and which virus concentration should be used to achieve an optimal silencing effect without killing to many cells (Figure 32). Furthermore, mAb4 recognizing all GlyRa subunits, should shed light on the effect of KCC2 knockdown onto the GlyR. Indeed, the GlyRa subunit expression decreases according to augmented virus concentration (Figure 32). The same is true for gephyrin represented by the mAb7 antibody. Gephyrin provides the connection of the GlyR to the cytoskeleton (Poulopoulos et al. 2009). Interestingly, only mAb7 exhibits that effect, 408 in contrast does not show any significant change in expression. Actin was thereby used as loading control and hence for normalization in the statistics

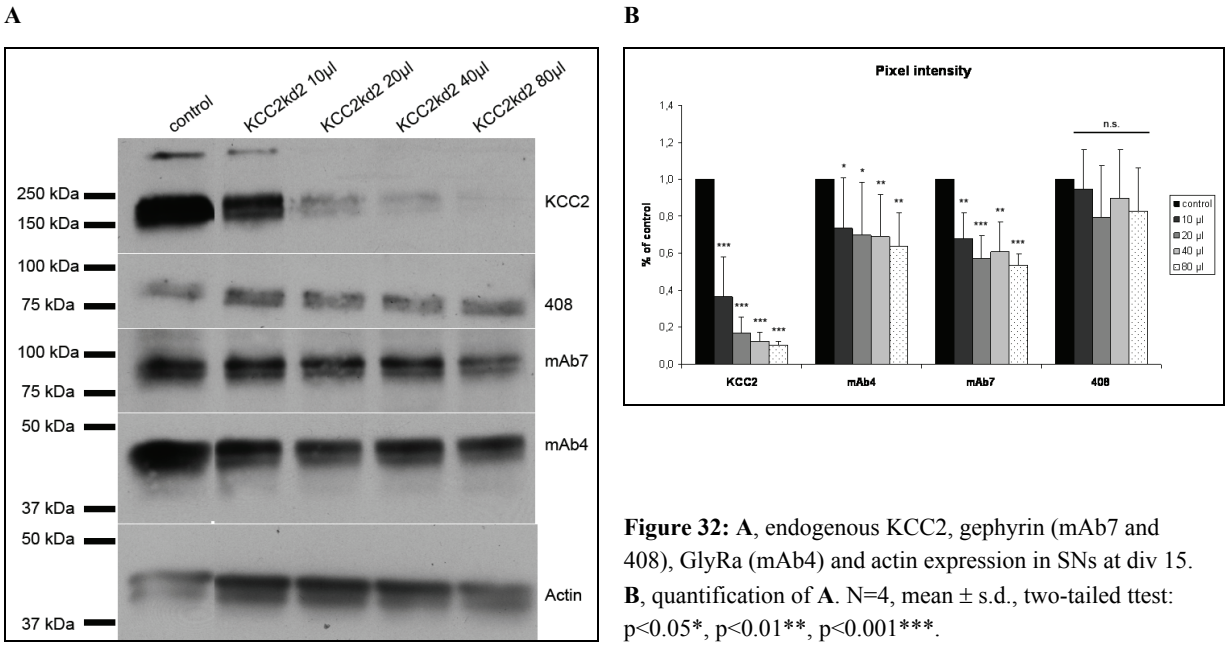

Figure 32: A, endogenous KCC2, gephyrin (mAb7 and 408), GlyRa (mAb4) and actin expression in SNs at div 15. **B**, quantification of **A**. N=4, mean ± s.d., two-tailed ttest: p<0.05*, p<0.01**, p<0.001***.

According to these observations, the question arises if other receptors also are affected by the knockdown of KCC2. Expression of NMDAR1 is significantly increased in knockdown cells (Figure 33). The GlyRa1 subunit expression decreases according to augmenting virus titre but the reduction only becomes significant at the highest virus concentration. Expression of the GlyRa2 subunit remains unchanged.

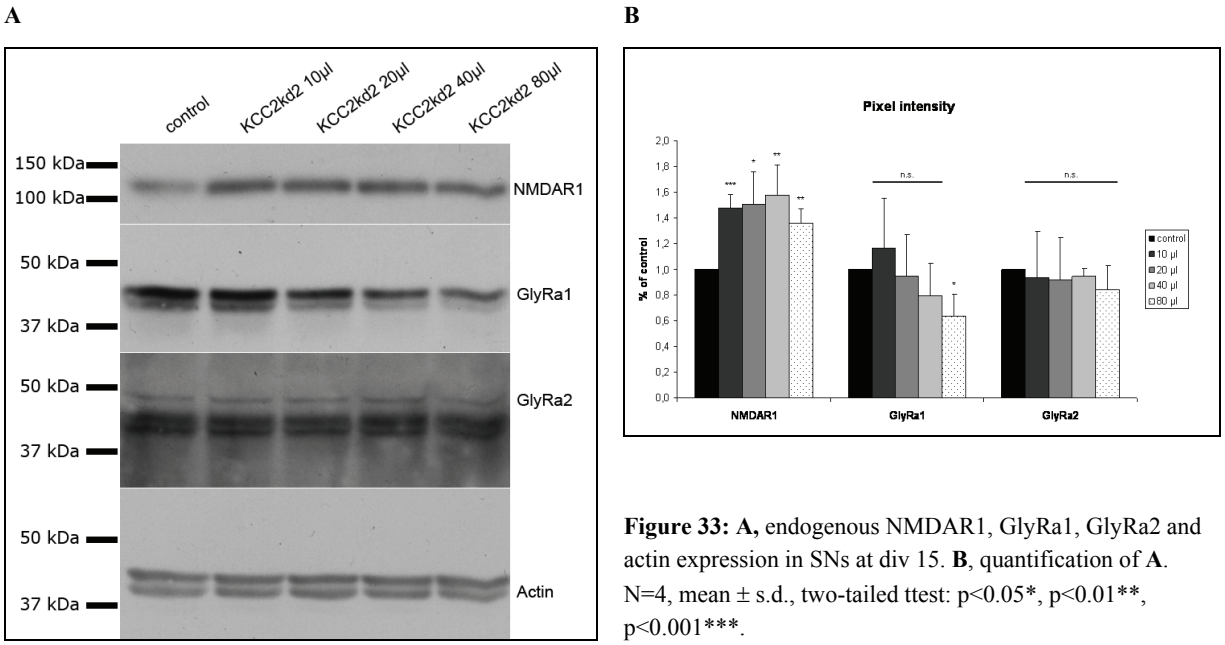

Figure 33: A, endogenous NMDAR1, GlyRa1, GlyRa2 and actin expression in SNs at div 15. **B**, quantification of **A**. N=4, mean ± s.d., two-tailed ttest: $p<0.05$*, $p<0.01$**, $p<0.001$***.

For immunoreactivity localization, only cells infected with KCC2kd2mm were used as control. Therefore, it was necessary to determine whether the mismatch sequence evokes significant changes in protein expression during time.

Determination of receptor and KCC2 protein in control, mismatch and knockdown cultures

To test the possible effects of the mismatch sequence, SNs were infected with KCC2kd2 or KCC2kd2mm or remained uninfected. Protein levels of KCC2, GlyRa (mAb4), gephyrin (mAb7 and 408), GlyRa2 and tubulin were determined at three different time points (div 8, 15 and 22, Figure 34A). Via semi-quantitative analysis (Figure 34B-D), the relative differences in the protein expression levels of infected cells could be compared to uninfected cells (con).

On the one hand, the analysis clarifies that at all investigated time points the mismatch sequence does not evoke any significant changes in protein expression. On the other hand, it becomes clear that the effects of the knockdown reach their maximum not before the third week in culture (div 22). The down regulation of KCC2 expression remains from div 15 on the lowest level (20% of control and mismatch). However, the effects of the knockdown onto the GlyR and gephyrin come in later. Gephy-

rin expression even is significantly up regulated at div 8. One week later in turn, mAb7 signal is significantly decreased. After three weeks in culture finally, GlyR subunits and gephyrin are significantly down regulated. The expression of the juvenile GlyRa2 subunit and the 408 signal remain unchanged during the whole time of investigation.

A

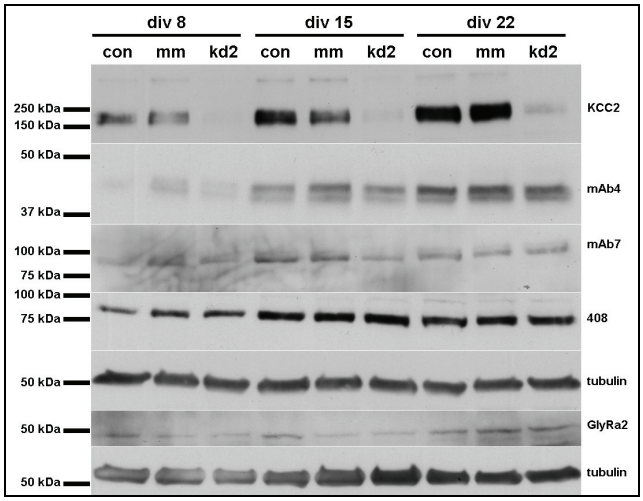

B: div 8

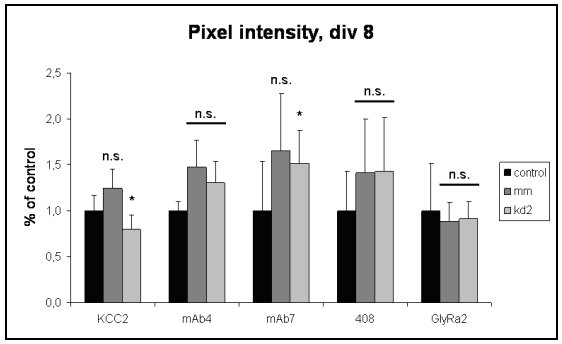

C: div 15

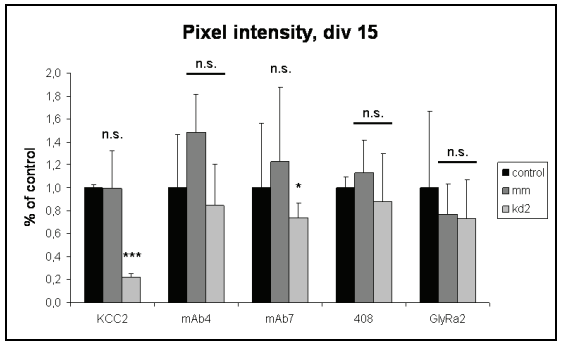

D: div22

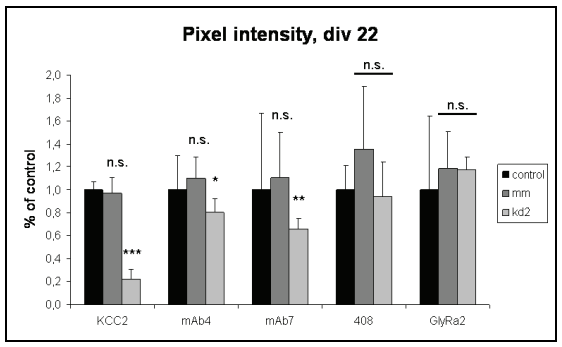

Figure 34: A, endogenous KCC2, GlyRa (mAb4), gephyrin (mAb7 and 408), GlyRa2 and tubulin expression in SNs at div 8, 15 and 22. **B**, **C** and **D** quantifications of **A** respectively. N=3, mean ± s.d., two-tailed ttest: $p<0.05$*, $p<0.01$**, $p<0.001$***. con: uninfected cells, mm: cells infected with KCC2kd2mm, kd2: cells infected with KCC2kd2.

After these immunoblot studies, the GlyR subunits and some other synaptic markers should be shown as immunoreactivities in fixed cells. A more pronounced effect is expected from those studies because thereby it is possible to discriminate between infected and uninfected cells via GFP expression. In immunoblot studies, the results consist of a mixture of infected and uninfected cells.

Localization of immunoreactivities

For visualizing the GlyRa subunits, antibody mAb4 was used. MAb2 specifically stains GlyRa1 clusters and mAb7 represents gephyrin. Moreover, GlyRa2, $GABA_AR$, KCC2, GFP, PSD 95 and VIAAT were visualized. Illustration of KCC2 sheds light on the knockdown efficiency, GFP signal reveals infected cells, PSD°95 serves as a control for synaptic proteins being independent of the GlyR complex and VIAAT gives information about the presynaptic component. First, infection of the cells and an efficient knockdown of KCC2 ought to be confirmed.

Verification of Infection and KCC2 Knockdown

To show cells carrying the virus, cultures were stained for GFP. Because the pure green signal of the infected and thus GFP expressing cells was too low, the GFP signal was additionally amplified by a well working FITC-conjugated GFP antibody. Information about a KCC2 knockdown evoked by KCC2kd2 but not by KCC2kd2mm gave the KCC2-1 antibody. Indeed, the cells of the mismatch cultures were infected (green) and KCC2 positive (red) at the same time. However, cells infected by KCC2kd2 virus do not exhibit normal or rather any KCC2 expression. For the statistical analysis, 11-12 pictures of GFP-positive cells were taken per culture. Subsequently the numbers of GFP-positive, KCC2-positive and both, GFP- and KCC2-positive cells were determined. For all three investigated time points (div 15, 22 and 36) the same effect appears. There is no significant difference in the number of GFP-positive cells between the two conditions. However, significant differences appear in the number of KCC2-positive cells and in the number of both KCC2- and GFP-positive cells (Figure 35, Figure 36 and Figure 37). Below, representing cells are shown.

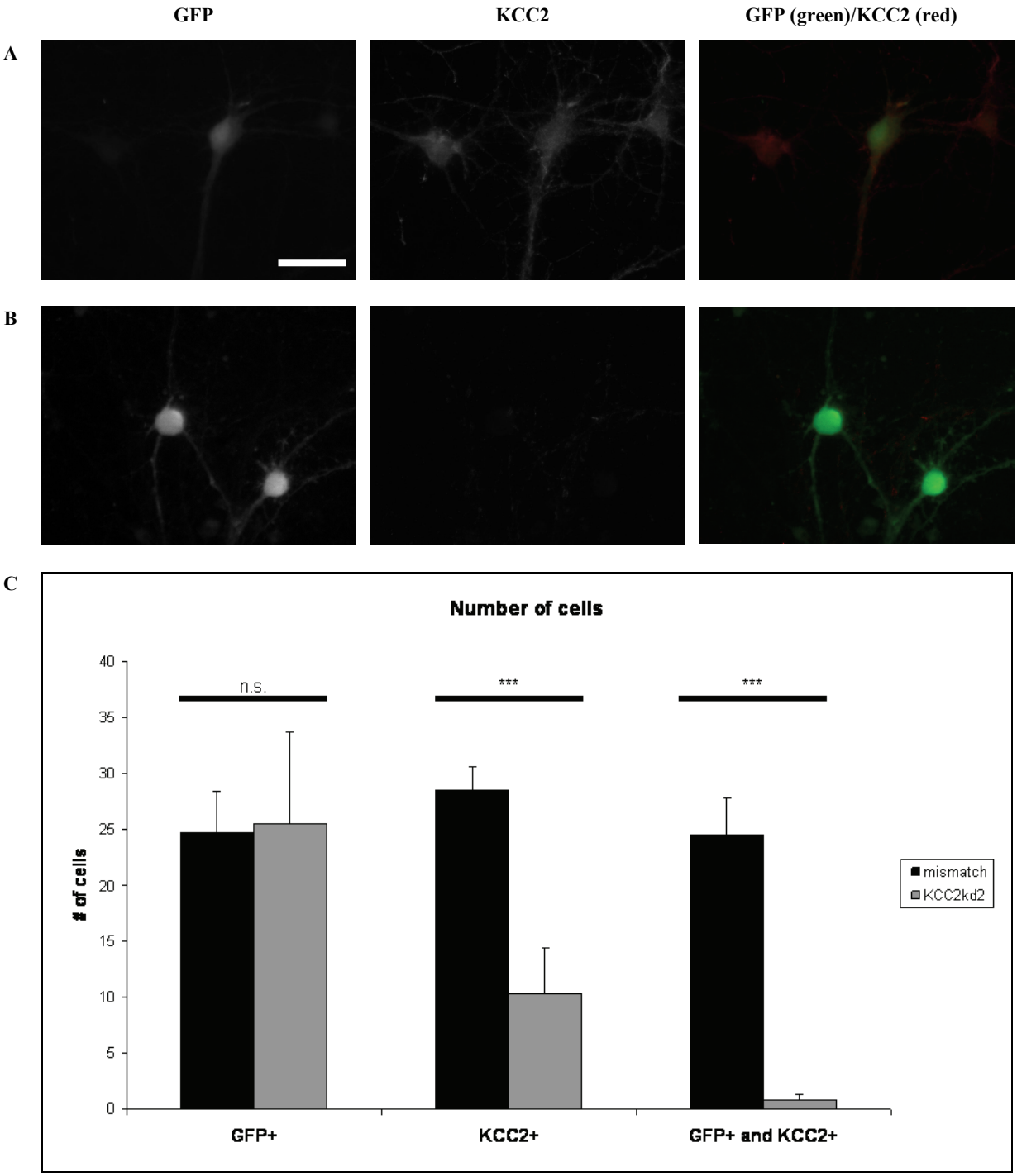

Figure 35: GFP- and endogenous KCC2-immunoreactivity in div 15 SNs. **A**, cells infected with KCC2kd2mm. **B**, cells infected with KCC2kd2. **C**, quantification of mismatch (black bars) and knockdown (gray bars) cultures. N=4, mean ± s.d., two-tailed ttest: p<0.001***, scale bar=30 µm.

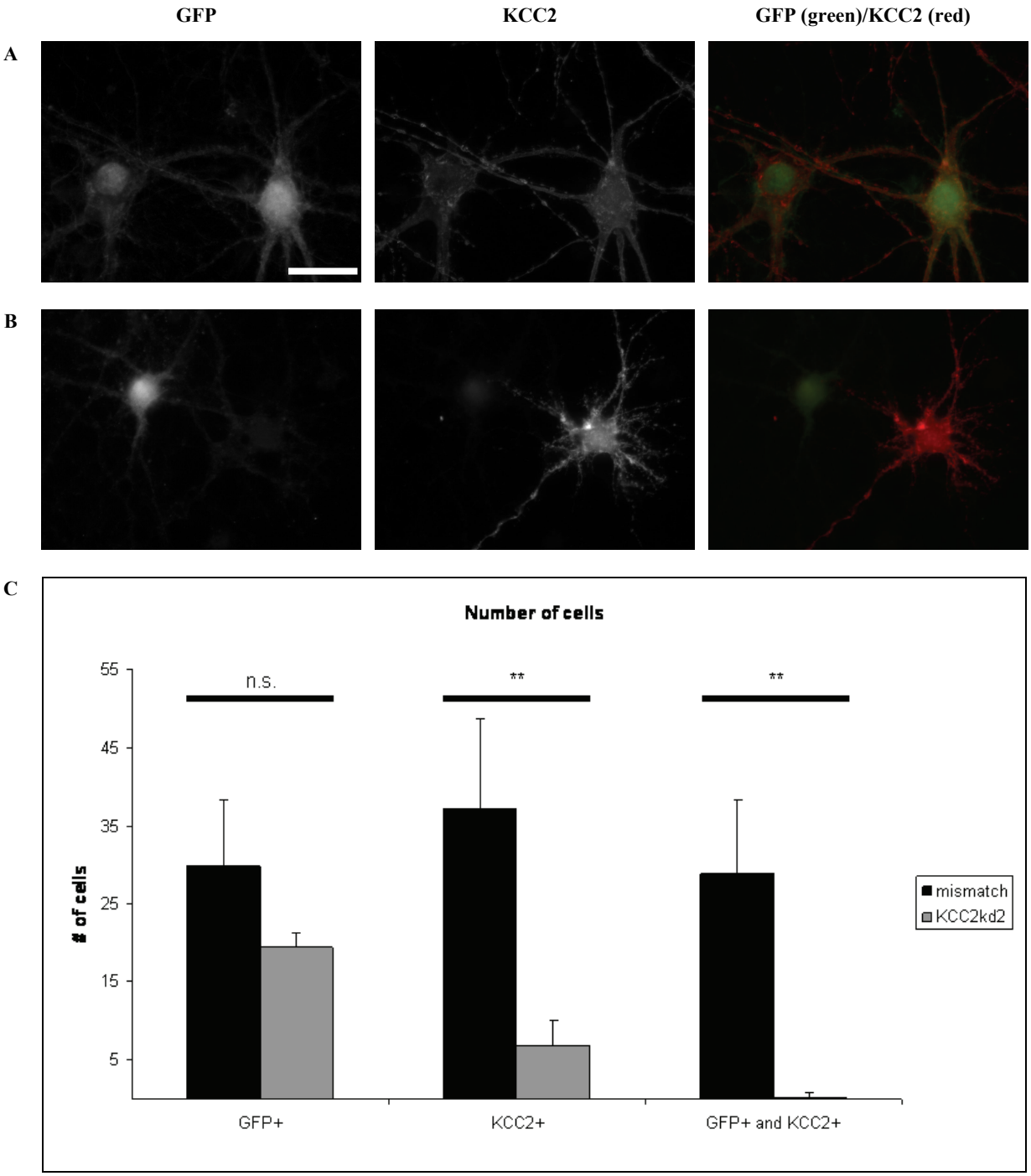

Figure 36: GFP- and endogenous KCC2-immunoreactivity in div 22 SNs. **A**, cells infected with KCC2kd2mm. **B**, cells infected with KCC2kd2. **C**, quantification of mismatch (black bars) and knockdown (gray bars) cultures. N=4, mean ± s.d., two-tailed ttest: $p<0.01$**, scale bar=30 µm.

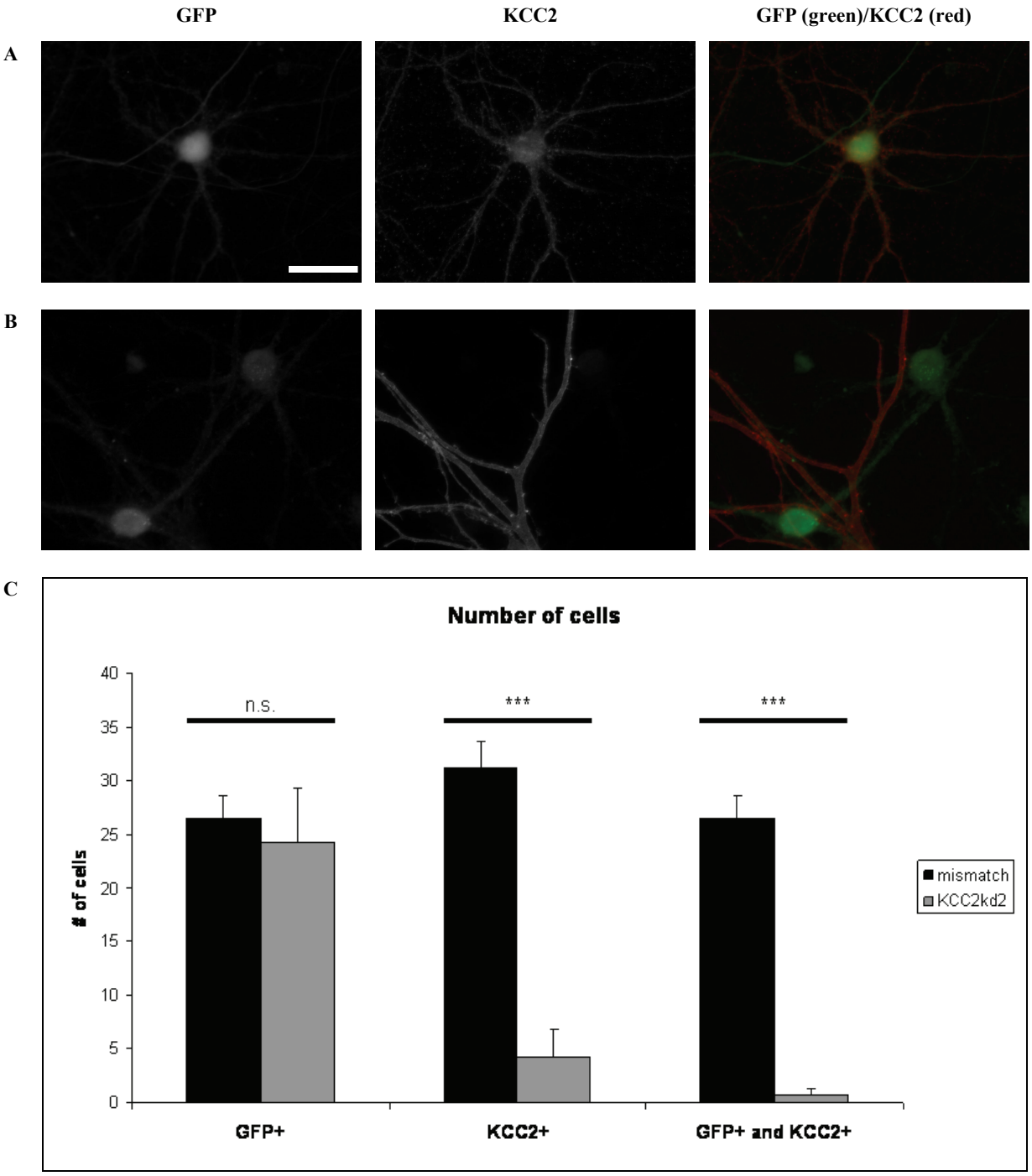

Figure 37: GFP- and endogenous KCC2-immunoreactivity in div 36 SNs. **A**, cells infected with KCC2kd2mm. **B**, cells infected with KCC2kd2. **C**, quantification of mismatch (black bars) and knockdown (gray bars) cultures. N=4, mean ± s.d., two-tailed ttest: $p<0.001$***, scale bar=30 µm.

After infection and knockdown confirmation, the next step was to investigate effects of the KCC2 knockdown onto the GlyR subunits.

Effects of KCC2 knockdown onto the GlyR alpha subunits

To achieve a first impression, cells were stained with mAb4 to examine if the knockdown has a general effect on the GlyR. Typical cells, such as used for the statistics, are presented below. For quantitative measurements, 11-12 images per culture were taken. Afterwards, regions of interest (ROIs) being 30 µm of dendrite next to the soma were determined and analyzed. Therefore, all puncta within the ROIs were scanned for their number, size (µm²) and gray value (fluorescence intensity). Per cell, all dendrites were recorded if possible. Background region was determined and thus subtracted from the signal for all pairs of mismatch and knockdown cultures individually. The following images are results of 4 independent experiments. At div 15, significant differences in number, size and gray value of GlyRa puncta occur (Figure 38).

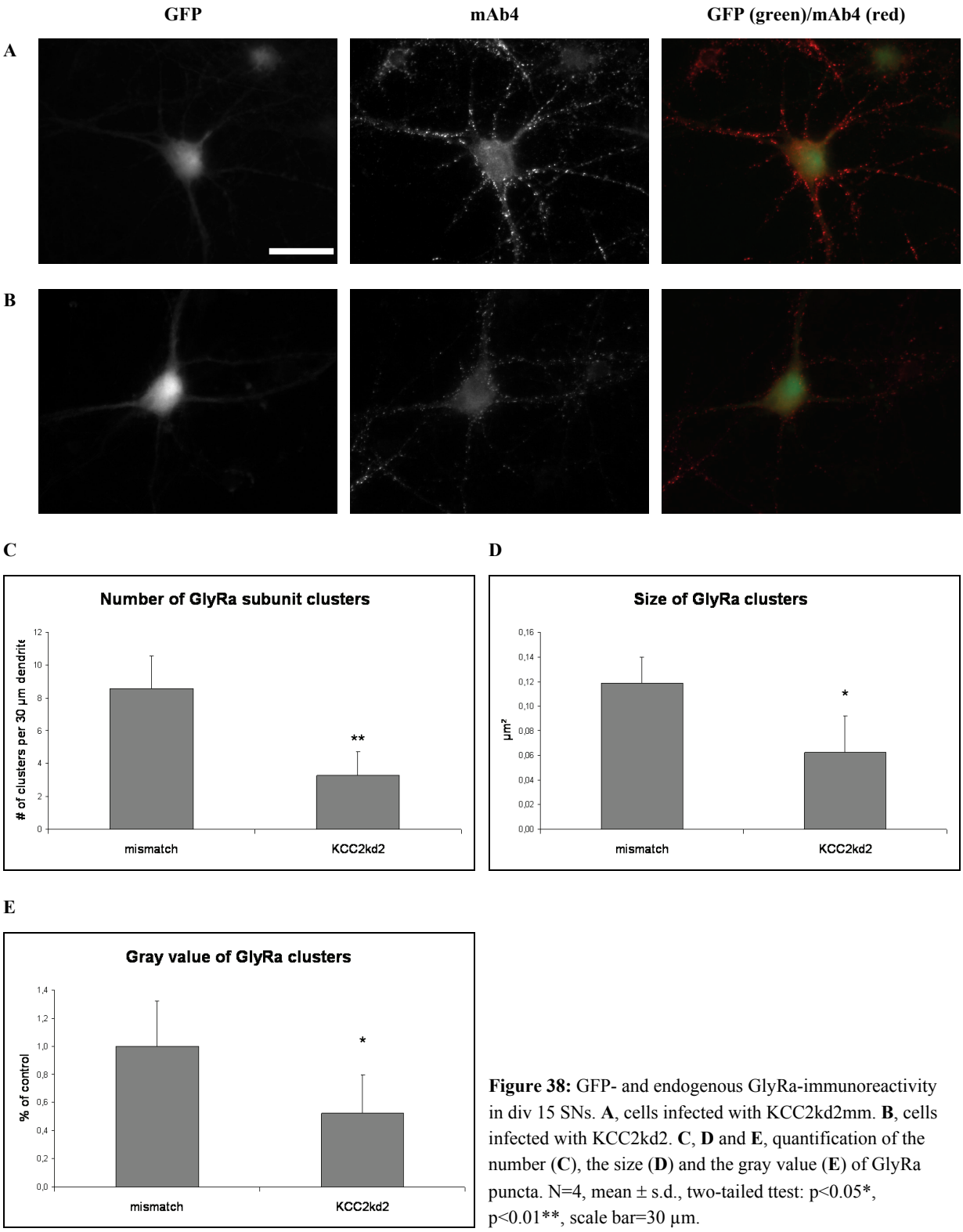

Figure 38: GFP- and endogenous GlyRa-immunoreactivity in div 15 SNs. **A**, cells infected with KCC2kd2mm. **B**, cells infected with KCC2kd2. **C**, **D** and **E**, quantification of the number (**C**), the size (**D**) and the gray value (**E**) of GlyRa puncta. N=4, mean ± s.d., two-tailed ttest: $p<0.05$*, $p<0.01$**, scale bar=30 µm.

These results reveal that there are less GlyRa clusters in knockdown cultures. The remaining clusters are smaller and glow weaker than cells of the mismatch control.

At div 22, mismatch and knockdown cultures also differ significantly in all three categories (Figure 39).

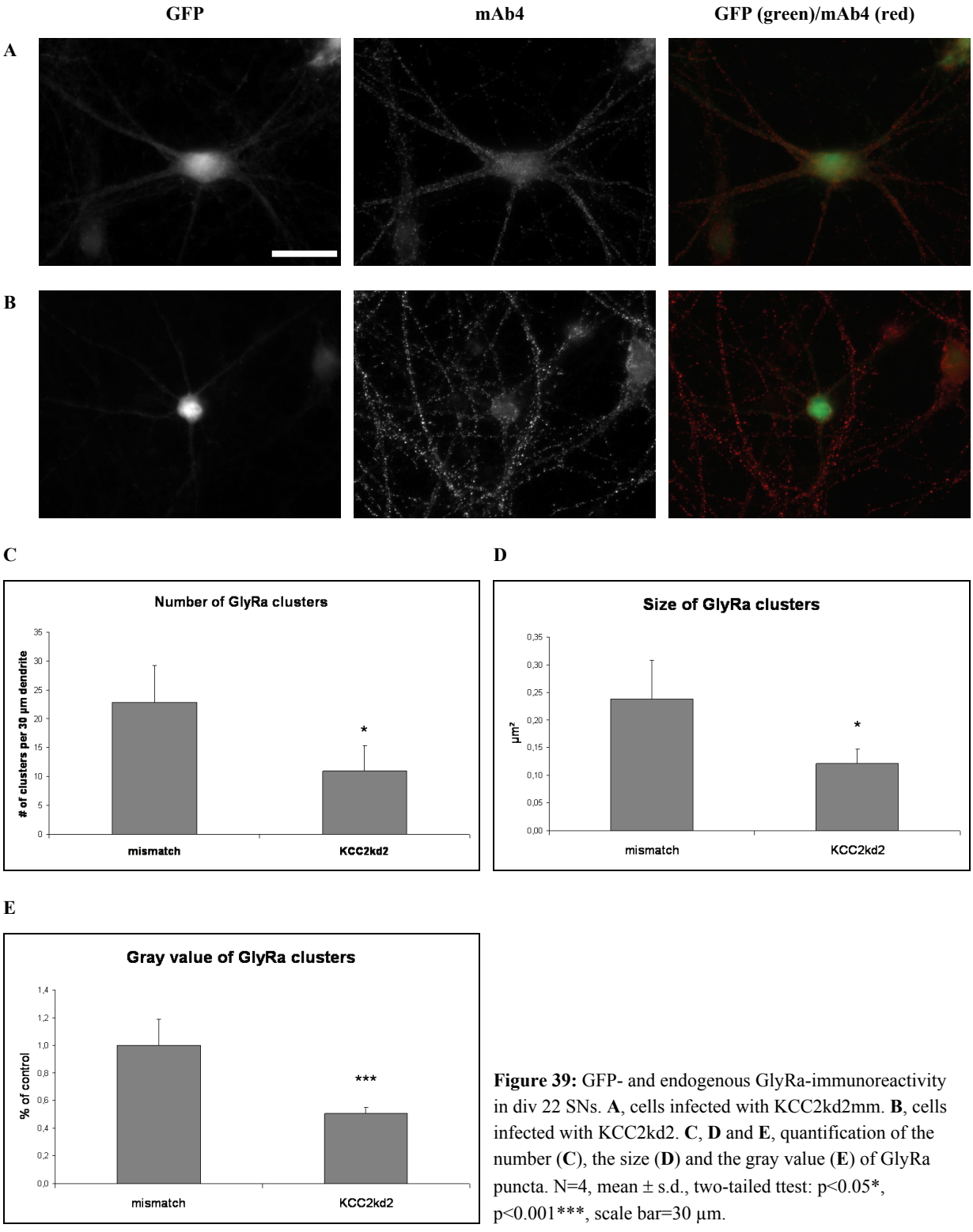

Figure 39: GFP- and endogenous GlyRa-immunoreactivity in div 22 SNs. **A**, cells infected with KCC2kd2mm. **B**, cells infected with KCC2kd2. **C**, **D** and **E**, quantification of the number (**C**), the size (**D**) and the gray value (**E**) of GlyRa puncta. N=4, mean ± s.d., two-tailed ttest: $p<0.05$*, $p<0.001$***, scale bar=30 µm.

Even towards five weeks in culture, the knockdown still is intact and directs significant alterations of the observed parameters (Figure 40).

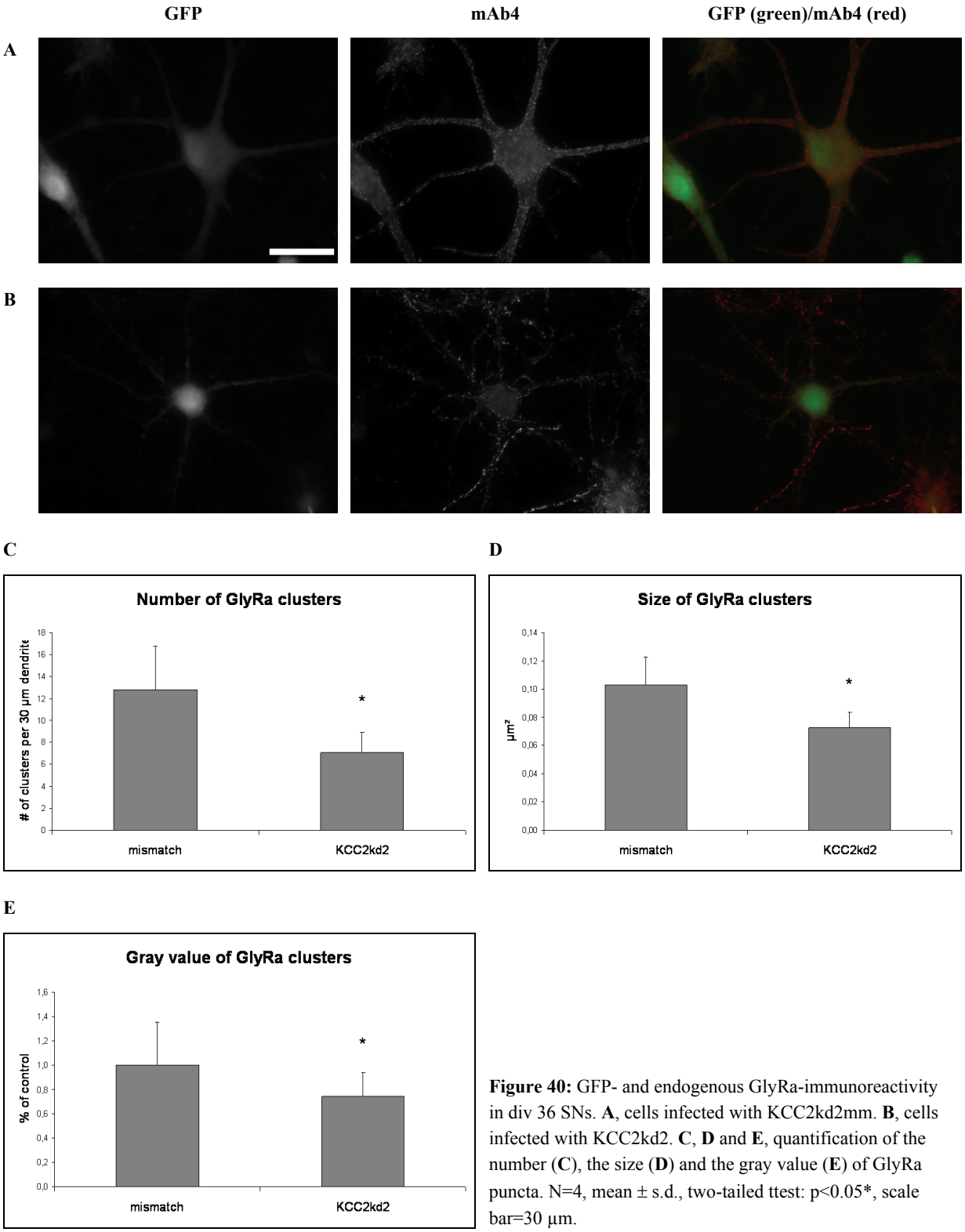

Figure 40: GFP- and endogenous GlyRa-immunoreactivity in div 36 SNs. **A**, cells infected with KCC2kd2mm. **B**, cells infected with KCC2kd2. **C**, **D** and **E**, quantification of the number (**C**), the size (**D**) and the gray value (**E**) of GlyRa puncta. N=4, mean ± s.d., two-tailed ttest: $p<0.05$*, scale bar=30 µm.

According to these observations, the effects ought to be specified more precisely. Therefore, the adult and the juvenile GlyRa subunits respectively were investigated.

Effects of KCC2 knockdown onto the adult GlyRa1 subunit

Since immunoblots already had shown that the adult GlyRa1 subunit is expressed to a lower level in knockdown cultures, its proportion was examined first. Antibody mAb2 is able to detect the adult GlyRa1 subunit specifically. The effect should turn out stronger compared to the mAb4 results, because the presumably unaltered contribution of the GlyRa2 subunit is abolished. Actually, this observation is made at div 15. Cells carrying the knockdown construct form less, smaller and weaker glowing clusters than the cells of the mismatch cultures (Figure 41).

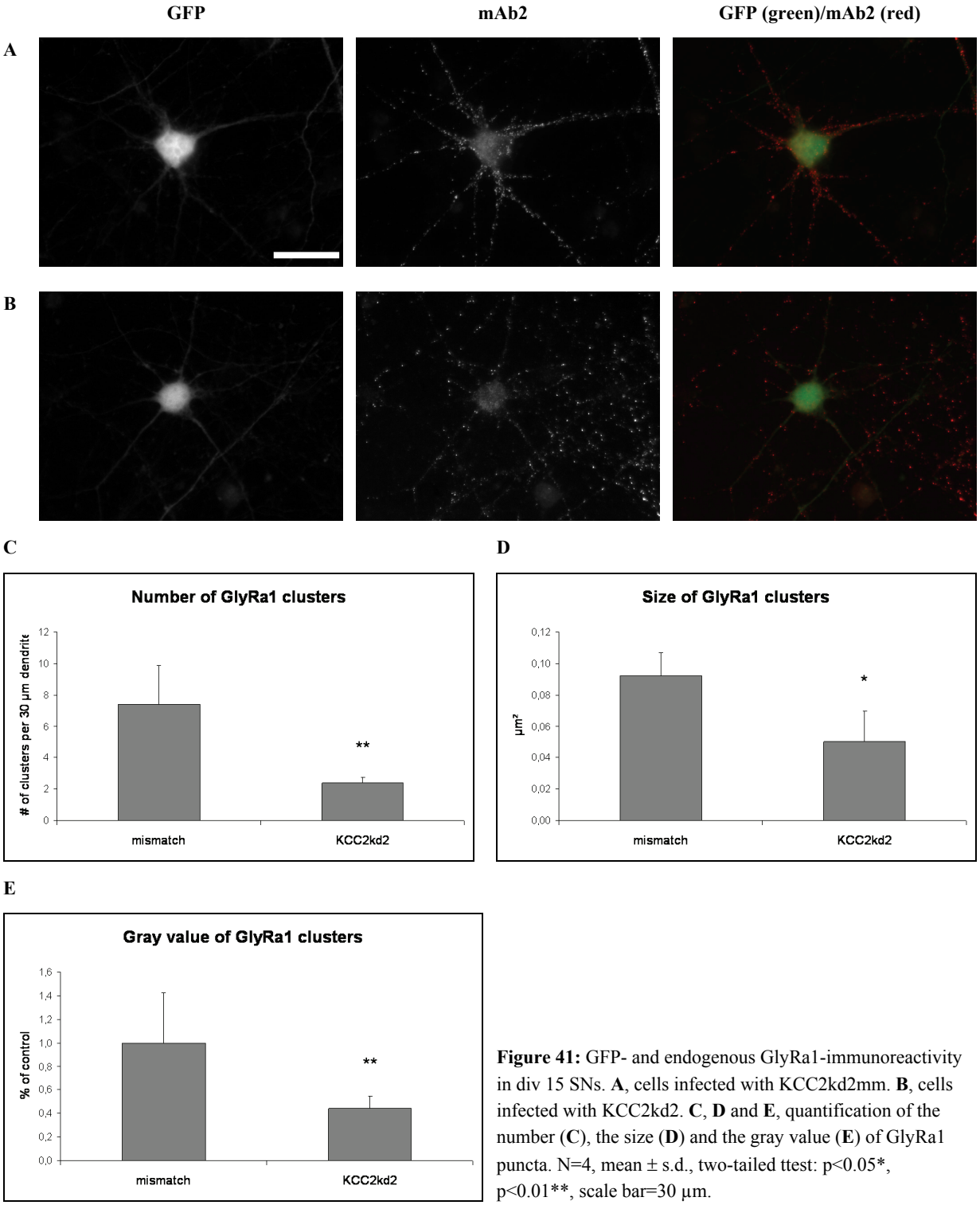

Figure 41: GFP- and endogenous GlyRa1-immunoreactivity in div 15 SNs. **A**, cells infected with KCC2kd2mm. **B**, cells infected with KCC2kd2. **C**, **D** and **E**, quantification of the number (**C**), the size (**D**) and the gray value (**E**) of GlyRa1 puncta. N=4, mean ± s.d., two-tailed ttest: $p<0.05$*, $p<0.01$**, scale bar=30 µm.

One week later in culture, the effects still are existent (Figure 42).

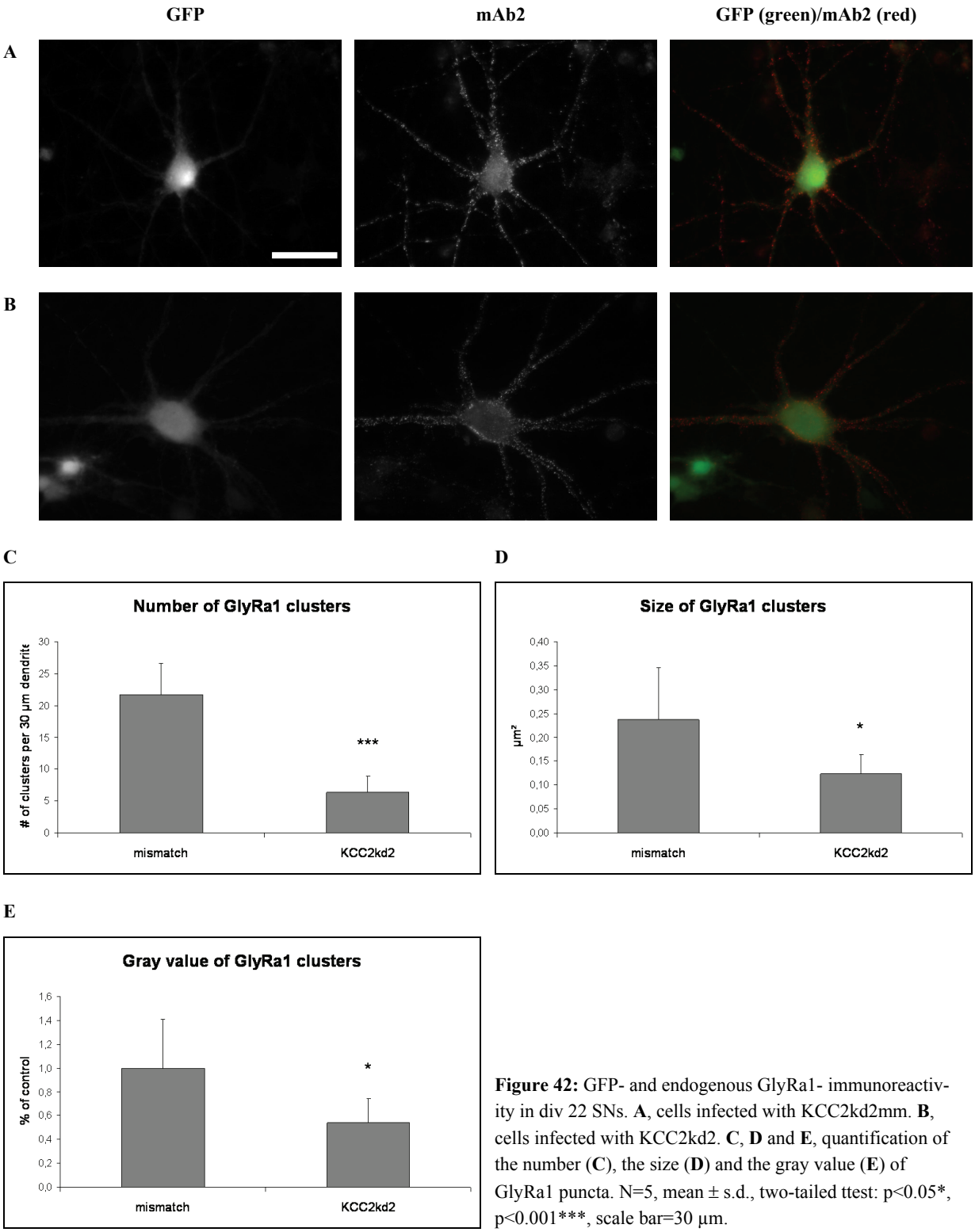

Figure 42: GFP- and endogenous GlyRa1- immunoreactivity in div 22 SNs. **A**, cells infected with KCC2kd2mm. **B**, cells infected with KCC2kd2. **C**, **D** and **E**, quantification of the number (**C**), the size (**D**) and the gray value (**E**) of GlyRa1 puncta. N=5, mean ± s.d., two-tailed ttest: $p<0.05$*, $p<0.001$***, scale bar=30 µm.

Towards five weeks in culture, there is no longer a difference in the gray value of GlyRa1 puncta between mismatch and knockdown cells. Nevertheless, there still is a less pronounced effect in the number and the size of the GlyRa1 clusters (Figure 43).

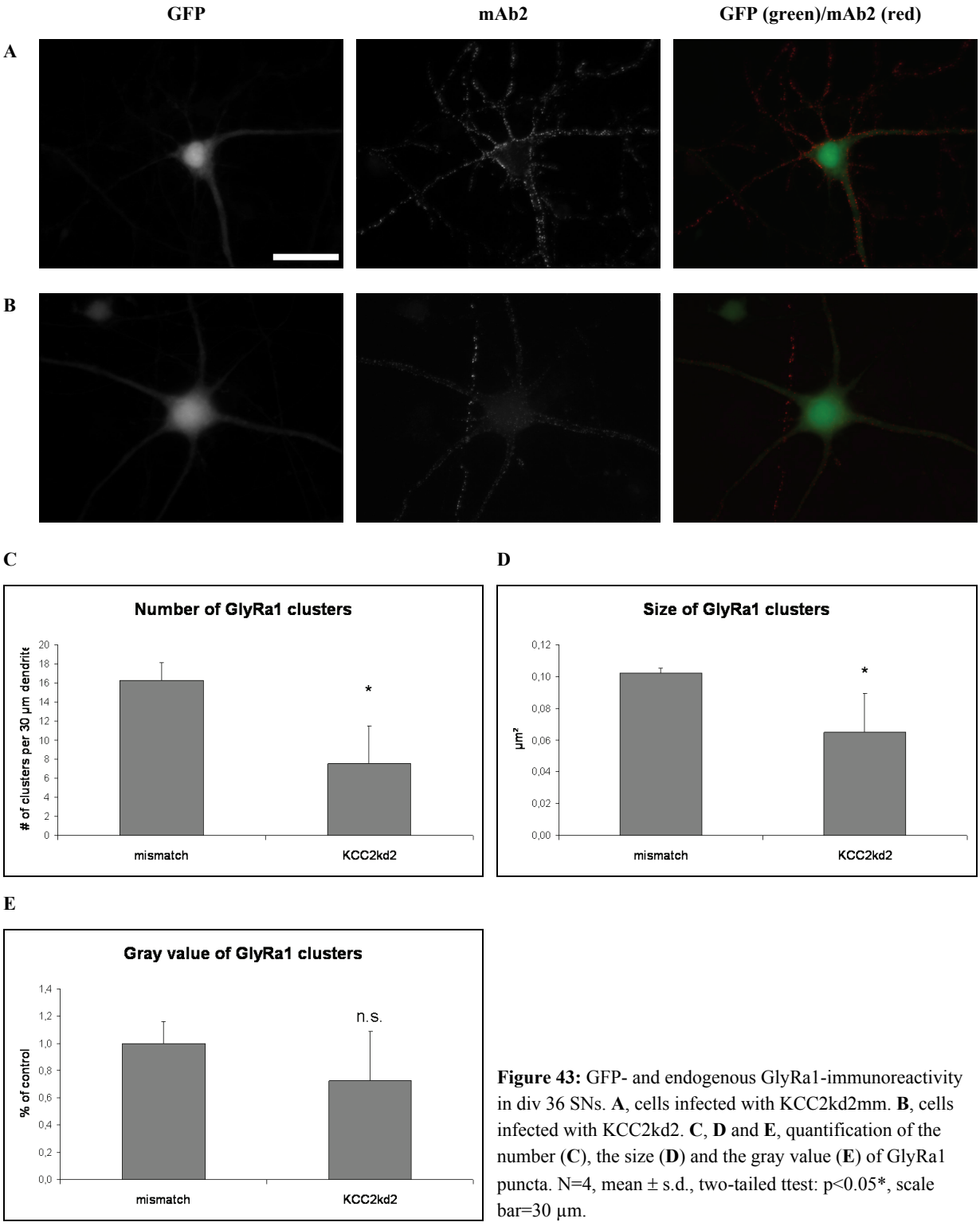

Figure 43: GFP- and endogenous GlyRa1-immunoreactivity in div 36 SNs. **A**, cells infected with KCC2kd2mm. **B**, cells infected with KCC2kd2. **C**, **D** and **E**, quantification of the number (**C**), the size (**D**) and the gray value (**E**) of GlyRa1 puncta. N=4, mean ± s.d., two-tailed ttest: $p<0.05$*, scale bar=30 µm.

Obviously, the expression of the GlyRa1 subunit is seriously altered by knocking down KCC2 expression. It is examined as follows, whether, as in immunoblots suggested, the GlyRa2 subunit is not concerned by these alterations.

Effects of KCC2 knockdown onto the juvenile GlyRa2 subunit

To test, whether knockdown of KCC2 has consequences for the expression of the GlyRa2 subunit, the protein was detected by use of an antibody made in goat. The only secondary antibody giving a cross reaction-free signal was αgt-cy2. Hence, the infected cells cannot be identified. Instead, only KCC2-positive cells were imaged in mismatch cultures and KCC2-negative cells were imaged in knockdown cultures. Therefore, it has to be assumed that also few uninfected cells contribute to the statistics.

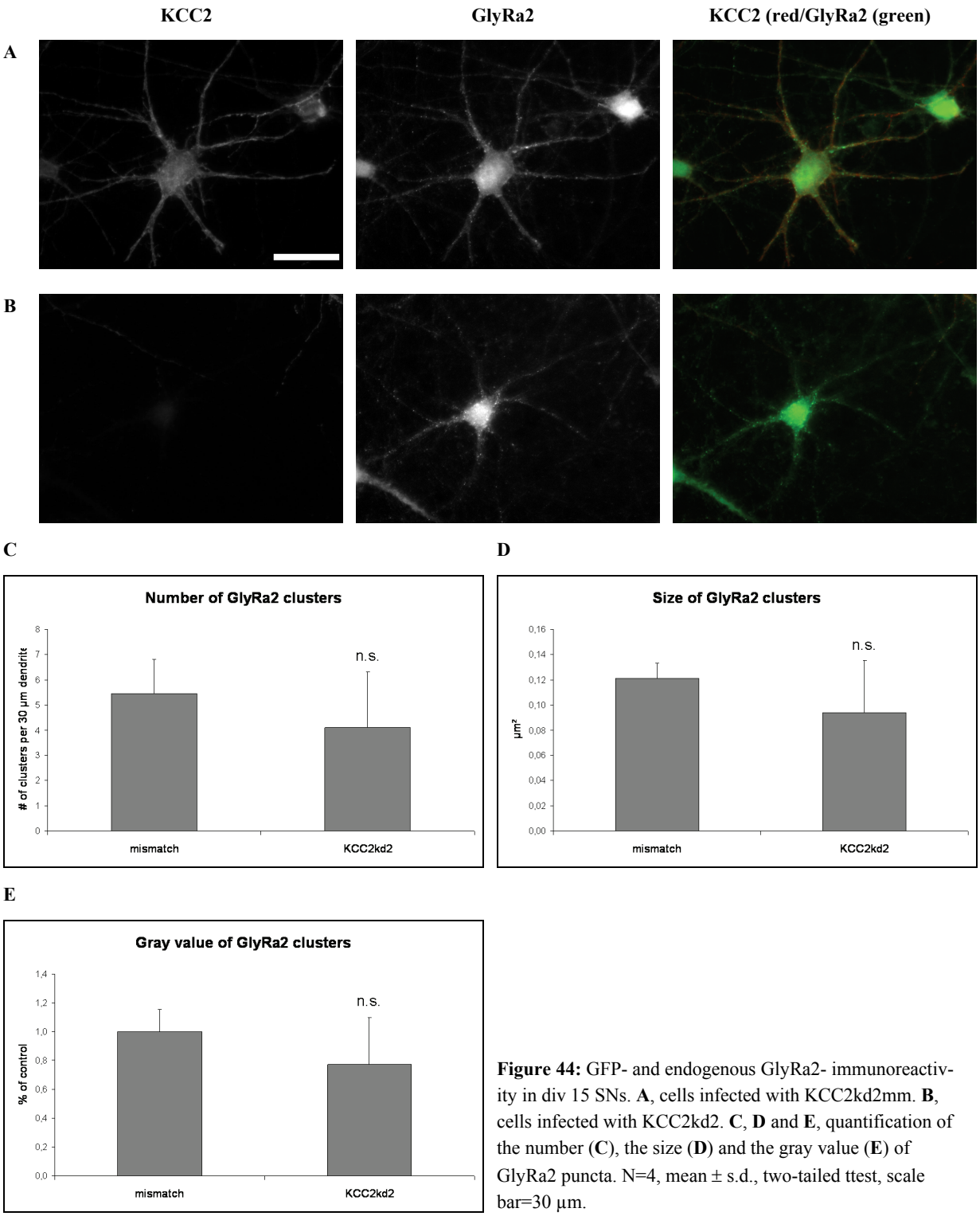

Figure 44: GFP- and endogenous GlyRa2- immunoreactivity in div 15 SNs. **A**, cells infected with KCC2kd2mm. **B**, cells infected with KCC2kd2. **C**, **D** and **E**, quantification of the number (**C**), the size (**D**) and the gray value (**E**) of GlyRa2 puncta. N=4, mean ± s.d., two-tailed ttest, scale bar=30 µm.

Immunoblot analysis implies the juvenile GlyRa2 subunit not to be concerned by the knockdown. Indeed, there are no significant differences between the mismatch and knockdown cultures at div 15 (Figure 44).

At div 22, an unexpected significant decrease in the number of GlyRa2 clusters in knockdown cultures occurs (Figure 45C). The other parameters do not exhibit any alteration (Figure 45D and E).

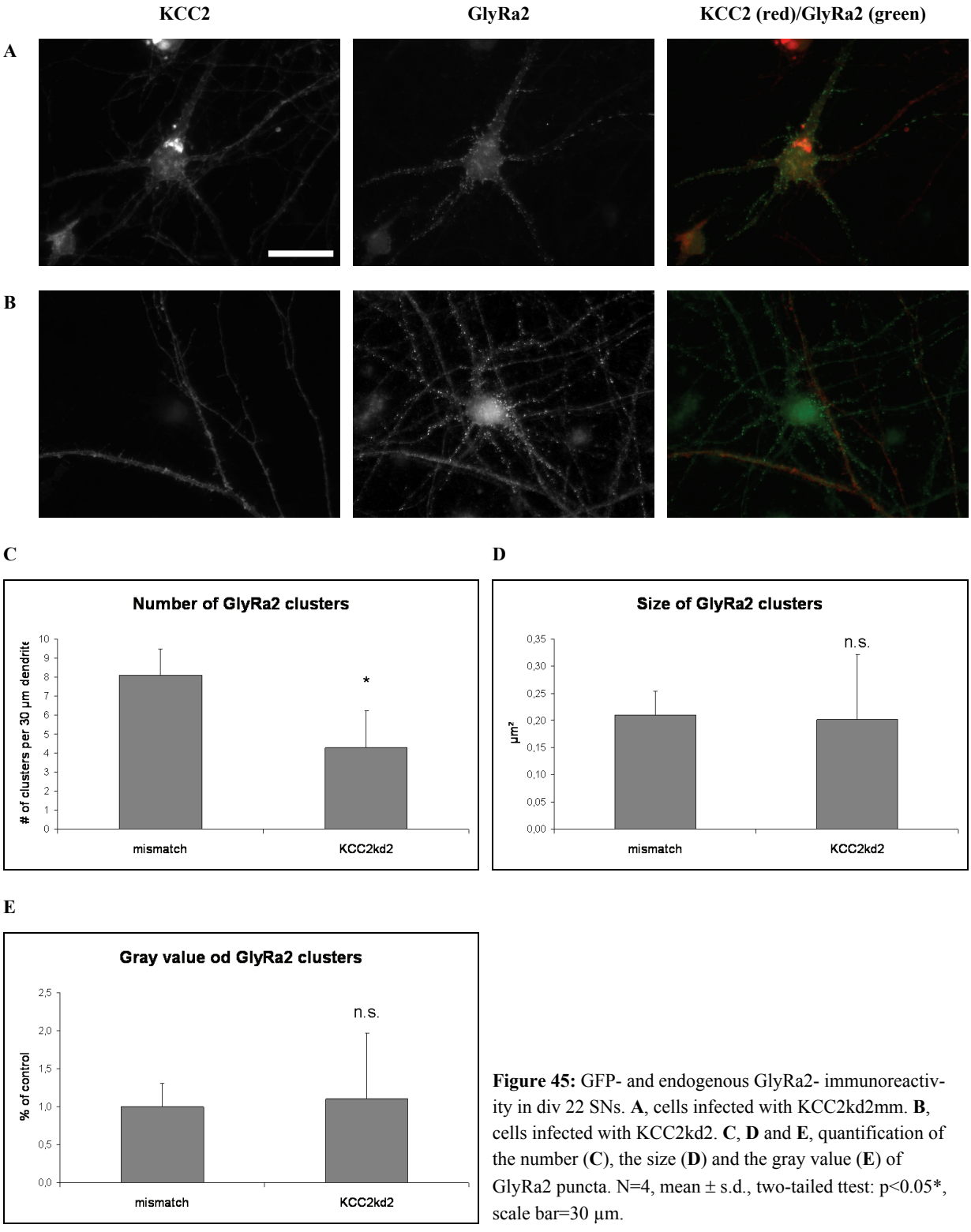

Figure 45: GFP- and endogenous GlyRa2- immunoreactivity in div 22 SNs. **A**, cells infected with KCC2kd2mm. **B**, cells infected with KCC2kd2. **C**, **D** and **E**, quantification of the number (**C**), the size (**D**) and the gray value (**E**) of GlyRa2 puncta. N=4, mean ± s.d., two-tailed ttest: $p<0.05$*, scale bar=30 µm.

At div 36, the number of GlyRa2 clusters in mismatch and knockdown cultures does no longer exhibit any significant difference (Figure 46C). Furthermore, the size and the gray value of GlyRa2 clusters remain unchanged (Figure 46D and E).

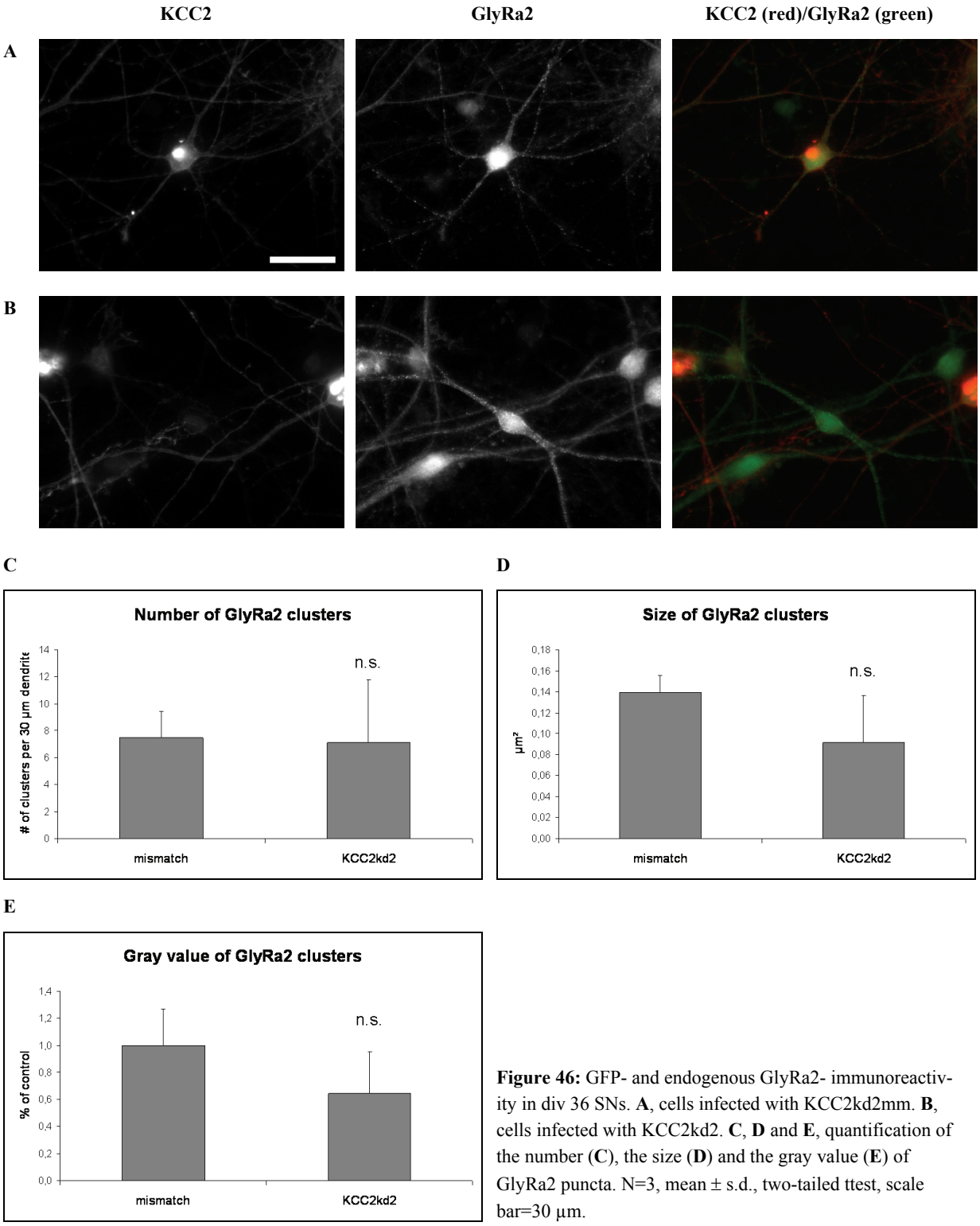

Figure 46: GFP- and endogenous GlyRa2- immunoreactivity in div 36 SNs. **A**, cells infected with KCC2kd2mm. **B**, cells infected with KCC2kd2. **C**, **D** and **E**, quantification of the number (**C**), the size (**D**) and the gray value (**E**) of GlyRa2 puncta. N=3, mean ± s.d., two-tailed ttest, scale bar=30 µm.

As previously indicated, gephyrin, comprising an anchoring function for the GlyR complex, also exhibits a diminished expression evoked by KCC2 knockdown. Thus, the immunoreactivity is determined as well.

Effects of KCC2 knockdown onto gephyrin expression

As shown in various publications, the GlyRb subunit owns a binding site for the anchor protein gephyrin. Gephyrin forms a lattice-like structure underneath the membrane to which the GlyRb subunit is allowed to bind (Poulopoulos et al. 2009). Since the GlyR appears to form hetero-oligomers consisting of GlyRa1 and GlyRb subunits, it might be obvious, that together with the decrease in GlyRa1 expression, gephyrin expression is diminished as well (Figure 47). However, due to the small differences in GlyRa2 expression one cannot suggest less gephyrin expression. That subunit forms amongst others homo-oligomers and does not necessarily bind to gephyrin. Immunoblots already demonstrated a drop of the gephyrin expression in knockdown cultures revealed by mAb7 detection. MAb7 exhibits rounded structures within the cultures. These patterns are presumably glial cell nuclei. This characteristic nuclei stain of mAb7 is well known.

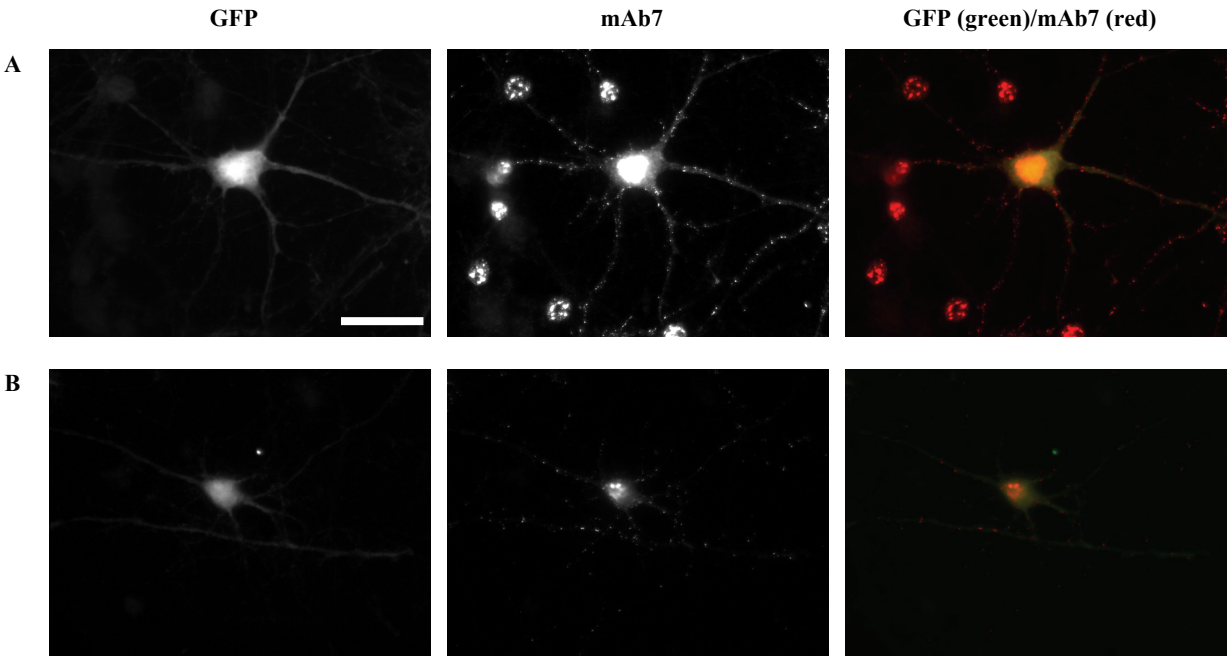

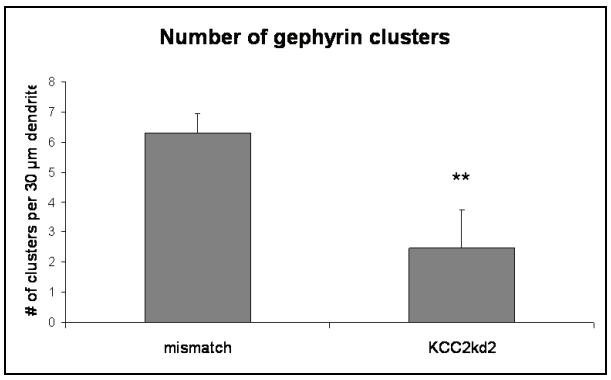

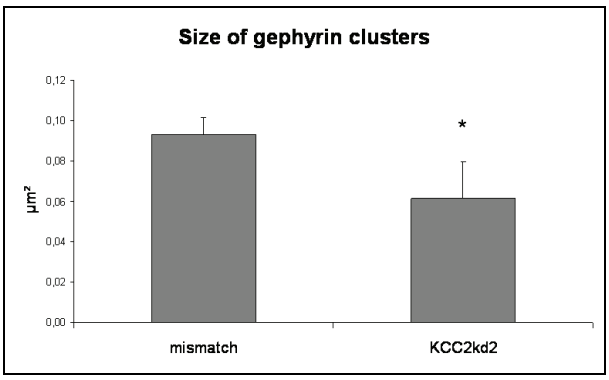

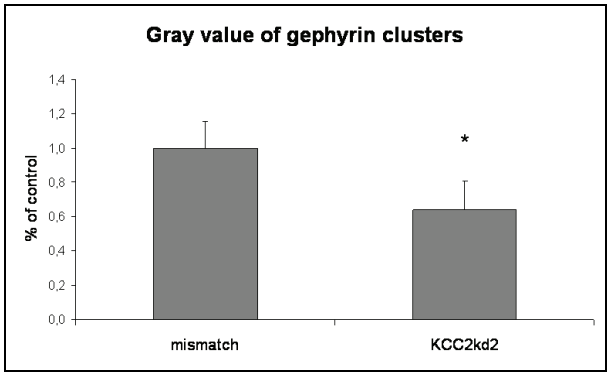

Figure 47: GFP- and endogenous gephyrin-immunoreactivity in div 15 SNs. **A**, cells infected with KCC2kd2mm. **B**, cells infected with KCC2kd2. **C**, **D** and **E**, quantification of the number (**C**), the size (**D**) and the gray value (**E**) of gephyrin puncta. N=4, mean ± s.d., two-tailed ttest: $p<0.05$*, $p<0.01$**, scale bar=30 µm.

The effect still is present one week later in development (Figure 48). The knockdown cultures exhibit diminished values in two parameters (Figure 48C and D). The remaining clusters in knockdown cells do not exhibit a weaker fluorescence than clusters of mismatch cells anymore (Figure 48E).

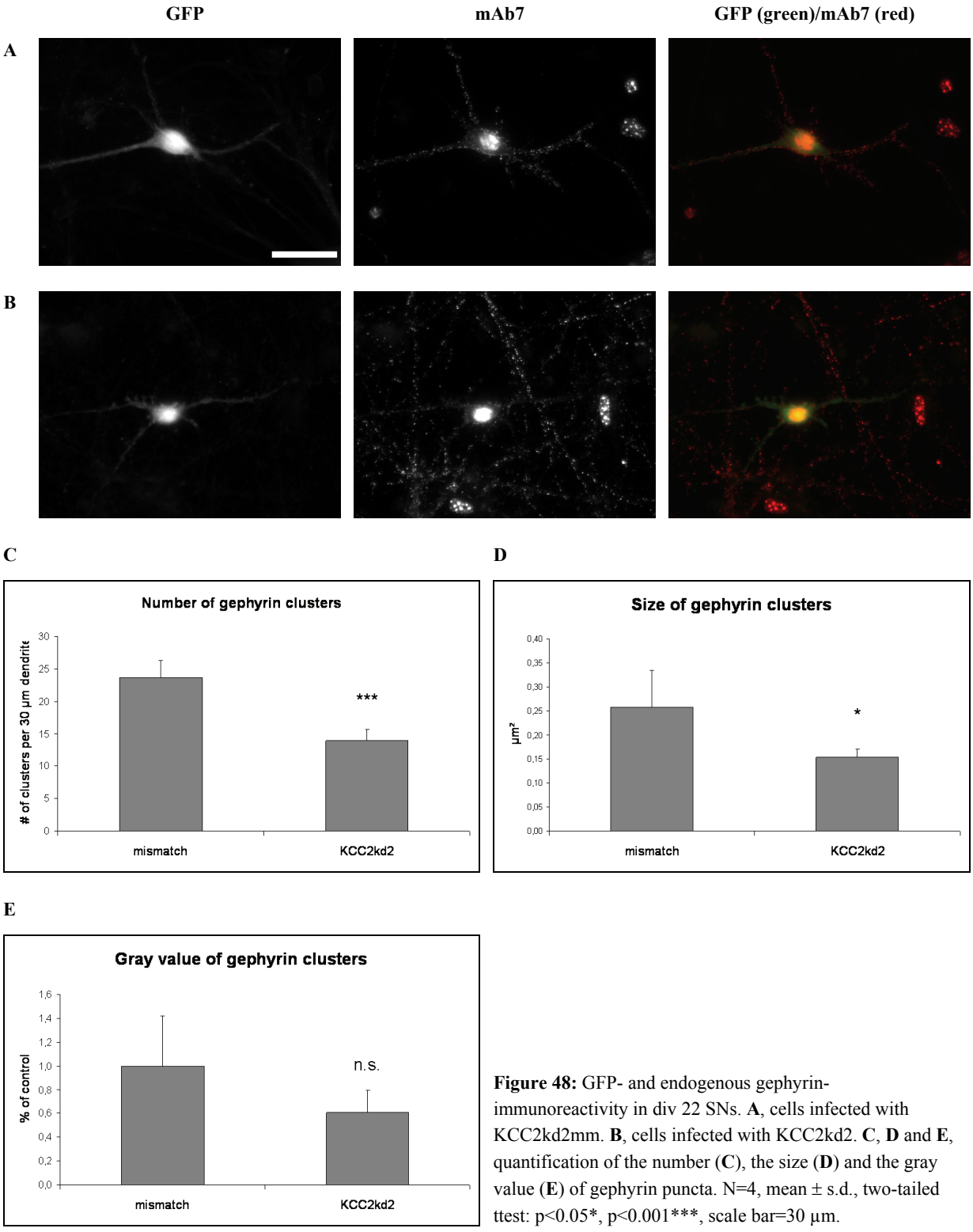

Figure 48: GFP- and endogenous gephyrin-immunoreactivity in div 22 SNs. **A**, cells infected with KCC2kd2mm. **B**, cells infected with KCC2kd2. **C**, **D** and **E**, quantification of the number (**C**), the size (**D**) and the gray value (**E**) of gephyrin puncta. N=4, mean ± s.d., two-tailed ttest: $p<0.05$*, $p<0.001$***, scale bar=30 µm.

Not until five weeks in culture, the observed effects start to neutralize. The differences between knockdown and mismatch cells become smaller at this point (Figure 49D and E). The only remaining significant effect is found in the number of clusters (Figure 49C).

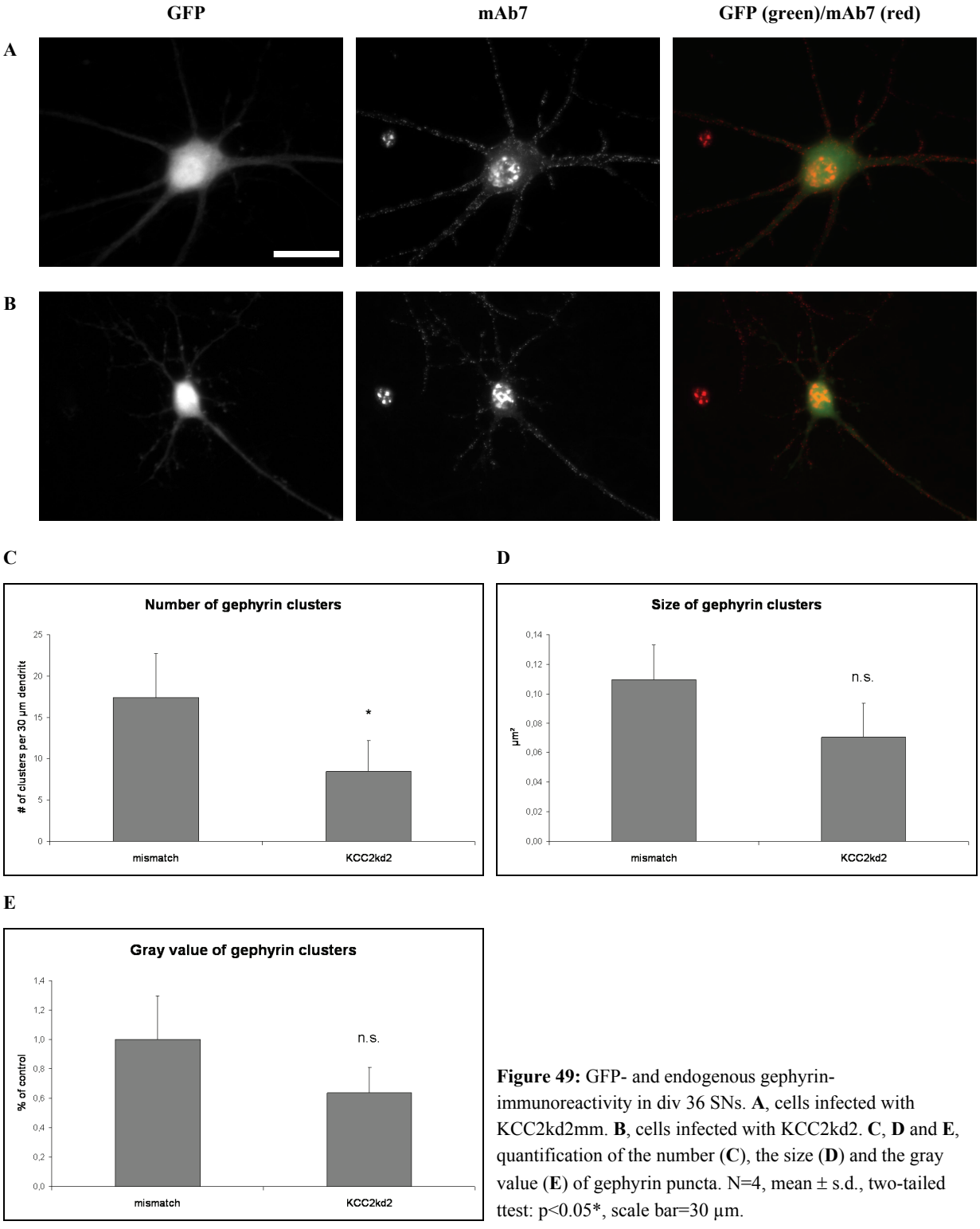

Figure 49: GFP- and endogenous gephyrin-immunoreactivity in div 36 SNs. **A**, cells infected with KCC2kd2mm. **B**, cells infected with KCC2kd2. **C**, **D** and **E**, quantification of the number (**C**), the size (**D**) and the gray value (**E**) of gephyrin puncta. N=4, mean ± s.d., two-tailed ttest: $p<0.05$*, scale bar=30 µm.

Additional to the GlyR subunits and gephyrin, other synaptic proteins were examined to exclude a general loss of synapses or shrinking of synapses. This should restrict the effect to the GlyR.

Effects of KCC2 knockdown on PSD 95 expression

The next explored protein was PSD 95. This neuron-specific protein assembles underneath the postsynaptic membrane where it forms scaffolds for anchoring synaptic receptors such as AMPARs or NMDARs. It is not shown to interact with the GlyR. At div 15, no obvious alterations in the taken parameters are present (Figure 50). Indeed the standard deviation in all trials is very high suggesting a quite variable expression of this protein.

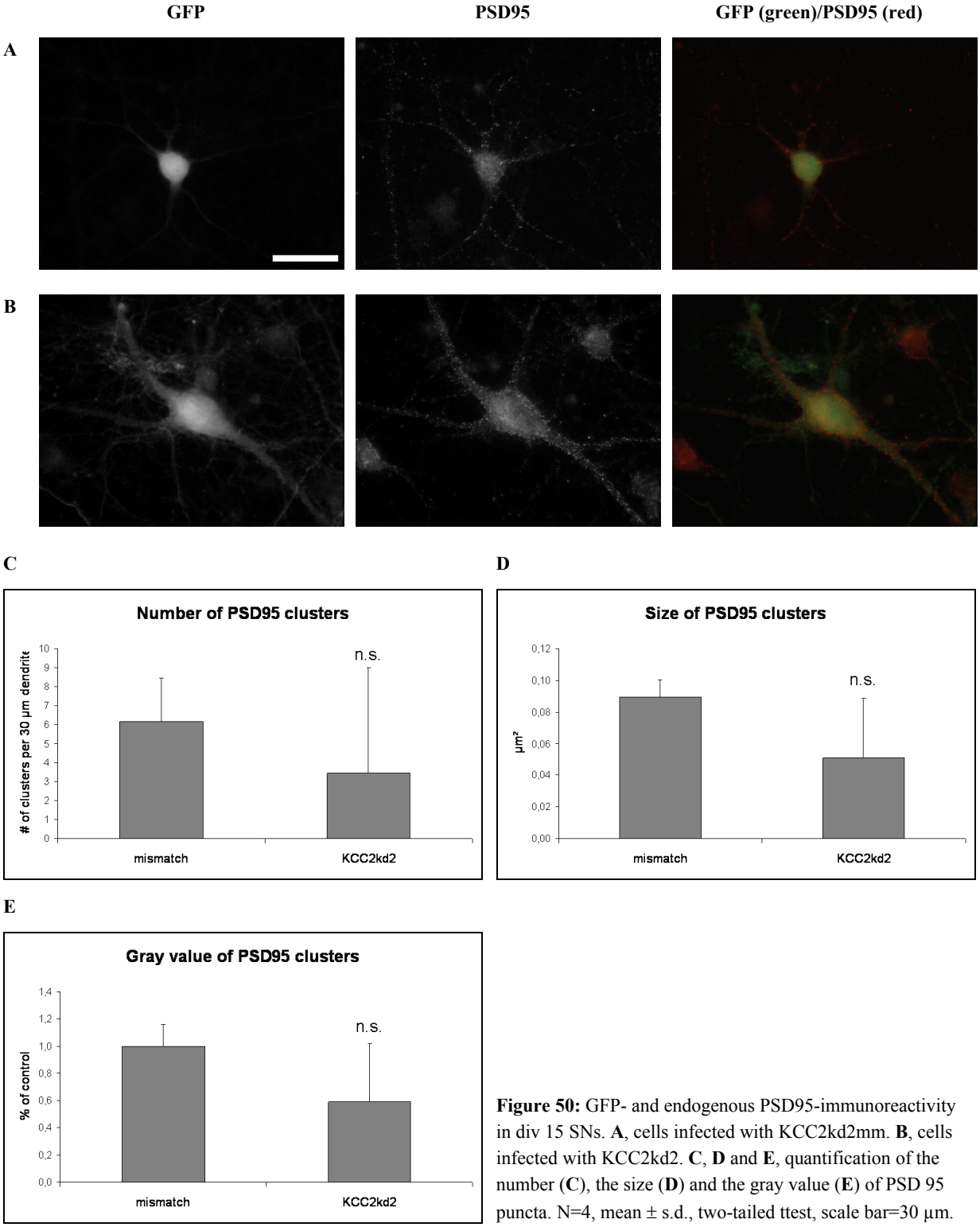

Figure 50: GFP- and endogenous PSD95-immunoreactivity in div 15 SNs. **A**, cells infected with KCC2kd2mm. **B**, cells infected with KCC2kd2. **C**, **D** and **E**, quantification of the number (**C**), the size (**D**) and the gray value (**E**) of PSD 95 puncta. N=4, mean ± s.d., two-tailed ttest, scale bar=30 µm.

One week later, still no significant differences between the two conditions occur (Figure 51). The variability within the trials remains high. However, based on these data, one can conclude that the number and the size of the PSD 95 puncta increase during synaptogenesis and decrease in turn after termination of synaptogenesis.

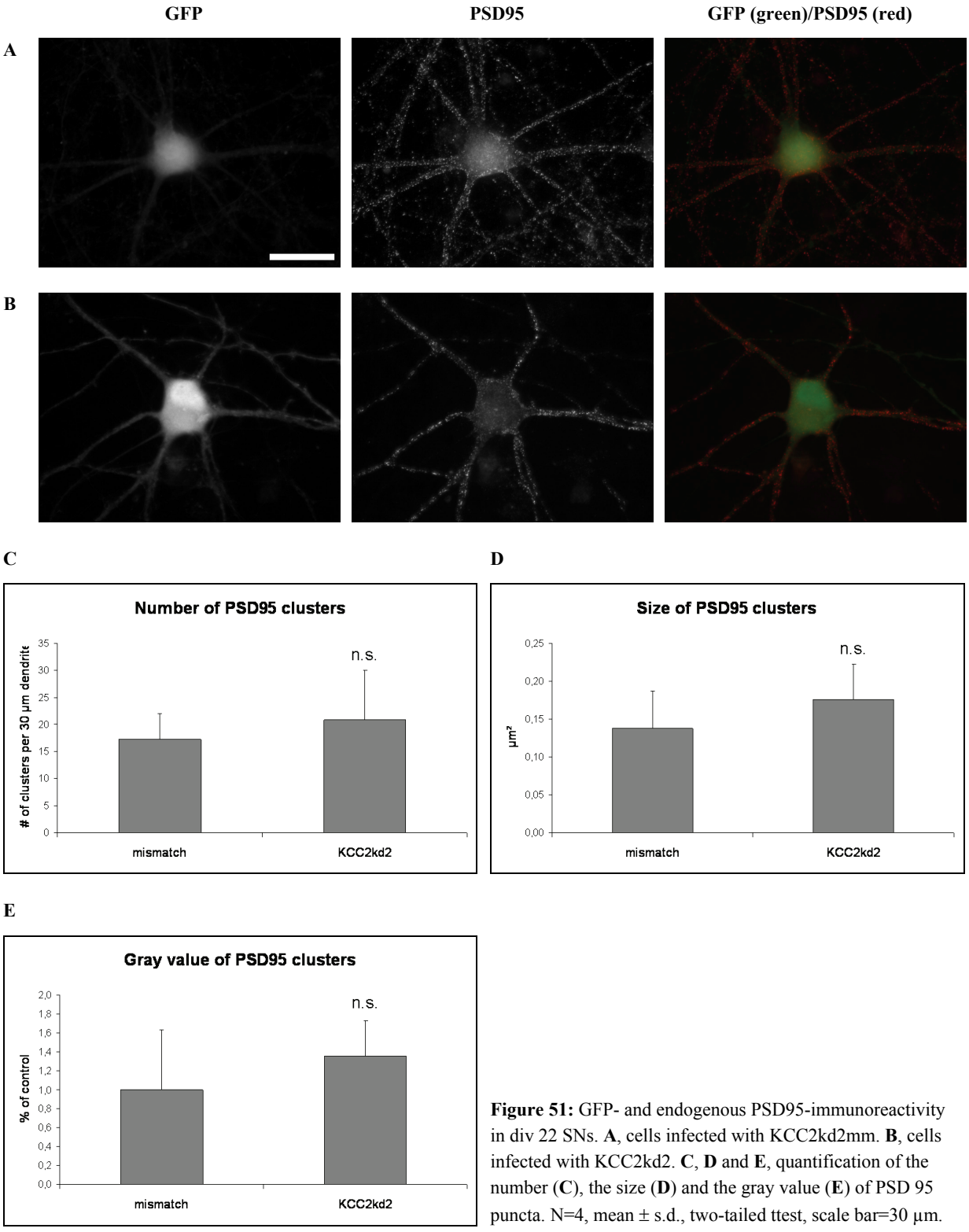

Figure 51: GFP- and endogenous PSD95-immunoreactivity in div 22 SNs. **A**, cells infected with KCC2kd2mm. **B**, cells infected with KCC2kd2. **C**, **D** and **E**, quantification of the number (**C**), the size (**D**) and the gray value (**E**) of PSD 95 puncta. N=4, mean ± s.d., two-tailed ttest, scale bar=30 µm.

At the last proved time point (div 36) no significant differences between mismatch and knock-down cells appear as well (Figure 52).

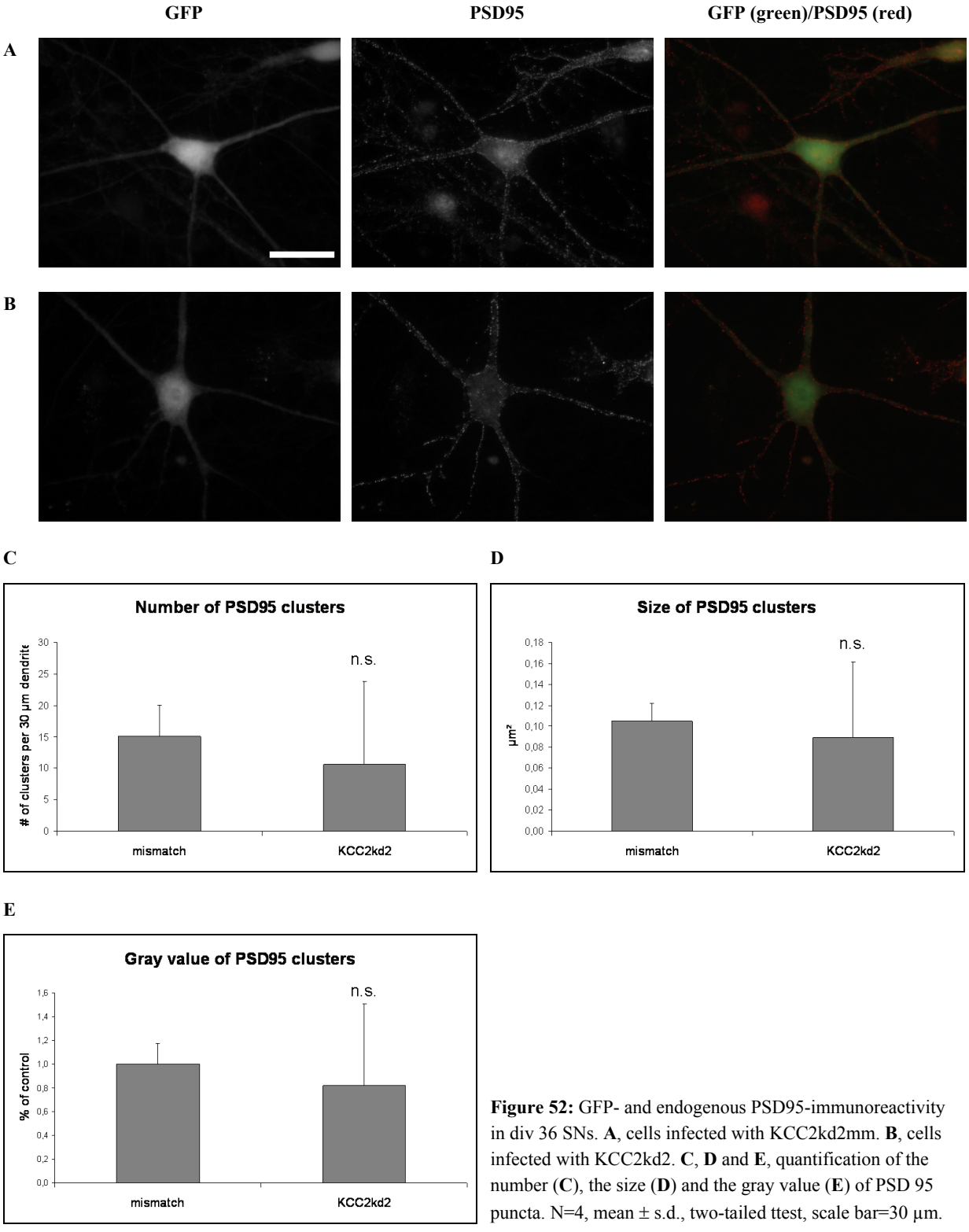

Figure 52: GFP- and endogenous PSD95-immunoreactivity in div 36 SNs. **A**, cells infected with KCC2kd2mm. **B**, cells infected with KCC2kd2. **C**, **D** and **E**, quantification of the number (**C**), the size (**D**) and the gray value (**E**) of PSD 95 puncta. N=4, mean ± s.d., two-tailed ttest, scale bar=30 µm.

After demonstrating that a GlyR independent synaptic protein is not concerned by the KCC2 knockdown, the next interesting step was to investigate the second inhibitory receptor type in the CNS, namely $GABA_AR$.

Effects of KCC2 knockdown on $GABA_AR$ expression

To test whether the effects caused by KCC2 knockdown in SNs are true for both inhibitory receptors or exclusively for the GlyR, the $GABA_AR$ expression was investigated, too. The $GABA_AR$ mainly is expressed in higher brain regions such as cortex, hippocampus, cerebellum, basal ganglia and thalamus, but low expression remains in the spinal cord (Dumoulin et al. 2000). For these studies, the antibody $GABA_AR$ bd17, which recognizes both the β2 and the β3 subunit of the $GABA_AR$, was used.

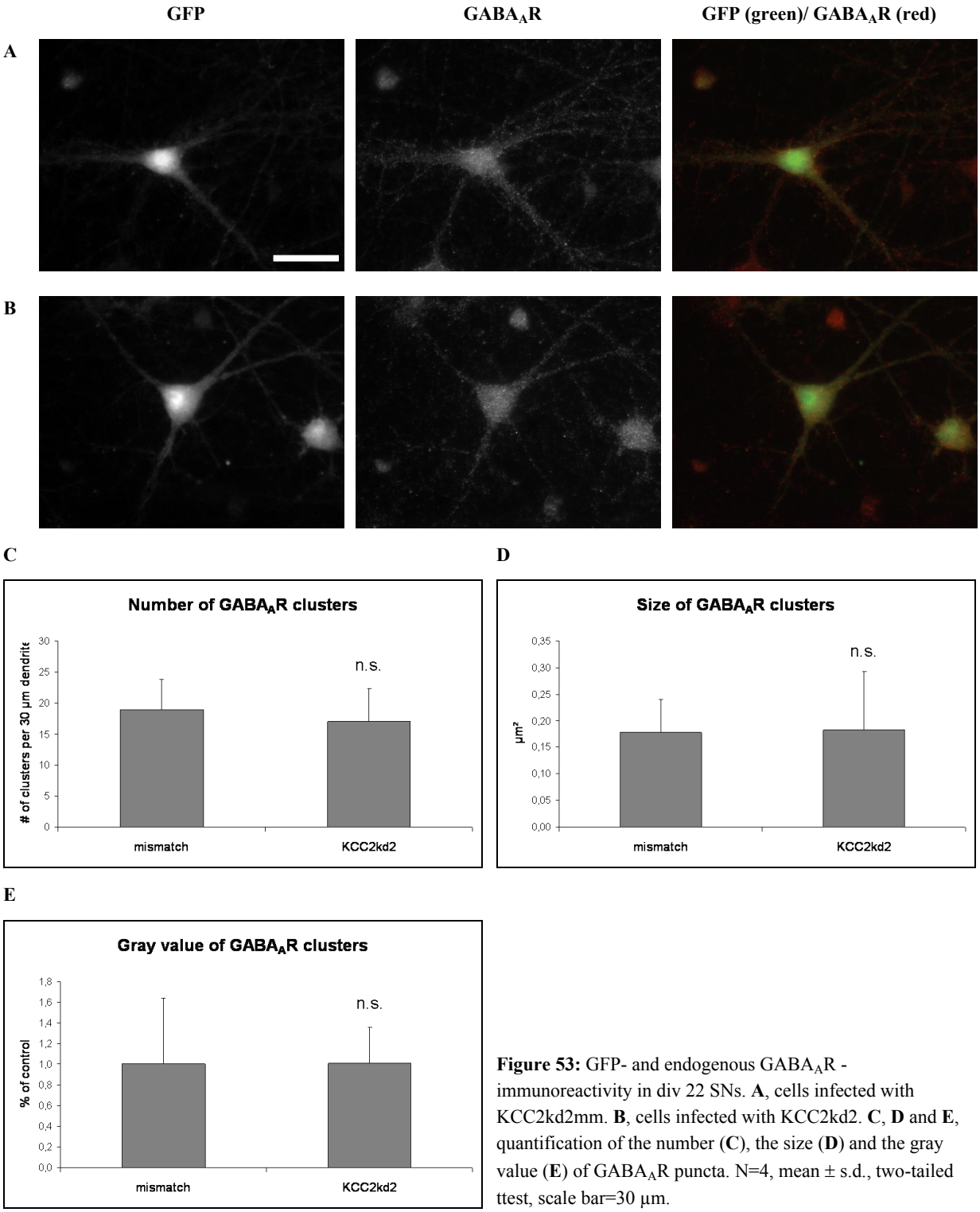

Figure 53: GFP- and endogenous $GABA_AR$ -immunoreactivity in div 22 SNs. **A**, cells infected with KCC2kd2mm. **B**, cells infected with KCC2kd2. **C**, **D** and **E**, quantification of the number (**C**), the size (**D**) and the gray value (**E**) of $GABA_AR$ puncta. N=4, mean ± s.d., two-tailed ttest, scale bar=30 µm.

However, bd17 was not able, to detect of any useful signal at div 15. Hence, this study starts not until div 22. As in the preceding PSD 95 investigation, there is no detectable difference in any parameter between the two conditions at div 22 (Figure 53).

Towards five weeks in culture, cells develop less puncta. A significant decrease in the number of $GABA_AR$ clusters in knockdown cells compared to mismatch cells occurs (Figure 54). The other two parameters remain unchanged.

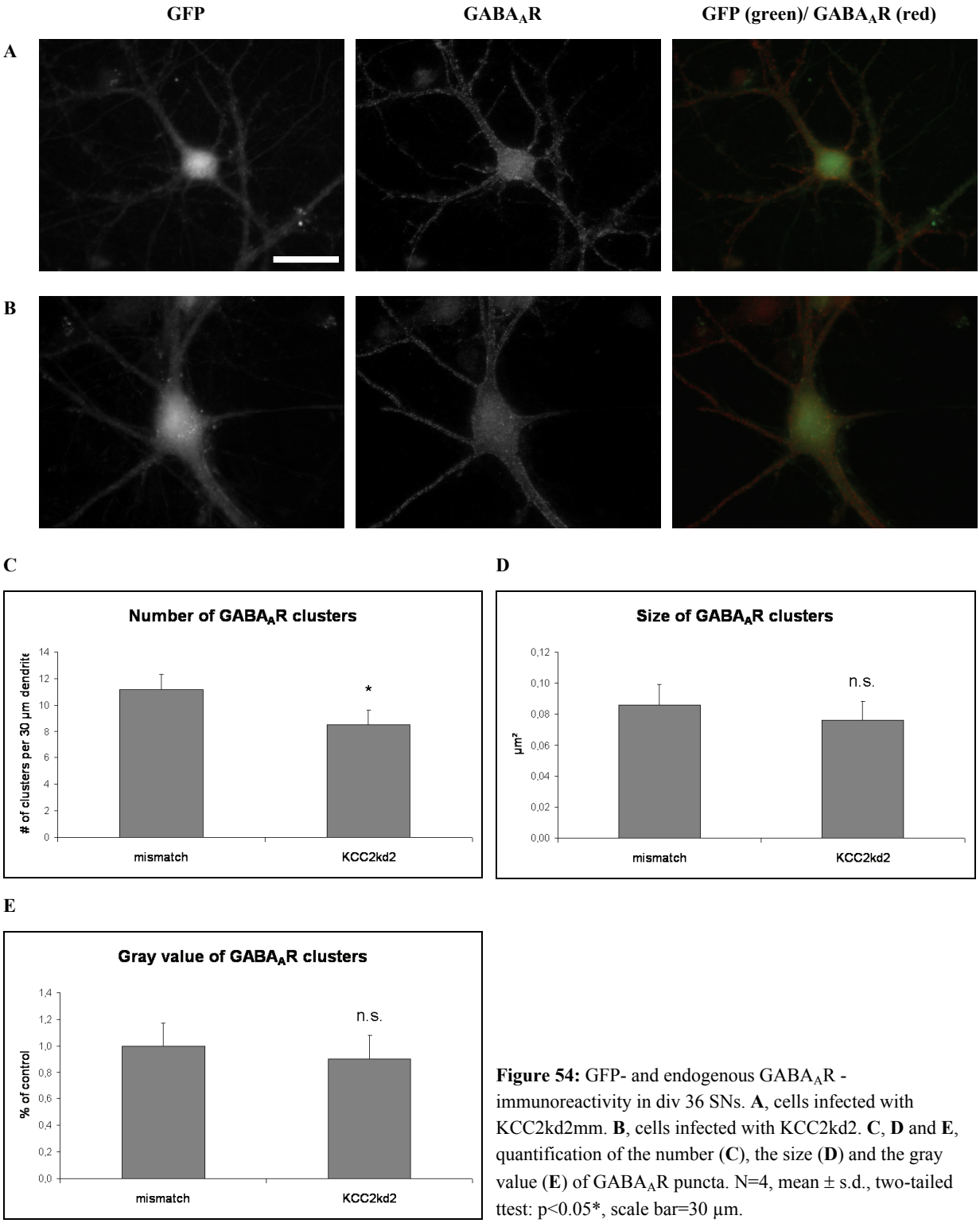

Figure 54: GFP- and endogenous $GABA_AR$ -immunoreactivity in div 36 SNs. **A**, cells infected with KCC2kd2mm. **B**, cells infected with KCC2kd2. **C**, **D** and **E**, quantification of the number (**C**), the size (**D**) and the gray value (**E**) of $GABA_AR$ puncta. N=4, mean ± s.d., two-tailed ttest: $p<0.05$*, scale bar=30 µm.

After determining the expression of all the postsynaptic proteins, the presynaptic component should be investigated as well.

Effects of KCC2 knockdown on VIAAT expression

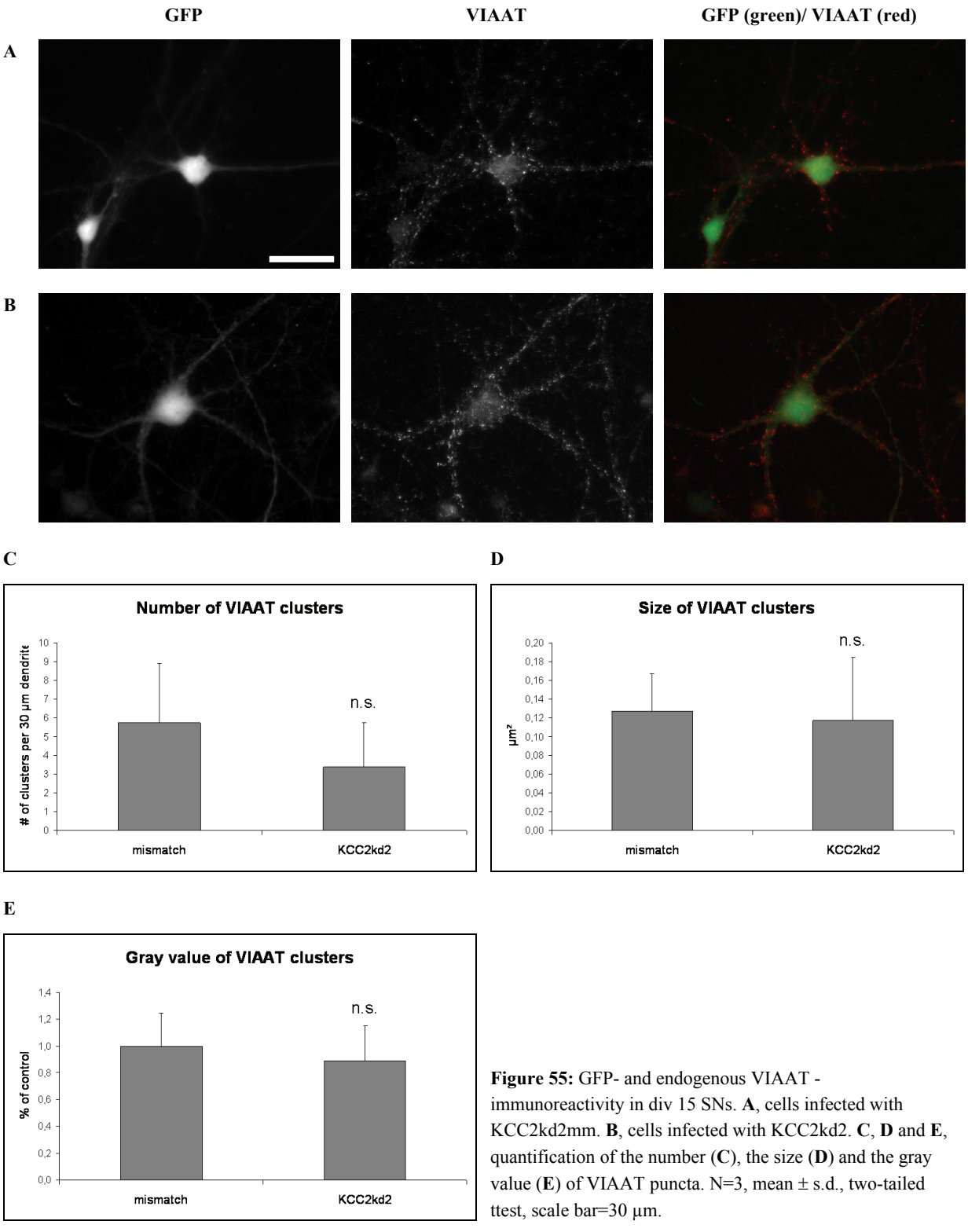

Figure 55: GFP- and endogenous VIAAT -immunoreactivity in div 15 SNs. **A**, cells infected with KCC2kd2mm. **B**, cells infected with KCC2kd2. **C**, **D** and **E**, quantification of the number (**C**), the size (**D**) and the gray value (**E**) of VIAAT puncta. N=3, mean ± s.d., two-tailed ttest, scale bar=30 µm.

After investigating different postsynaptic proteins, mainly receptors, it also was necessary to look at the presynaptic component. Therefore, VIAAT expression was determined in the noted assay.

VIAAT is a transmembrane protein storing GABA and glycine in synaptic vesicles. KCC2 knockdown does not lead to any effect in VIAAT expression at div 15 (Figure 55).

After three weeks in culture, no significant effect between mismatch and knockdown cultures can be determined (Figure 56). This implicates that KCC2 knockdown does not alter the presynaptic component.

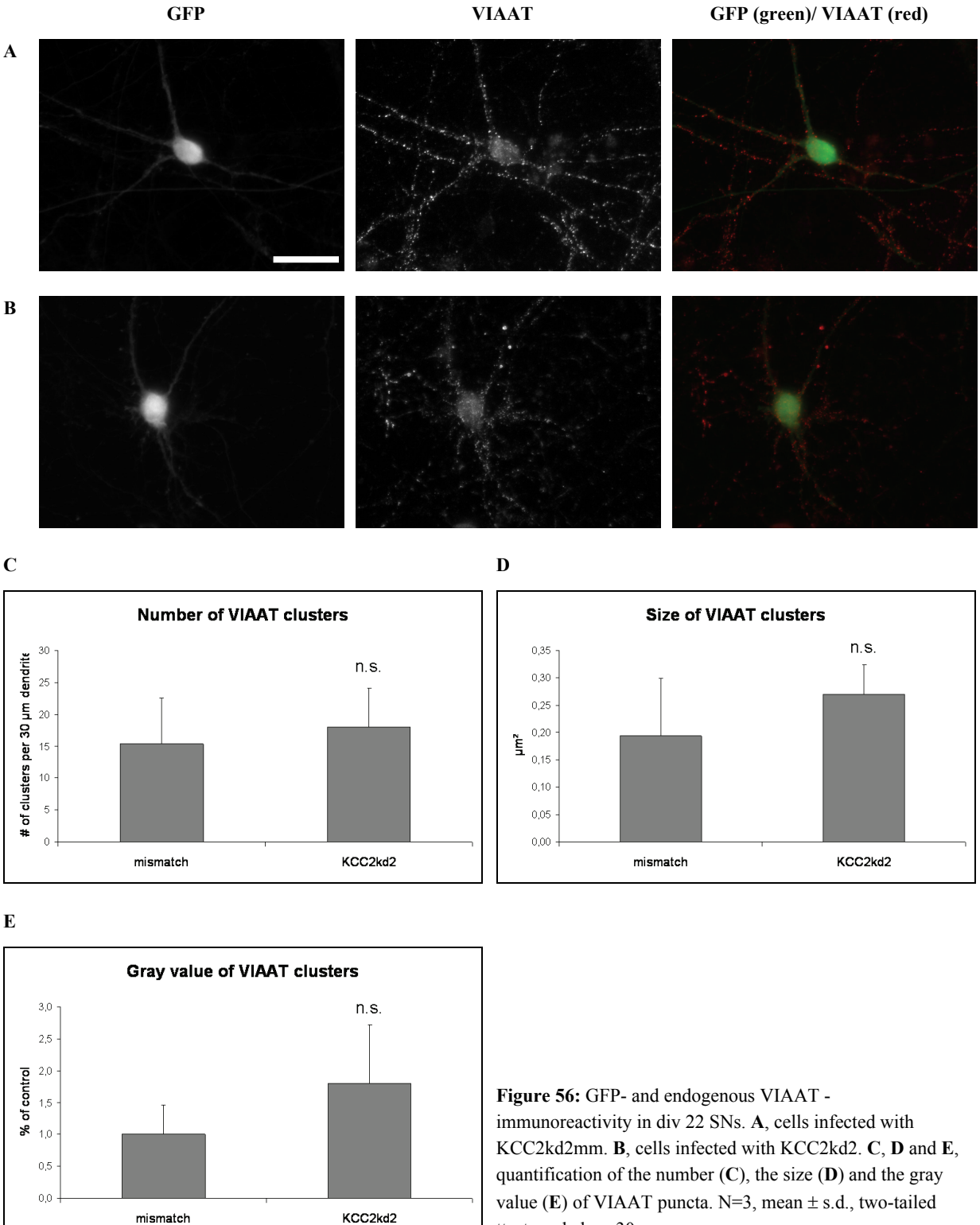

Figure 56: GFP- and endogenous VIAAT -immunoreactivity in div 22 SNs. **A**, cells infected with KCC2kd2mm. **B**, cells infected with KCC2kd2. **C**, **D** and **E**, quantification of the number (**C**), the size (**D**) and the gray value (**E**) of VIAAT puncta. N=3, mean ± s.d., two-tailed ttest, scale bar=30 µm.

It was not possible to quantify VIAAT immunoreactivity at div 36 because at that time point too many and large VIAAT puncta aroused. Thus, the VIAAT study had to end with div 22 data.

5. Discussion

5.1. Specificity of attached antibodies

Upon longer exposure of the hyperfilm to the membrane (3 min versus 30 sec.) the αGlyRa1 (rb) antibody also exhibits weak bands in the lanes containing lysates of HEK cells transfected with GlyRa2 and GlyRa3 subunits. This indicates that αGlyRa1 is also able to bind the other GlyR subunits to a small extent. Nevertheless, the latter antibody was used for semi-quantitative studies, because after analysis of the data, the results were different from mAb4 data. MAb4 is the antibody recognizing all α subunits. αGlyRa2 (gt) is clearly specific for the GlyRa2 subunit. The immunoblot signal is exclusively found in the GlyRa2 lane and immunoreactivity experiments were well defined. The only disadvantage of using this antibody was that it could only be detected using a cy2-conjugated secondary antibody resulting in a green signal. Usually, cells infected with lentivirus were detected by their green appearance because they hold a GFP reporter gene, which in turn had to be enhanced by an additional antibody staining. Therefore, in cultures stained with αGlyRa2, it was not possible to distinguish between infected and non-infected cells. Thus, the quantification of those cultures includes non-infected cells. Data resulting from the work with αGlyRb were not quantified.

5.2. Expression profiles of the GlyR subunits

As shown before (Malosio et al. 1991b), mRNA of the GlyRa1 subunit is not present in hippocampal neurons. This phenomenon was now confirmed by RTq-PCR data. The achieved GlyRa1 ΔCT values differ strongly and are relative high, indicating an extreme late start of amplification. Together, the results point to a lack of GlyRa1 mRNA in the hippocampus at the investigated time points. Similar to Malosio's data the mRNA level of the GlyRa2 subunit decreases with time. This is already visible in the RT-PCR studies and later clarified in RTq-PCR experiments. Therefore, it seems that in hippocampal neurons potentially a switch in the assembly of the GlyR occurs. Thereby, the GlyRa2 subunit cannot be replaced by the GlyRa1 subunit but rather by GlyRa3 or another GlyR alpha subunit being expressed instead of GlyRa2. The most probable explanation could be that in hippocampus most of the GlyRs consist of α2 and β subunits in adulthood. The existence of α2β heteromeric GlyRs has been indicated in some studies (Haverkamp et al. 2004, Veruki et al. 2007, Takahashi et al. 1992). Arguments for this assumption are the increasing amount of GlyRb subunit and the slight decrease of GlyRa2 RNA levels. It seems that in early development, α2 homomeric GlyRs but also (to a lower extent) α2β GlyRs are expressed in the hippocampus. During development, the number of α2β GlyRs might increase whereas the number of α2 homomeric GlyRs might decrease. As the ratio of α and β subunits is determined to 2:3, the bigger amount of GlyRb RNA can be explained. However, one

could assume that either the RNA level of GlyRb has to be one third higher than that of GlyRa2 implying only heteromeric receptors in adulthood or even the same or lower regarding the remaining homomeric α2 receptors. This problem is solved by the GlyRb subunit also forming heteromeric receptors with the α3 subunit.

According to the relative amount, the RNA data are further confirmed by the protein levels. The immunoblots show that more GlyRb than GlyRa2 material is present in hippocampal cultures. Also fitting with the RNA data is the fact, that GlyRb protein level is decreasing before it is augmented shortly prior achieving adulthood. In contrast, the immunoblot suggests GlyRa2 protein level also to be increased during development not matching with the RNA data. This might point to another thought. Maybe there are more α2 homomeric receptors present in the adult hippocampus than suggested or/and the GlyRa2 subunit is more stable in the membrane and therefore less RNA is needed in adulthood.

In terms of spinal neurons, all four subunits are present at the investigated time points. Yet the RT-PCR studies show that the amount of GlyRa1 RNA is increasing during development. The other subunits do not exhibit big changes. In contrast, the RTq-PCR studies clearly show the augmenting expression levels of the GlyRa1, GlyRa3 and GlyRb subunit as well as the decrease of GlyRa2 RNA expression during development. The juvenile GlyRa2 subunit is likely to be replaced by the GlyRa1 subunit. This thought is clarified by the cross of the two curves around div 15. The very early up regulation of GlyRb RNA and GlyRa3 RNA also being up regulated but shifted backwards compared to GlyRa1, argue for the preferred formation of heteromeric α1β and α3β GlyRs. The number of heteromeric α2β and homomeric α2 GlyRs seems to become smaller during the investigated time period. The amount of GlyRb RNA is similar to that in HCNs. From div 4 on, GlyRb reaches the highest level compared to the other subunits. At the last investigated time point (div 28), GlyRb shows almost twice the amount of the GlyRa subunits. Surprisingly, in adulthood GlyRa2 RNA still is the most frequent α subunit expressed in SNs. This phenomenon leads to the conclusion that in adulthood probably a mixture of heteromeric α1β, α2β and α3β GlyRs are expressed as well as presumptive α2 homomeric, non-synaptic receptors.

The immunoblot studies are not meaningful. GlyRa2 protein level seems not to be changed during the time window and GlyRb protein bands are hardly recognizable. It seems that the GlyRb protein level arises until div 21 and decreases in turn between div 21 and div 28. Since the αGlyRb antibody did not continue to work properly, the immunoblot data are not trustworthy.

5.3. Characterization of KCC2 expression in spinal neurons

As shown in previous studies, KCC2 is up regulated during development (Clayton et al. 1998, Lu et al. 1999). In this study, KCC2 RNA expression reaches the highest value at div 21 *in vitro* but the protein level achieves a peak already at div 14. The peak of the protein level at div 14 indicates the

highest amount of KCC2 being present around the time point of the developmental switch. The shift between protein and RNA level of one week is hardly to explain. It may be, that the turnover rate of KCC2 protein becomes faster after the ion ratio within the cell has been changed and so the RNA level still is augmented while the protein level already is declining. In contrast, it is obvious, that after turning the ion ration within the cell, KCC2 can act slower and therefore less protein is sufficient. In adulthood, the ion rate just has to be maintained and not be changed any more, requiring less activity. Therefore, KCC2 protein and RNA levels are lower in adulthood than around the developmental switch. The *in vivo* situation resembles the *in vitro* data. KCC2 protein level first is up regulated and subsequent down regulated to a certain extent. The peak of protein expression thereby resides around P22 indicating that cultured cells develop faster.

5.4. Altered expression of GlyR subunits and KCC2 upon blockade of glycinergic transmission

Strychnine application is used for blockade of glycinergic transmission. It is known, that strychnine treatment of SN cultures directs large intracellular structures consisting of aggregated GlyR and gephyrin protein (Kirsch and Betz 1998). These structures presumably are endosomes. In this study, the contribution of GlyR activity to the subunit switch should be clarified. Continuous strychnine application leads to a slight decrease in KCC2 expression compared to untreated cells. This indicates the GlyR to have a certain influence over KCC2 expression. In 2007, Fiumelli and Woodin reviewed, that the same happened upon chronic $GABA_AR$ blockade (Fiumelli and Woodin, 2007). The developmental up regulation of KCC2 failed to occur and the switch from excitatory to inhibitory was delayed. Dose-response studies demonstrate, that this effect reaches the significant level not until div 14. The use of 2 µM strychnine thereby leads to a 50% down regulation of KCC2 expression. Different procedures are possibly responsible for the observed effect. First, GlyR activity is partly necessary for the developmental up regulation of KCC2 and hence changes of the ion ratio. This suggestion is supported by the fact, that the down regulation of KCC2 expression only is significant at div 14, being the critical time point for the developmental switch. This in turn would implicate that the influence of GlyR activity does not start until the transmission has become inhibitory. However, since no complete down regulation of KCC2 occurs, other factors like BDNF, EGR4 and CIP1 (Wenz et al. 2009, Fiumelli and Woodin 2007, Uvarov et al. 2006) might contribute and even are more deciding. Another possibility is, that GlyR activity impairs KCC2 turnover leading to more KCC2 protein to be removed from the membrane and degraded subsequently. As, until now still little is known about involvement of the GlyR in gene regulation, no precise prediction can be made.

By further investigation, it should be clarified whether Ca^{2+}-influx upon GlyR activity is responsible for changes in KCC2 expression. Blocking the entire neurotransmission in the SN cultures by TTX application indeed directs a 50% down regulation of KCC2 but also mAb7 signal confirming the data

obtained by strychnine application. Since BAPTA (able to bind the entire free Ca^{2+} in the culture) treatment also directs KCC2 down regulation, it becomes clear that Ca^{2+} may play a role in the regulation of KCC2 expression. Interestingly, 408 signal, also representing gephyrin, was not altered. This might be explained by a putative specificity of mAb7 to phosphorylation states of gephyrin, which was not known until now. Thus, blockade of transmission and inhibition of Ca^{2+} signalling may influence the phosphorylation state of gephyrin, which in turn could be crucial for gephyrin scaffold formation.

To simply block Ca^{2+} influx, cells were treated with the L-type Ca^{2+} channel blockers nifedipin and verapamil on the one hand and with the Ca^{2+} chelator EGTA, not being able to cross the cell membrane. Interestingly, no changes in KCC2 expression were obtained upon blocking L-type channels and no significant alterations appeared to the KCC2-monomer bands by catching all free-floating Ca^{2+} ions of the medium. However, two observations were quite clear: upon EGTA treatment, a prominent KCC2 oligomer band formed and mAb7 signal was abolished completely. This finding implicates that the absence of Ca^{2+} leads to closer or stronger KCC2 complexes. Thus, Ca^{2+} may help to loosen the complex. Without Ca^{2+}, even SDS and urea cannot completely destroy the complexes. The phenomenon of the stronger KCC2 oligomer band was also observed in BAPTA-treated cells (not clearly visible in the presented immunoblot) but was not quantified.

The described experiments show, that KCC2 expression, which is decreased by strychnine application is not dependent on Ca^{2+}-influx through L-type Ca^{2+} channels but on the Ca^{2+} being already inside the cell and somehow on GlyR activity. The latter might induce a still unknown signalling pathway. KCC2 oligomer stability in turn is dependent on either the presence of Ca^{2+}, on Ca^{2+} entering the cell via other than L-type channels such as R-, T-, N-, P- or Q-type Ca^{2+} channels or at last on Ca^{2+} being released from intracellular Ca^{2+} sources. Thus, Ca^{2+} is important for the decomposition ability of KCC2 complexes and the phosphorylation state of gephyrin. Thereby, Ca^{2+} is likely to mediate activation or inhibition of kinases and/or phosphatases respectively, which in turn regulate the phosphorylation states of KCC2 and gephyrin. Blockade of the entire transmission by TTX concerns KCC2 expression as well. This result is a combination of different blocked channels whereas GlyRs and AMPARs seem to play the most important role.

The reciprocal assay, based on treating cells grown in glycine-free medium with glycine did not direct the expected contrary results namely an increase in KCC2 signal compared to untreated cells. Indeed a small increase in KCC2 expression is visible in treated cells at div 14 but this modification is unfortunately not significant. Since KCC2 signal is also developing in cells grown in glycine-free medium, the thought arises that GlyR activity is not essential for KCC2 expression, which is contrary to the results obtained before. More likely is the maybe inaccurate experimental approach. Perhaps glycine should have been applied for a longer time or in a higher concentration. Another aspect is that the glycine-free medium was not excluded to contain other GlyR agonists like β-alanine or taurine. Two additional controls, being cells grown in regular NB^{++++} and treated with strychnine as well as cells grown in glycine-free NB^{++++} and treated with strychnine, would have shed light on the results.

5.5. Effects of KCC2 knockdown

5.5.1. Design of shRNA sequences

For the infection of neurons only lentiviral particles containing the kd2 oligo were used. This sequence exhibits the biggest success in the knockdown of recombinant KCC2 expression in HEK cells. KCC2kd2mm, a sequence similar to KCCkd2 but containing three mutations served as a potent non-silencing control. Indeed, the trial to clone the mutated sequence of KCC2 (KCC2mut) into the viral vector pFSGW failed. This DNA fragment carries three silent mutations within the sequence that is targeted by KCC2kd2. Recombinantly expressed in neurons infected by KCC2kd2, KCC2mut is supposed to rescue the knockdown effect. Unfortunately, it was not successful cloned into the lentiviral expression vector. Nevertheless, its robustness against the silencing construct was impressively demonstrated in transfected HEK cells.

5.5.2. Effects of KCC2-Knockdown in HCNs

After confirming KCC2kd2 to be capable to induce an almost complete knock down of recombinantly expressed KCC2 in a cell line system, it further is shown to also direct the down regulation of the endogenous protein. In HCNs, even 20 µl of the lentiviral suspension were sufficient to almost completely abolish endogenous KCC2 expression. Furthermore, mAb7 signal is dramatically reduced in cells infected with 80 µl virus suspension, indicating a correlation between KCC2 expression and the mentioned phosphorylation state of gephyrin. In contrast, 408 signal, also representing gephyrin protein is not altered. GlyRa subunits, represented by mAb4 also exhibit diminished expression. It would be interesting to find out whether decreased GlyRa subunit expression causes gephyrin down regulation or the other way around. Furthermore, it is possible, that both, GlyRa and gephyrin expression are impaired by the lack of KCC2, being independent on each other.

5.5.3. Effects of KCC2 knockdown in SNs

5.5.3.1. Semi-quantitative determination of protein levels on immunoblots

KCC2 expression in SNs also is concerned by KCC2kd2. In a dose-dependent manner, KCC2 is down regulated according to increasing virus amounts. Similar to the situation in HCNs, GlyRa and gephyrin subunit expression is decreased upon higher virus amounts. In contrast, knockdown of KCC2 evokes a significantly increased NMDAR expression. Whereas GlyRa2 expression is unchanged upon KCC2 knockdown, GlyRa1 subunit expression is significantly reduced in cells infected with the highest virus concentration. These findings suggest a model, in which cells lacking KCC2 remain in a juvenile state. They might miss the maturation caused by the activity of KCC2, being responsible for changing the ion ratio in wild type cells. Representative for a juvenile state would be a GlyRa2 expres-

sion similar to control cells or even higher resembling younger neurons. Indeed, GlyRa2 expression remains unchanged, whereas the mature subunit, GlyRa1, is down regulated. The latter also suggests the cells, to reside in a juvenile state. As shown in immunoblots before, GlyRa2 protein level is not decreasing with time indicating KCC2 expression not to be crucial for regulating the juvenile GlyR form but rather being responsible for the maturation of the cell by exclusively modifying GlyRa1 expression. The latter might be a hint to the phenomenon, that GlyRa2 knockout mice do not exhibit the startle disease as seen in their GlyRa1 knockout counterparts. Possibly, GlyRa2 is not crucial for the maturation, but rather GlyRa1. Moreover, studies about a possible up regulation of the GlyRa1 subunit in GlyRa2 knockout mice still are lacking. It is not clear, whether the pure presence of KCC2 or rather its activity is sufficient for the GlyRa1 up regulation during development. If the activity of KCC2 is responsible for the successful expression of mature GlyRs, either the chloride level or the switch to a hyperpolarizing response upon channel opening may be crucial. This thesis is supported by the fact, that in mature cells Ca^{2+} signalling, which still arises in juvenile neurons upon depolarization, is no longer given. The other idea, in which the single presence of KCC2 is sufficient to induce expression of mature GlyRs might be supported by another study, demonstrating, that even inactive KCC2 is able to rescue a spine formation defect (Li et al. 2007). In their study, lack of KCC2 in cortical neurons directs immature spine morphology fitting with this study, in which lack of KCC2 leads to a juvenile phenotype of SNs regarding GlyR subunit expression. The increase in NMDAR expression in knockdown cultures may reflect a compensating mechanism of the cells to augment the number of potential Ca^{2+}-influx possibilities, which in turn are needed for a successful maturation. The depolarizations, being evoked by juvenile GlyRs, might therefore be crucial for an accumulation of Ca^{2+} within intracellular stores. This Ca^{2+} then is needed for further maturation of the cell. Factors for the maturation might be the putative Ca^{2+}-dependent stabilization of KCC2 oligomers or formation of gephyrin scaffolds. The latter would explain why BAPTA and continuous GlyR blockade induces KCC2 down regulation but not o/n application of EGTA and Ca^{2+} channel blockers. Furthermore, it might be fruitful, to determine NMDAR expression in GlyRa2 knockout mice. It could be that, in order to compensate for the loss of GlyRa2, NMDAR expression is up regulated, to ensure Ca^{2+} influx into the neurons in early development.

5.5.3.2. Determination of receptor and KCC2 protein in control, mismatch and knockdown cultures

The time course experiment sheds light on the development of the expression patterns of the examined proteins. KCC2 expression indeed is down regulated upon KCC2kd2 infection suggesting the sequence to operate properly. KCC2kd2mm in turn is not able to induce a knockdown of KCC2 expression. Even towards three weeks in culture, while the knockdown cells undergo a strong down regulation in KCC2 expression, mismatch cells do not exhibit significant changes in KCC2 expression.

GlyR subunits indeed are up regulated in SNs upon infection, but the changes are not significant. Cells, carrying the knockdown sequence, in turn undergo a slight decrease in mAb4 signal at div 15 and even a significant diminishment of the latter at div 22. This is consistent with the data obtained in the experiments before (Figure 32). Unexpected was the initial augmentation of the mAb7 signal at div 8. Yet one week later, mAb7 signal is significantly depleted compared to control and mismatch cultures. Another week later, the expression is even stronger reduced. These data also are in line with earlier results. The increase of mAb7 expression at div 8 might result from the signals, still being too weak for an exact quantification. At none of the investigated time points, GlyRa2 and 408 signals were significantly altered upon KCC2 depletion. This indicates, as already shown before, that the juvenile subunit is not concerned by the lack of KCC2, and that antibody 408 labels another form of gephyrin than mAb7 recognizes, whereas expression of the former one is not concerned upon KCC2 down regulation. Because mAb4 signal is altered upon KCC2kd2 infection but not GlyRa2 signal, expression of one of the adult subunits namely GlyRa1 or GlyRa3 has to be responsible therefore. As shown before GlyRa1 may be the subunit accounting for the changes in mAb4 signals.

Important for the following studies, is finally that the mismatch construct is not able to induce significant changes in the expression of the investigated proteins. Beside, it is remarkable that KCC2 expression is slightly, albeit not significantly, up regulated. The same is true for mAb4 and mAb7 signals, which in turn is consistent with the correlated down regulation of those three proteins.

5.5.3.3. Localization of Immunoreactivities

As expected, GFP positive (GFP^+) cells, which contain the virus, show almost no KCC2 immunoreactivity when infected with the knockdown construct KCC2kd2, whereas they exhibit red immunoreactivity representing KCC2 signal when infected with the mismatch control KCC2kd2mm. It is also visible, that the total number of KCC2 positive cells is reduced in cultures infected with KCC2kd2. The described effect is present at all investigated div stages (div 15, 22 and 36). Thus, we could successfully demonstrate that cells indeed are infected by lentiviral particles (GFP expression) and that infected cells exhibit a down regulation of KCC2 expression indicating our knockdown construct KCC2kd2 to work properly.

After the confirming infection of the cells and the existence of a knockdown effect, GlyRa subunit expression was investigated using mAb4, which recognizes all GlyR α subunits. Thereby it turned out that the expression of the GlyR is concerned by KCC2kd2. At div 15, number of clusters, size of clusters and the fluorescence intensity are significantly diminished upon KCC2 knockdown. This is also true for the two older stages div 22 and div 36.

To discriminate between the juvenile and the adult GlyRa subunit, specific antibodies were used. MAb2 recognizes the adult form, whereas αGlyRa2 stains the juvenile subunit. First, the adult subunit, GlyRa1, was investigated. As immunoblots already suggested, the expression of GlyRa1 might be diminished upon KCC2 knockdown. Indeed, GlyRa1 expression exhibits a reduced expression in neu-

rons infected with the knockdown construct. This is another indication for the cells to rest in a juvenile stage and not to augment GlyRa1 expression upon KCC2 knockdown. First, the number of GlyRa1 puncta is diminished, indicating that less synapses containing the adult GlyR are formed. Secondly, the size of the clusters is smaller than in cells containing the mismatch construct. This points to a smaller active zone in KCC2 knockdown cultures. The reduction in the gray volume, representing the fluorescence intensity of the GlyRa1 clusters, suggests a smaller number of GlyRa1 receptors in the synapses. Since the cluster size is also diminished, the receptor density might not be affected. Indeed, the density of the receptors within the synapses was determined by dividing the gray value by the cluster size. In no single case, a significant difference between mismatch and knockdown cultures was achieved. After three weeks in culture, the number of GlyRa1 clusters is reduced stronger than after two weeks. Towards five weeks in culture in turn, the effects become less strong. The gray value of GlyRa1 clusters even does not exhibit significant differences between mismatch and KCC2kd2 cultures. The dilution of the effects upon a long time in culture might represent an upcoming compensation by the cells. In contrast, GlyRa2 expression is in most cases not concerned by the knockdown. The only parameter, which undergoes a significant change between knockdown and mismatch cells, is the number of clusters in div 22 neurons. It is not clear why the number of GlyRa2 clusters is reduced in knockdown cultures at the indicated time point. Obviously, there are less synapses containing the GlyRa2 subunits indicating that GlyRa2 also is concerned by the KCC2 knockdown but to a smaller extent than the adult receptor. In all other parameters no significant alterations between mismatch and knockdown cultures occur. This confirms the thesis that upon persisting in a juvenile stage the up regulation of GlyRa1 is reduced or completely left out. As expected, in mismatch cultures expression of the GlyR α subunits decreases from div 15 (eight clusters per 30 µm dendrite) to div 22 (22 clusters per 30 µm dendrite) representing the growing number of GlyRa containing synapses in the cell. Surprisingly after three weeks in culture, the number of GlyRa clusters decreases in turn (12 clusters per 30 µm dendrite). It is probable that after achieving adulthood, cells reduce the number of juvenile receptors. The same procedure is true for the expression of the GlyRa1 subunit suggesting the cell to remove receptors containing the adult subunit. However, it is also possible, that the turnover rate of the GlyR becomes decelerated in adulthood. Since mAb4 signal is stronger reduced than mAb2 signal, it might be that synapses containing the GlyRa3 subunit also are removed from the membrane and abolished. The GlyRa2 signal increases during the third week in culture and remains at eight puncta per 30 µm dendrite. In knockdown cells in turn, the number of GlyRa clusters is half of that of mismatch cultures. In addition, an increase during the third week is remarkable as well as the decrease until div 36 but always exhibiting only half as many clusters as mismatch cells. This suggests that from begin of the measurement on less GlyRa clusters are present in knockdown cells but undergo as well as mismatch cells the mentioned alteration in their number during development. Thereby it is not clear which subunit causes the decrease in expression during the fifth week in culture because both, mAb2 and GlyRa2 signal even increase in that time period.

Since it was not clear so far why or how the reduction of GlyRa1 expression came, gephyrin as a GlyR anchoring protein was investigated as well. Thereby only mAb7 studies were performed because 408 antibody was not achieved to give a useful immunoreactivity signal in my hands. Generally, the number of gephyrin puncta behaves similar to that of the GlyR. Starting with about six clusters per 30 µm dendrite at div 15, the number of gephyrin clusters is quadruplicated during the following week but decreases until div 36 where it reaches about 17 clusters per 30 µm dendrite. The size of the puncta undergoes an analogue course. As already shown via immunoblots, the strongest reduction in mAb7 signal occurs around div 22, directly after the GlyR subunit switch is thought to take place. In knockdown cultures, the described rise and decline of gephyrin expression also occurs, but the number of clusters always remains significantly lower than in mismatch cells. The question arising from these results is, whether the reduction of gephyrin causes the loss of GlyR clusters or the other way around. Kling et al. postulate that GlyRa1 may be an important regulator of gephyrin accumulation because they found a drastic down regulation of gephyrin protein in membrane preparations of the spinal cord of GlyRa1 knockout mice (*oscillator,* Kling et al. 1997). Thus, the reduction of GlyRa1 might evoke the loss of gephyrin clusters. However, Kling et al. did not determine the gephyrin protein level of the whole cell. Therefore, it remains unclear whether gephyrin forms the large aggregates within the cytoplasm known from Kirsch and Betz (Kirsch and Betz 1998) or whether the overall gephyrin expression is reduced in their experiments. In this study, no intracellular gephyrin aggregates are formed upon KCC2 knockdown. This would suggest that reduced GlyRa1 expression directs a down regulation of gephyrin. Regarding the results from Lévi et al., indicating that loss of gephyrin causes loss of GlyR clusters (Lévi et al. 2004) it is also possible, that the down regulation of gephyrin evokes a decrease in GlyRa1 expression. A last but also probable presumption could be that KCC2 down regulation is responsible for both GlyRa1 and gephyrin reduction. This would indicate that the absence of KCC2 protein or the predicted high chloride level in the cells respectively is able to regulate GlyRa1 and/or gephyrin expression. From div 22 on, the fluorescence intensity and from div 36 on also the size of the gephyrin clusters respectively are no longer significantly reduced. The same was already seen for GlyRa1 clusters indicating an upcoming, compensatory effect in the infected neurons.

In 2007, Li et al. demonstrated KCC2 to be crucial for spine development. They show abnormal dendritic spine morphologies in $KCC2^{-/-}$ cortical neuronal cultures. These spines exhibit a filopodia-like morphology and significantly longer protrusions compared to control cells (Li et al. 2007). The same phenomenon was observed but not analyzed in infected cells. Figure 48B and Figure 49B clearly demonstrate the altered protrusion morphology. During the study, I could observe more branched dendrites and longer spines in most neurons infected with KCC2kd2. These findings support Li's data on the one hand and on the other hand, the thesis that loss of KCC2 keeps the neurons back in a juvenile state. Another noticeable characteristic of the knockdown cells is that they appear smaller than the mismatch controls also supporting the latter.

To characterize further effects initiated by KCC2 knockdown, other synaptic markers were analyzed. One of them is PSD 95. Important for the study was, that PSD 95 is not shown to interact with gephyrin and/or the GlyR. PSD 95 has an anchoring function for AMPAR and NMDAR. Thus, synaptic components independent from the GlyR-gephyrin complex were analyzed for alterations. At div 15, the number of PSD 95 puncta accounts about six per 30 µm dendrite. During the next week, this value is more than duplicated and does not drop later on. The size of the PSD 95 clusters in turn behaves as that of the GlyR and gephyrin: it rises between div 15 and div 22 and declines until div 36. At no point in time, the measured values differ to significant extents. The high standard deviations of especially the knockdown cultures are a sign of a broad expression variability of PSD 95. In Li's study, the number of PSD 95 puncta was reduced in $KCC2^{-/-}$ neurons being not true for my study. Li et al also showed that the observed effect was not dependent on the function of KCC2 but probably on its interaction with the cytoskeleton. For my work, the latter imports that either loss of KCC2 function results in a juvenile chloride concentration within the cell or that loss of KCC2 in general gives rise to complex cytoskeletal alterations. The latter might suggest a mechanism in which KCC2 regulates gephyrin expression via complicate cytoskeletal interactions.

The next step was to explore the expression of $GABA_AR$ being another receptor to mediate inhibitory transmission. A first but not measured observation was that cells carrying $GABA_AR$ immunoreactivity did not exhibit differences in size. In contrast, knockdown cells positive for the GlyR or gephyrin appear to be smaller than their mismatch counterparts. The number of $GABA_AR$ puncta undergoes the same course as GlyRa1. The number of clusters rises between div 15 and div 22 and subsequently declines. The same happens to the size of $GABA_AR$ clusters. Except for the number of clusters at div 36, no significant differences occur in $GABA_AR$ expression comparing mismatch and knockdown cultures. It might be that $GABA_AR$ in general is less sensitive to KCC2 down regulation in SNs because it is not the main inhibitory receptor expressed. However, being confronted with the silencing construct for more than four weeks, even $GABA_AR$ receptor expression may be concerned. In summary, the effect onto the $GABA_AR$ remains mild or even is not present at all. This indicates $GABA_AR$ being not concerned because it fails to bind gephyrin. The latter hypothesis is postulated by Poulopoulos who found no direct interaction between gephyrin and the $GABA_AR$ (Poulopoulos et al. 2009). Furthermore, this thesis would support the earlier idea of KCC2 knockdown to induce gephyrin down regulation, which in turn affects GlyR expression. Moreover, these results indicate, that $GABA_AR$ does not compensate for the reduction in GlyRa1 expression

The last synaptic component, which has been examined in the present study, was the expression of the presynaptically localized vesicular inhibitory amino acid transporter (VIAAT). During the investigated time period, the number of VIAAT puncta was triplicated and the size of the clusters was almost duplicated. At div 36, it was no longer possible to measure these parameters because the VIAAT signal became to strong and hence unclear. However, no significant changes of the critical parameters occurred suggesting the presynapse to remain completely untouched by KCC2 knockdown.

As already mentioned, for all immunoreactivities and all time points, the quotient of the "gray value" and the "size" of the puncta was generated. Since the obtained data did not exhibit significant changes, they are not shown in the thesis. The conclusion is that the density of the single receptors within the puncta is not altered at all.

In summary, by means of the PCR data, a switch in the mRNA expression of the juvenile GlyRa2 and the adult GlyRa1 subunit can be determined around div 14. To the same time point, KCC2 protein and RNA expression reaches a maximum *in vitro* and *in vivo* suggesting a possible linkage of KCC2 and the GlyR expression and/or activity. Furthermore, KCC2 expression and stability might be dependent on GlyR activity, evoking Ca^{2+} influx or on Ca^{2+} presence in general. Thereby, Ca^{2+} might play a role in regulating kinase or phosphatase activity, which in turn modifies the phosphorylation state of KCC2 and/or gephyrin. The fact, that phosphorylation states indeed are altered upon application of the mentioned inhibitors and chelators is supported by the absence of mAb7 and PS-6 signal in treated cultures. However, the other way around, suppression of KCC2 protein expression clearly directs down regulation of the adult GlyR alpha subunit and gephyrin without affecting the expression of other synaptic proteins like e.g. $GABA_AR$ or VIAAT.

In conclusion, the results indicate a complex correlation of KCC2 and the GlyR, rather GlyRa1, which are supposed to be dependent on each other to a certain extent. First, KCC2 expression, activity or maybe localization in the membrane is dependent on GlyR activity. Activation of the latter induces a depolarization of the cell and the subsequent Ca^{2+} influx into the cell. Ca^{2+} in turn is able to evoke kinase- or phosphatase-determined alteration in the phosphorylation state of KCC2. KCC2 achieves a more or less stable conformation dependent on its phosphorylation state, which again is important for its activity. On the other hand, an almost complete knockdown of KCC2 expression in cultured spinal neurons alters the expression of GlyRa1 and the scaffolding protein gephyrin, which is connected to the adult form of the GlyR. Either the presence of a high chloride level inhibits GlyRa1 expression in any way, so that the maturation of the cell is initiated by a decreasing intracellular chloride level, or the presence of KCC2 has an influence onto GlyRa1 expression via the cytoskeleton. This is also probable since it was already shown that KCC2 owns binding sites for cytoskeletal proteins, which yet are different from the cytoskeletal proteins, gephyrin is able to bind. Nevertheless, it is possible, that unknown connections among cytoskeletal proteins, KCC2, gephyrin and the GlyR facilitate the described regulation. It also is possible that the adult GlyR is not allowed to be anchored to the cytoskeleton at synaptic sites caused by the reduction of gephyrin upon KCC2 knockdown. Subsequently, the GlyR molecules are removed from the membrane and degraded within the cell. Unfortunately, the level of the GlyRb subunit could not be determined. This would have shed light to the latter question, because when removed from the membrane, the whole GlyR pentamer including the GlyRb subunits would be concerned. A last probability is that the reduction in GlyRa1 expression results from transcriptional regulation.

A probable model could be that the activity of the juvenile GlyR, triggering an excitatory response, is needed for accumulation of Ca^{2+} within intracellular stores. Ca^{2+} in turn is somehow responsible for the successful work, the stability or the phosphorylation state of KCC2. KCC2 subsequently, changes the ion ratios within the cell, which in turn directs maturation of the cell in terms of increased gephyrin and/or GlyRa1 expression.

6. Future aspects

My work evokes more questions than it could answer. Initiated by the results of the treatments, the question came up which role Ca^{2+} is playing in stabilizing the KCC2 tetramer and thereby its ability to transport ions. In collaboration with a physiologically arranged research group, the activity of KCC2 could be investigated using specific blockers for KCC2 or measuring Rb^{+} uptake by the cells following the described treatments. This could shed light on whether Ca^{2+} is able to alter KCC2 activity via destabilization of the complex. Furthermore, it has to be clarified if KCC2 indeed is phosphorylated or dephosphorylated upon Ca^{2+} influx or presence. Cloning experiments to identify possible phosphorylation sites as well as treatment with specific kinase and phosphatase inhibitors may help to answer the latter.

For the glycine treatments, more controls are needed such as cells grown in NB^{++++} but treated with strychnine as well as cells grown in glycine-free NB^{++++} also treated with strychnine. This would better mimic the silent GlyR.

Additional to the mismatch shRNA, a rescue construct should have been adapted. However, I was not able to clone the mutated KCC2 sequence into the lentiviral vector. The collaboration with a versed molecular biology research group may result in a functional rescue control. Cells transduced by both, the knockdown and the rescue construct should no longer exhibit the effects evoked by KCC2 knockdown. Moreover, switching off the TrkB receptor (receptor for BDNF) by RNAi or specific inhibitors, might direct the same effects than the KCC2 knockdown. Additionally, other components of the KCC2 signalling pathway or KCC2 regulators should be investigated. An early overexpression of KCC2 in cultured neurons may lead to the opposite effect, consisting of an early onset of GlyRa1 up regulation. In addition, the low, mature chloride level and therewith the hyperpolarizing transmission state should be achieved earlier in development.

A functionally inactive form of KCC2 transfected or transduced to the SNs may give information about the dependence of the GlyRa1 expression on KCC2 activity.

Further insights in the association of KCC2 and the GlyR may be achieved by investigating KCC2 knockout animals. KCC2 knockout mice as well as conditional knockout mice already are available at the moment. Cross-sections of the spinal cord from knockout animals should be taken and analyzed for GlyR subunit and gephyrin immunoreactivities. The results should be compared to wild type animals and the results of this thesis. The consequential issues might show whether the expression of the adult GlyR alpha1 subunit also is down regulated in knockout mice. Possibly, some compensatory effects would be observed as well.

In terms of knockout animals, also the GlyRa2 knockout mouse should be examined. The GlyRa2 knockout mouse might exhibit an up regulation in either another than the GlyRa2 subunit or even in NMDAR to compensate for the loss of the alpha2 subunit.

Furthermore, the silencing sequence could be injected to the spinal cord of newborn rats, which might be analyzed two ore more weeks later. Therefore, cross-sections of the spinal cord should be investigated for GlyR subunit and gephyrin immunoreactivity as well.

7. Abbreviations

ΔCT	Difference of the CT-values of the control an the investigated gene
AMPAR	α-Amino-3-hydroxy-5-methyl-4-isoxazol-Propionic acid receptor
APS	Ammoniumpersulfate
APV	Amino-Phosphonopentanoate
AraC	Cytarabin
BDNF	Brain derived neurothrophic factor
bp	Basepairs
BSA	Bovine serum albumin
$CaCl_2$	Calciumdichloride
cDNA	Copy DNA
CT	Cycle Threshold (cycle of the RTq-PCR, in which the enzyme-substrate curve changes from the linear to the Plateau-phase)
DABCO	1,4-Diazabicyclo[2.2.2]octan
div	Days in vitro
Dk	Donkey
DMEM	Dulbecco's modified Eagle Medium
DMSO	Dimethylsulfoxide
dNTP	Deoxyribonucleotide-Triphosphate
DOC	Sodium Deoxycholate
ds	Double stranded
E	Embryonic day
ECL	Enhanced Chemiluminescence
EDTA	Ethylendiamine-tetraacetate
EGFP	Enhanced green fluorescent protein
et al.	et alteri
EtBr	Ethidiumbromide
EtOH	Ethanol
FBS/FCS	Fetal bovine/calf serum
$GABA_AR$	γ-Aminobutteric Acid A-Receptor
GFP	Green fluorescent protein
GlyR	Glycine receptor
GlyT2	Glycine transporter subtype 2
gpig	Guinea pig
gt	Goat
HBSS	Hanks balanced salt solution
HCN	Hippocampal neuron/hippocampal neuronal
HEK	Human embryonic kidney
HRP	Horse raddish peroxidase
HS	Horse Serum
IB	Immunoblot

IR	Immunoreactivity
KCC2	Potassium chloride cotransporter 2
kd	Knockdown
KOH	Potassiumydroxide
LB	Luria-Bertani
M	Mol per litre
mA	Milliampere
MAP	Microtubule associated protein
MCS	Multiple cloning site
MEF	Mouse embryonic fibroblast
MeOH	Methanol
$MgCl_2$	Magnesiumdichloride
Milli-Q	Double distilled water
mIPSC	Miniature inhibitory postsynaptic current
mm	mismatch
mM	Millimol per litre
$MnCl_2$	Mangandichloride
ms	Mouse
n.s.	Not significant
NB	Neurobasal
NL	Neuroligin
NMDAR	N-Methyl-D-Aspartate receptor
o/d	Over day
o/n	Over night
OD	Optical density
P	Postnatal day
P/S	Penicillin/Streptomycin
PAGE	Polyacrylamide gelelectrophoresis
PBS	Phosphate buffered saline
PET	Polyethylenterephthalate
PFA	Paraformaldehyde
pH	Potentia hydrogenii (cologarithm of the activity of dissolved hydrogen ions)
PIPES	Piperazine-1,2-bis[2-ethanesulfonic acid]
PMSF	Phenylmethylsulphonylfluoride
pS	picoSiemens
PSD 95	Postsynaptic Density Protein 95
PVDF	Polyvinylidenfluoride
rb	Rabbit
RIPA	Radio immunoprecipitation assay
RNAi	RNA interference
rpm	Rounds per minute
RT	Room temperature

RT-PCR	Reverse Transcriptase Polymerase chain reaction)
RTq-PCR	Real Time quantitative PCR
s.d.	Standard deviation
S2	Safety-Level 2
SDS	Sodiumdodecylsulfate
shRNA	short hairpin RNA
SN	Spinal neuron/spinal neuronal
SOB	Super optimal broth
sp	Sheep
SW	Swing-out rotor
TBS	Tris-buffered saline
TBS-T	Tris-buffered saline + Tween-20
TEMED	N,N,N',N'-Tetramethylethylenediamine
Tris	Trimethylsilylsilan
TWEEN-20	Polyoxyethylen(20)-sorbitan-monolaurate
UT	Untransfected
UZ	Ultrazentrifugation/Ultrazentrifuge
V	Volt
VIAAT	Vesicular Inhibitory Amino Acid Transporter
Wnt	Wingless (wg) Integrated (Int)
xg	X-times acceleration of gravitiy

8. References

Adragna NC, Fulvio MD, Lauf PK. Regulation of K–Cl cotransport: from function to genes. J Membr Biol. 201: 109–137, 2004.

Beato M, Groot-Kormelink PJ, Colquhoun D, Sivilotti LG. The activation mechanism of alpha1 homomeric glycine receptors. J Neurosci. 24: 895-906, 2004.

Becker CM, Hoch W, Betz H. Glycine receptor heterogeneity in rat spinal cord during postnatal development. EMBO J. 7: 3717-26, 1988.

Betz H, Laube B. Glycine receptors: recent insights into their structural organization and functional diversity. J Neurochem. 97: 1600-1610, 2006.

Blaesse P, Airaksinen MS, Rivera C, Kaila K. Cation-chloride cotransporters and neuronal function. Neuron 61: 820-838, 2009.

Blaesse P, Guillemin I, Schindler J, Schweizer M, Delpire E, Khiroug L, Friauf E, Nothwang HG. Oligomerization of KCC2 correlates with development of inhibitory neurotransmission. J Neurosci. 26: 10407-10419, 2006.

Bluem R, Schmidt E, Corvey C, Karas M, Schlicksupp A, Kirsch J, Kuhse J. Components of the translational machinery are associated with juvenile glycine receptors and are redistributed to the cytoskeleton upon aging and synaptic activity. J Biol Chem. Dec 28: 37783-37793, 2007.

Boettger T, Rust MB, Maier H, Seidenbecher T, Schweizer M, Keating DJ, Faulhaber J, Ehmke H, Pfeffer C, Scheel O, Lemcke B, Horst J, Leuwer R, Pape HC, Völkl H, Hübner CA, Jentsch TJ. Loss of K-Cl co-transporter KCC3 causes deafness, neurodegeneration and reduced seizure threshold. EMBO J. 22: 5422-5434, 2003.

Buckwalter MS, Cook SA, Davisson MT, White WF, and Camper SA. A frameshift mutation in the mouse α1 glycine receptor gene (Glra1) results in progressive neurological symptoms and juvenile death. Hum Mol Genet. 78: 2025–2030, 1994.

Caron L, Rousseau F, Gagnon E, Isenring P. Cloning and functional characterization of a cation–Cl-cotransporter-interacting protein, J Biol Chem. 275: 32027–32036, 2000.

Charrier C, Ehrensperger MV, Dahan M, Lévi S, Triller A. Cytoskeleton regulation of glycine receptor number at synapses and diffusion in the plasma membrane. J Neurosci. 26: 8502-8511, 2006.

Chudotvorova I, Ivanov A, Rama S, Hübner CA, Pellegrino C, Ben-Ari Y, Medina I. Early expression of KCC2 in rat hippocampal cultures augments expression of functional GABA synapses. J Physiol. 566: 671-679, 2005.

Clayton GH, Owens GC, Wolf JS, Smith RL. Ontogeny of cation-Cl2 cotransporter expression in rat neocortex. Brain Res Dev Brain Res. 109: 281–292, 1998.

Dahan M, Lévi S, Luccardini C, Rostaing P, Riveau B, Triller A. Diffusion dynamics of glycine receptors revealed by single-quantum dot tracking. Science 302: 442-445, 2003.

Devignot V, Prado de Carvalho L, Bregestovski P, and Goblet C. A novel glycine receptor α Z1 subunit variant in the zebrafish brain. Neuroscience 122: 449–457, 2003.

Dittgen T, Nimmerjahn A, Komai S, Licznerski P, Waters J, Margrie TW, Helmchen F, Denk W, Brecht M, Osten P. Lentivirus-based genetic manipulations of cortical neurons and their optical and electrophysiological monitoring in vivo. Proc Natl Acad Sci. USA. 101: 18206-18211, 2004.

Dresbach T, Nawrotzki R, Kremer T, Schumacher S, Quinones D, Kluska M, Kuhse J, Kirsch J. Molecular architecture of glycinergic synapses. Histochem Cell Biol. 130: 617-633, 2008.

Duan L, Yang J, Slaughter MM. Caffeine inhibition of ionotropic glycine receptors. J Physiol. 587: 4063-4075, 2009.

Ehrensperger MV, Hanus C, Vannier C, Triller A, Dahan M. Multiple association states between glycine receptors and gephyrin identified by SPT analysis. Biophys J. 92: 3706-3718, 2007.

Feng G, Tintrup H, Kirsch J, Nichol MC, Kuhse J, Betz H, Sanes JR. Dual requirement for gephyrin in glycine receptor clustering and molybdoenzyme activity. Science 282: 1321-1324, 1998.

Fiumelli H, Woodin MA. Role of activity-dependent regulation of neuronal chloride homeostasis in development. Curr Opin Neurobiol. 17: 81-86, 2007.

Fritschy JM, Benke D, Mertens S, Oertel WH, Bachi T, Möhler H. Five subtypes of type A gamma-aminobutyric acid receptors identified in neurons by double and triple immunofluorescence staining with subunit-specific antibodies. Proc Natl Acad Sci. USA: 6726-6730, 1992.

Fritschy JM, Harvey RJ, Schwarz G. Gephyrin: where do we stand, where do we go? Trends Neurosci. 31: 257-264, 2008.

Fritschy JM, Mohler H. $GABA_A$-receptor heterogeneity in the adult rat brain: differential regional and cellular distribution of seven major subunits. J Comp Neurol. 359: 154-194, 1995.

Gagnon KB, England R, Delpire E. Volume sensitivity of cation–Cl-cotransporters is modulated by the interaction of two kinases: Ste20-related proline-alanine-rich kinase and WNK4. Am J Physiol: Cell Physiol. 290: C134–C142, 2006.

Gamba G, Miyanoshita A, Lombardi M, Lytton J, Lee WS, Hediger MA, Hebert SC. Molecular cloning, primary structure, and characterization of two members of the mammalian electroneutral sodium-(potassium)-chloride cotransporter family expressed in kidney. J Biol Chem. 269 (26):17713-17722, 1994.

Gomeza J, Ohno K, Hulsmann S, Armsen W, Eulenburg V, Richter DW, Laube B, and Betz H. Deletion of the mouse glycine transporter 2 results in a hyperekplexia phenotype and postnatal lethality. Neuron 40: 797–806, 2003.

Graham BA, Schofield PR, Sah P, and Callister RJ. Altered inhibitory synaptic transmission in superficial dorsal horn neurones in spastic and oscillator mice. J Physiol. 551: 905–916, 2003.

Grenningloh G, Pribilla I, Prior P, Multhaup G, Beyreuther K, Taleb O, Betz H. Cloning and expression of the 58 kd beta subunit of the inhibitory glycine receptor. Neuron 4: 963-970, 1990.

Grenningloh G, Schmieden V, Schofield PR, Seeburg PH, Siddique T, Mohandas TK, Becker CM, Betz H. Alpha subunit variants of the human glycine receptor: primary structures, functional expression and chromosomal localization of the corresponding genes. EMBO 9: 771-776, 1990.

Grudzinska J, Schemm R, Haeger S, Nicke A, Schmalzing G, Betz H, Laube B. The beta subunit determines the ligand binding properties of synaptic glycine receptors. Neuron 45: 727-739, 2005.

Gulyás AI, Sík A, Payne JA, Kaila K, Freund TF. The KCl cotransporter, KCC2, is highly expressed in the vicinity of excitatory synapses in the rat hippocampus. Eur J Neurosci. 13: 2205-2217, 2001.

Hanus C, Ehrensperger MV, Triller A. Activity-dependent movements of postsynaptic scaffolds at inhibitory synapses. J Neurosci. 26: 4586-4595, 2006.

Hanus C, Vannier C, Triller A. Intracellular association of glycine receptor with gephyrin increases its plasma membrane accumulation rate. J Neurosci. 24: 1119-1128, 2004.

Harvey RJ, Depner UB, Wässle H, Ahmadi S, Heindl C, Reinold H, Smart TG, Harvey K, Schütz B, Abo-Salem OM, Zimmer A, Poisbeau P, Welzl H, Wolfer DP, Betz H, Zeilhofer HU, Müller U. GlyR alpha3: an essential target for spinal PGE2-mediated inflammatory pain sensitization. Science 304: 884-887, 2004.

Haverkamp S, Müller U, Zeilhofer HU, Harvey RJ, Wässle H. Diversity of glycine receptors in the mouse retina: localization of the alpha2 subunit. J Comp Neurol. 477: 399-411, 2004.

Hübner CA, Stein V, Hermans-Borgmeyer I, Meyer T, Ballanyi K, Jentsch TJ. Disruption of KCC2 reveals an essential role of K-Cl cotransport already in early synaptic inhibition. Neuron 30: 515-524, 2001.

Kim EY, Schrader N, Smolinsky B, Bedet C, Vannier C, Schwarz G, Schindelin H. Deciphering the structural framework of glycine receptor anchoring by gephyrin. EMBO J 26: 1385-1395, 2006.

Kins S, Betz H, Kirsch J. Collybistin, a newly identified brain-specific GEF, induces submembrane clustering of gephyrin. Nat Neurosci. 3: 22-9, 2000.

Kirsch J, Betz H. Glycine-receptor activation is required for receptor clustering in spinal neurons. Nature 392: 717-720, 1998.

Kirsch J, Betz H. The postsynaptic localization of the glycine receptor-associated protein gephyrin is regulated by the cytoskeleton. J Neurosci. 15: 4148-4156, 1995a.

Kirsch J, Betz H. Widespread expression of gephyrin, a putative glycine receptor-tubulin linker protein, in rat brain. Brain Res. 621: 301-310, 1993a.

Kirsch J, Kuhse J, Betz H. Targeting of glycine receptor subunits to gephyrin-rich domains in transfected human embryonic kidney cells. Mol Cell Neurosci. 6: 450-461, 1995b.

Kirsch J, Langosch D, Prior P, Littauer UZ, Schmitt B, Betz H. The 93-kDa glycine receptor-associated protein binds to tubulin. J Biol Chem. 266: 22242-22245, 1991.

Kirsch J, Wolters I, Triller A, Betz H. Gephyrin antisense oligonucleotides prevent glycine receptor clustering in spinal neurons. Nature 366: 745-748, 1993b.

Kirsch J. Glycinergic transmission. Cell Tissue Res. 326: 535-540, 2006.

Kling C, Koch M, Saul B, Becker CM. The frameshift mutation oscillator (Glra1(spd-ot)) produces a complete loss of glycine receptor alpha1-polypeptide in mouse central nervous system. Neuroscience 78: 411-417, 1997.

Kuhse J, Kuryatov A, Maulet Y, Malosio ML, Schmieden V, and Betz H. Alternative splicing generates two isoforms of the α 2 subunit of the inhibitory glycine receptor. FEBS Lett. 283: 73–77, 1991.

Leite JF, Cascio M. Structure of ligand-gated ion channels: critical assessment of biochemical data supports novel topology. Mol Cell Neurosci. 17: 777-792, 2001.

Lévi S, Logan SM, Tovar KR, Craig AM. Gephyrin is critical for glycine receptor clustering but not for the formation of functional GABAergic synapses in hippocampal neurons. J Neurosci. 24: 207-217, 2004.

Lewis TM, Schofield PR, McClellan AM. Kinetic determinants of agonist action at the recombinant human glycine receptor. J Physiol. 549: 361-374, 2003.

Li H, Khirug S, Cai C, Ludwig A, Blaesse P, Kolikova J, Afzalov R, Coleman SK, Lauri S, Airaksinen MS, Keinänen K, Khiroug L, Saarma M, Kaila K, Rivera C. KCC2 interacts with the dendritic cytoskeleton to promote spine development. Neuron 56: 1019-1033, 2007.

Liu A, Niswander LA. Bone morphogenetic protein signalling and vertebrate nervous system development. Nat Rev Neurosci. 6: 945-954, 2005.

Lu J, Karadsheh M, Delpire E. Developmental regulation of the neuronal-specific isoform of K-Cl cotransporter KCC2 in postnatal rat brains. J Neurobiol. 39: 558-568, 1999.

Lummis SC, Gundlach AL, Johnston GA, Harper PA, and Dodd PR. Increased -aminobutyric acid receptor function in the cerebral cortex of myoclonic calves with an hereditary deficit in glycine/strychnine receptors. J Neurochem. 55: 421–426, 1990.

Lynch JW. Molecular structure and function of the glycine receptor chloride channel. Physiol Rev. 84: 1051-1095, 2004.

Maas C, Tagnaouti N, Loebrich S, Behrend B, Lappe-Siefke C, Kneussel M. Neuronal cotransport of glycine receptor and the scaffold protein gephyrin. J Cell Biol. 172: 441-451, 2006.

Malosio ML, Grenningloh G, Kuhse J, Schmieden V, Schmitt B, Prior P, and Betz H. Alternative splicing generates two variants of the α1 subunit of the inhibitory glycine receptor. J Biol Chem. 266: 2048–2053, 1991a.

Malosio ML, Marquèze-Pouey B, Kuhse J, Betz H. Widespread expression of glycine receptor subunit mRNAs in the adult and developing rat brain. EMBO J. 10: 2401-2409, 1991b.

Meier H and Chai CK. Spastic, an hereditary neurological mutation in the mouse characterized by vertebral arthropathy and leptomeningeal cyst formation. Exp Med Surg. 28: 24–38, 1970.

Meier J, Vannier C, Serge A, Triller A, Choquet D. Fast and reversible trapping of surface glycine receptors by gephyrin. Nat Neurosci. 4: 253–260, 2001.

Mercado A, Mount DB, Gamba G. Electroneutral cation-chloride cotransporters in the central nervous system. Neurochem Res. 29: 17-25, 2004.

Meyer G, Kirsch J, Betz H, Langosch D.Neuron. Identification of a gephyrin binding motif on the glycine receptor beta subunit. 15: 563-572, 1995.

Mulhardt C, Fischer M, Gass P, Simon-Chazottes D, Guenet JL, Kuhse J, Betz H, and Becker CM. The spastic mouse: aberrant splicing of glycine receptor beta subunit mRNA caused by intronic insertion of L1 element. Neuron 13: 1003–1015, 1994.

Naldini L, Blömer U, Gage FH, Trono D, Verma IM. Efficient transfer, integration, and sustained long-term expression of the transgene in adult rat brains injected with a lentiviral vector. Proc Natl Acad Sci. USA 93: 11382-11388, 1996.

Naldini L, Blömer U, Gallay P, Ory D, Mulligan R, Gage FH, Verma IM, Trono D. In vivo gene delivery and stable transduction of nondividing cells by a lentiviral vector. Science 272: 263-267, 1996.

Nikolic Z, Laube B, Weber RG, Lichter P, Kioschis P, Poustka A, Mulhardt C, and Becker CM. The human glycine receptor subunit α3. Glra3 gene structure, chromosomal localization, and functional characterization of alternative transcripts. J Biol Chem. 273: 19708–19714, 1998.

Papadopoulos T, Korte M, Eulenburg V, Kubota H, Retiounskaia M, Harvey RJ, Harvey K, O'Sullivan GA, Laube B, Hülsmann S, Geiger JR, Betz H. Impaired GABAergic transmission and altered hippocampal synaptic plasticity in collybistin-deficient mice. EMBO J. 26: 3888-3899, 2007.

Payne JA, Rivera C, Voipio J, Kaila K. Cation-chloride co-transporters in neuronal communication, development and trauma. Trends Neurosci. 26: 199-206, 2003.

Pfeiffer F, Simler R, Grenningloh G, Betz H. Monoclonal antibodies and peptide mapping reveal structural similarities between the subunits of the glycine receptor of rat spinal cord. Proc Natl Acad Sci. USA 81: 7224-7227, 1984.

Piechotta K, Weth F, Harvey RJ, Friauf E. Localization of rat glycine receptor alpha1 and alpha2 subunit transcripts in the developing auditory brainstem. J Comp Neurol. 438: 336-352, 2001.

Poulopoulos A, Aramuni G, Meyer G, Soykan T, Hoon M, Papadopoulos T, Zhang M, Paarmann I, Fuchs C, Harvey K, Jedlicka P, Schwarzacher SW, Betz H, Harvey RJ, Brose N, Zhang W, Varoqueaux F. Neuroligin 2 drives postsynaptic assembly at perisomatic inhibitory synapses through gephyrin and collybistin. Neuron 63: 628-642, 2009.

Price TJ, Cervero F, de Koninck Y. Role of cation-chloride-cotransporters (CCC) in pain and hyperalgesia. Curr Top Med Chem. 5: 547-555, 2005.

Rees MI, Harvey K, Ward H, White JH, Evans L, Duguid IC, Hsu CC, Coleman SL, Miller J, Baer K, Waldvogel HJ, Gibbon F, Smart TG, Owen MJ, Harvey RJ, and Snell RG. Isoform heterogeneity of the human gephyrin gene (GPHN), binding domains to the glycine receptor, and mutation analysis in hyperekplexia. J Biol Chem. 278: 24688–24696, 2003.

Rivera C, Voipio J, Payne JA, Ruusuvuori E, Lahtinen H. Lamsa K, Pirvola U, Saarma M, Kaila K. The K^+/Cl^- co-transporter KCC2 renders GABA hyperpolarizing during neuronal maturation. Nature 397: 251–255, 1999.

Ryan SG, Buckwalter MS, Lynch JW, Handford CA, Segura L, Shiang R, Wasmuth JJ, Camper SA, Schofield P, and O'Connell P. A missense mutation in the gene encoding the α1 subunit of the inhibitory glycine receptor in the spasmodic mouse. Nat Genet. 7: 131–135, 1994.

Ryan SG, Dixon MJ, Nigro MA, Kelts KA, Markand ON, Terry JC, Shiang R, Wasmuth JJ, and O'Connell P. Genetic and radiation hybrid mapping of the hyperekplexia region on chromosome 5q. Am J Hum Genet. 51: 1334–1343, 1992.

Shiang R, Ryan SG, Zhu YZ, Hahn AF, O'Connell P, and Wasmuth JJ. Mutations in the α1 subunit of the inhibitory glycine receptor cause the dominant neurologic disorder, hyperekplexia. Nat Genet. 5: 351–358, 1993.

Sola M, Bavro VN, Timmins J, Franz T, Ricard-Blum S, Schoehn G, Ruigrok RW, Paarmann I, Saiyed T, O'Sullivan GA, Schmitt B, Betz H, Weissenhorn W. Structural basis of dynamic glycine receptor clustering by gephyrin. EMBO J. 23: 2510-2519, 2004.

Takahashi T, Momiyama A, Hirai K, Hishinuma F, Akagi H. Functional correlation of fetal and adult forms of glycine receptors with developmental changes in inhibitory synaptic receptor channels. Neuron 9: 1155-1161, 1992.

Van Zundert B, Alvarez FJ, Tapia JC, Yeh HH, Diaz E, Aguayo LG. Developmental-dependent action of microtubule depolymerization on the function and structure of synaptic glycine receptor clusters in spinal neurons. J Neurophysiol. 91: 1036-1049, 2004.

Veruki ML, Gill SB, Hartveit E. Spontaneous IPSCs and glycine receptors with slow kinetics in wide-field amacrine cells in the mature rat retina. J Physiol. 581: 203-019, 2007.

Vinay L, Jean-Xavier C. Plasticity of spinal cord locomotor networks and contribution of cation-chloride cotransporters. Brain Res Rev. 57: 103-110, 2008.

Watanabe E, Akagi H. Distribution patterns of mRNAs encoding glycine receptor channels in the developing rat spinal cord. Neurosci Res. 23: 377-382, 1995.

Wenz M, Hartmann AM, Friauf E, Nothwang HG. CIP1 is an activator of the K+-Cl- cotransporter KCC2. Biochem Biophys Res Commun. 381: 388-392, 2009.

Zhang XB, Sun GC, Liu LY, Yu F, Xu TL. Alpha2 subunit specificity of cyclothiazide inhibition on glycine receptors. Mol Pharmacol. 73: 1195-1202, 2008.

Zhu L, Lovinger D, Delpire E. Cortical neurons lacking KCC2 expression show impaired regulation of intracellular chloride. J Neurophysiol. 93: 1557-1568, 2005.

Zufferey R, Nagy D, Mandel RJ, Naldini L, Trono D. Multiply attenuated lentiviral vector achieves efficient gene delivery in vivo. Nat Biotechnol. 9: 871-875, 1997.

Internetquellen

(zuletzt abgerufen am 20.05.2010):

http://de.wikipedia.org/wiki/Wikipedia:Hauptseite

http://www.ncbi.nlm.nih.gov/pubmed/

http://rzblx1.uni-regensburg.de/ezeit/index.phtml?bibid=UBHE&colors=3&lang=de

http://www.embryology.ch/allemand/vcns/moelle03.html

Hiermit erkläre ich an Eides statt, dass ich die vorliegende Dissertation selbstständig und ohne unerlaubte Hilfsmittel durchgeführt habe.

Bretten, den 20.05.2010

Stefanie Schumacher